SYNTHESIS OF DNA-TEMPLATED FUNCTIONAL MATERIALS AND THEIR APPLICATIONS

A Dissertation

Presented to the Faculty of the Graduate School

of Cornell University

In Partial Fulfillment of the Requirements for the Degree of

Doctor of Philosophy

by

Jong Bum Lee

May 2009

SYNTHESIS OF DNA-TEMPLATED FUNCTIONAL MATERIALS AND THEIR APPLICATIONS

Jong Bum Lee, Ph. D.

Cornell University 2009

DNA has been used to guide the self-assembly of functional materials in this dissertation. Based on programmability of DNA, Y-shaped DNA (Y-DNA) and X-shaped DNA (X-DNA) were precisely labeled with fluorescence and quencher dyes. From these precise labelings, the stability of Y- and X-shaped DNA was studied by the Förster resonance energy transfer (FRET) method. In addition, the thermal stability of DNA nanostructures self-assembled from Y- and X-shaped DNA was thoroughly investigated. The nanosurface energy transfer (NSET) method was employed to monitor the conformation change of the nanostructures with nano-scale sensitivity. The effects of junctions on the thermal stability dendrimer-like DNA (DL-DNA) and DNA hydrogel were also studied with various types of FRET pair labeled building blocks.

Based on the multivalency and anisotropicity of DNA nanostructures, DNA-templated assembly of multifunctional nano-architectures was achieved. By ligation of branched DNA labeled with quantum dots, gold nanoparticles, and polyethylene glycol monoacrylate, **a**nisotropic, **b**ranched, and **c**rosslinkable monomers (ABC monomers) were created. Because of the precise labeling of multi-moieties on a single entity, DNA nano-architectures showed multifunctions such as optical coding, amplifying signal by polymerization, and detecting pathogen DNA. A target-driven

polymerization by the ABC monomer achieved highly-sensitive pathogen detection. In addition, the polymers were used as a biocompatible multi-drug delivery vector.

DNA-templated technology was applied in generating a novel functional DNA hydrogel. The formation of the gel was based on physical interactions of elongated DNA strands by rolling circle chain reaction (RCCR). Unlike traditional DNA based hydrogel, this novel DNA hydrogel was thermally stable, since it did not depend on base pairing. The new DNA hydrogel behaved like fluid but still held a specific shape and gel properties. In addition, the hydrogels showed thermoplastic property which allows hydrogel to be easily reshaped by molding and heating. With these excellent characteristics, our liquid-like DNA hydrogels were developed as an injectable extracellular matrix for tissue engineering.

BIOGRAPHICAL SKETCH

Jong Bum Lee was born and raised on a farm which had hundreds of dairy cows. His favorite thing was to make small houses for baby cows and fed them. He chose chemical engineering as his major after he graduated from Seoul High School. After four-year college life in Sogang University, he spent another two years in the same school for MS degree with achievement for developing a method to fabricate protein chips.

In 2004, he went to professor Luo's group at Cornell for his Ph. D degree. After one year, he got married with Jee Young Lee. On August 4th, 2008, his lovely daughter, Claire Siyeon Lee, was born. She makes him smile every day and gives him energy for his research. After fruitful four and half years in Luo's group, he will begin exciting postdoctoral work.

To my parents, my sisters, my wife, and my daughter

ACKNOWLEDGMENTS

I would like to thank my academic advisor, Prof, Dan Luo, for his support and guidance. He was patiently teaching me the beauty of research in the past four and half years. His passion for research will have a great influence on my future. I will never forget the enjoyable experience in Luo's group. I would also like to thank the other members of thesis committee, Prof. Chih-Chang Chu and Prof. Christopher Umbach for valuable comments and advices.

I also deliver my thanks to all members of our lab, Hisakage Funabash, Nokyoung Park, Wenlong Cheng, Liang Ding, Soong Ho Um, Yougen Li, Young Hoon Roh, Mark Hartman, Mike Campolongo, Shawn Tan, Thua Nguyen Nhi Tran, Pichamon Kiatwuthinon for their technical help. Their discussions and comments were also very appreciated.

For encouragement in the final stage of my Ph.D. degree, I specially thank my lovely wife, Jee Young Lee, and my lovely daughter, Claire Siyeon Lee. I also appreciate to my sisters, brother-in-laws, nieces, and nephew for their encouragement. At the end, I give my appreciation to my parents, Kyu Ho Lee and Young Ja Cho, for their endless love and support in whatever and wherever I decided to do and go.

TABLE OF CONTENTS

LIST OF FIGURES

LIST OF TABLES

CHAPTER 1

Introduction: DNA as a Template for Nanotechnology

1.1 Properties of DNA

DNA molecules play an important role as the genetic material encoding biological information in the central dogma[1, 2]. Since each strand of DNA is made of a backbone plus sequences of four bases: adenine (A), guanine (G), cytosine (C), and thymine (T), a myriad of biological information can be stored. In nature, DNA is predominantly found as double stranded (dsDNA), which is formed based on the hydrogen bond interaction between adenine and thymine (A-T pairing) and guanine and cytosine (G-C pairing)[3]. Since G-C pairing involves three hydrogen bonds, it is more stable than A-T pairing, which involves two hydrogen bonds. Therefore, dsDNA containing more GC pairs are more stable than those consisting of fewer G-C[4] pairs.

Watson-Crick base pairing allows two single stranded DNA (ssDNA) to form dsDNA in the opposite direction (one from 5' to 3' and the other from 3' to 5'). Because of the precise base pairing, DNA is so far the most readily programmable and reliably predictable molecule. The programmably assembled dsDNA can be separated into two ssDNA molecules by heat, high pH, or low salt concentration[5-9]. Denatured ssDNA can reassemble back to dsDNA by cooling or lowering the pH. This programmability and reversibility are extremely useful properties for employing DNA as a scaffold in constructing novel nanomaterials.

Mechanically, DNA is flexible or rigid depending on length. The persistence length of dsDNA is about 50 nm (about 150 base pairs (bps)) while ssDNA is very flexible with a persistence length of 1nm[10, 11]. The width of the double helix is about 2nm and the length increment of each base pair is about 0.34 nm[12]. Therefore, each helix turn, which consists of ten base pairs, increases 3.4 nm. Based on the well studied properties of DNA, the length of DNA molecules can be exactly controlled to an accuracy of 0.34 nm.

As a generic material, DNA is biocompatible, stable, and water soluble and can be easily manipulated. Many enzymatic methods are available to manipulate DNA[13]. For example, more than 3000 restriction enzymes can cut DNA at specific sites and ligase enzymes can covalently and specifically connect DNA. In addition, various polymerases can elongate DNA. More importantly, polymerases using the technique of polymerase chain reaction (PCR) can amplify a template DNA exponentially. In addition to these enzymatic manipulations, DNA strands are easily modified by a variety of small chemicals at both the 5' phosphate and 3' hydroxy groups[14].

1.2 Branched DNA as an anisotropic building block

1.2.1. Anisotropy of building blocks

Anisotropic interactions through chemical, physical, or biosynthetic methods are powerful tools for introducing multiple functions in a single building block[15]. The uniqueness of anisotropic building blocks, in contrast to isotropic spherical colloids, is binding selectivity. Unlike isotropic materials, which have been found to lack precise control in building up complex structures, anisotropic building blocks are moving closer to building architectures with structural complexity due to their interaction anisotropy. Although asymmetrically shaped particles have been synthesized, including triangles[16], half shells[17], tetrapods[18], tripods[19], stars[20], and X-shapes[21], polydispersity of these particles can still hinder binding selectivity. DNA based building blocks seem to be unique in this regard, providing remarkable control over intermolecular interactions.

1.2.2. DNA-based nanoparticle assemblies

Toward the functional application of DNA for novel molecular assemblies, DNA has been employed to program the self-assembly of nanoparticle based

structures. Alivisatos and Mirkin are the frontier of DNA directed assembly of nanoparticles[22]. Earlier work by Alivisatos and coworkers reported that complementary DNA oligonucleotides could be used to organize nanoparticles[23]. In this article, a strategy to align 1.4nm gold nanoparticles (AuNP) functionalized with single-stranded DNA along the complementary single-stranded DNA templated was described. Either "Head to tail" or "Head to head" patterns were achieved and imaged by transmission electron microscopy (TEM). In addition, Alivisatos's group has also patterned various sized AuNPs and successfully synthesized hybrid assemblies of quantum dots (QD) and AuNPs by DNA directed synthesis[24, 25]. Earlier work by Mirkin and coworkers showed that complimentary DNA could be used for assembling macroscopic materials with 13nm AuNPs[26]. In these articles, AuNPs were separately functionalized with two different thiol-modified single stranded DNA. These two single stranded DNA were linked by introducing a linker DNA which was complementary to both single stranded DNA on the AuNPs. By hybridization, aggregations of AuNPs were formed and shown by TEM images with well-ordered structures. This controlled manner of AuNP aggregation was applied to colorimetric DNA detection by monitoring the change of color depending on the degree of aggregation[27].

1.2.3. Branched DNA

In nature, most DNA molecules are either linear or circular forms. Therefore, to create a variety of functional structures from DNA, it is necessary to synthesize DNA structure in multiple dimensions like branched DNA. Holiday junction DNA, which occurs naturally in living systems, is a key intermediate in DNA metabolism, particularly in the processes of replication, recombination, and repair.

Seeman pioneered DNA nanotechnology from creating synthetic branched DNA to constructing highly ordered complex DNA nanostructures[2, 28]. Although the branch point of Holliday junctions in nature can be relocated by virtue of the homologous sequences, branched DNA can be designed to include fixed junctions with three to eight arms[29]. Yan also developed addressable DNA-based molecular tweezers based on four-arm DNA junctions[30]. The sequence design for these building blocks has been based on empirical rules[31]. Although some computer simulation and modeling have been applied to designing the structure of basic building blocks[32], the general method for sequence designs of complicated structures still needs to be improved.

1.2.4. Anisotropy of branched DNA

Luo's group has created Y-shaped DNA and X-shaped DNA which consist of three or four ssDNA, respectively[33-35] (Figure 1.1). Each ssDNA can be linked to chemical entities. In addition, these ssDNA can be designed to have specific extra sequences, called sticky ends, which enable branched DNA to covalently connect to other specific branched DNA (via complementary sticky ends) through a controlled and enzymatic method. With this type of method, branched DNA can form an ideal multivalent and anisotropic building block, although the shape can be symmetrical. The branches can be easily labeled to almost any chemical moieties as long as they can be conjugated to a DNA strand.

1.3 Structural DNA nanotechnology

1.3.1. 2D DNA assemblies

The major challenge to achieve well-defined 2D DNA assemblies was to generate rigid branched DNA[36]. Seeman improved the rigidity of DNA structure by

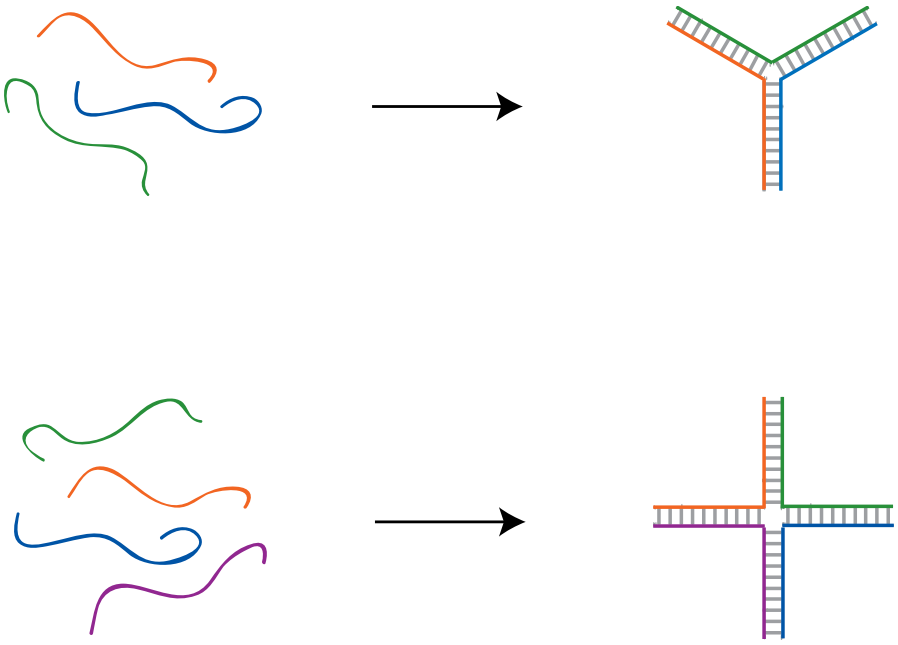

Figure 1.1. Y-shaped DNA and X-shaped DNA are synthesized by annealing temperature with three or four ssDNA, respectively. (images adapted from [33] and [34])

developing a double-crossover (DX) and triple-crossover (TX) DNA[29]. These DNA scaffolds have been applied to guide the positioning of materials in nano-precision[37, 38]. For example, Yan's group used 2D DNA lattices to array gold nanoparticles, proteins, and fluorescence dyes (Figure 1.2)[39-42]. DNA aptamers which can recognize specific proteins with specific sequences were easily anchored on a DNA lattice and thrombins were precisely arrayed on the DNA lattice by anti-thrombin aptamers[43]. Since aptamers can be found for other proteins by the systematic evolution of ligands by exponential enrichment (SELEX), the DNA lattice can easily organize any protein by aptamer-protein interaction. Mao also reported hexagonal 2D arrays with three-point-star DNA motifs[44]. Moving beyond the lattice structure, Rothemund's group significantly improved the synthesis of a variety of 2D shapes[45]. They successfully synthesized stars, smiley faces and even more complicated shapes with their DNA origami approach (Figure 1.3). Kjems's group achieved the synthesis of DNA origami dolphin-shaped structures[46]. Interestingly, these DNA dolphins can shake their tails depending on the temperature with this research group's ingenious sequence design. Thus, control of molecules or structures can be easy by employing 2D DNA structures.

1.3.2. 3D DNA assemblies

Using the various branched DNA structures including DNA tiles, 3D DNA assemblies have been reported in a variety of topologies. Seeman synthesized 3D DNA cubes[47]. This was the first construction of a closed polyhedral DNA structure. Luo's group created 3D DNA hydrogel from X-shaped DNA by T4 DNA ligation (Figure 1.4)[34]. In the work performed by this group, palindromic sticky ends were used to enhance the efficiency of liagation. Since the double stranded X-shaped DNA was less rigid than the double-crossover or triple crossover branched DNA, the resultant assembly formed 3D structures instead of 2D lattices. Although a typical

building block, or tile, is rigid, Reif and LaBean successfully synthesized DNA tube circumferences by constructing DNA lattices using a flexible and single stranded DNA motif[48]. The flexible DNA motif allowed them to precisely program the tube geometry. Most recently, Mao successfully synthesized tetrahedron, dodecahedron and buckyball DNA structures with three-point-star motifs (Figure 1.5)[49]. By controlling the flexibility and concentration of the motifs, the complicated 3D DNA structures were precisely constructed via one-pot assembly in tens of nanometer scale.

Turberfield reported 3D DNA tetrahedron which was able to change its shape in response to specific fuel single stranded DNA[50, 51]. With their biocompatibility, these 3D DNA structures have shown great potential as a drug carrier.

1.4 DNA-templated polymerization

1.4.1. DNA-templated chemical polymerization

DNA-templated polymerization of building blocks has great potential for precise control of sequence-defined polymers with structures and properties which are difficult to achieve by typical polymerization[52]. For example, the DNA-templated polymerization could be achieved by phosphoramidates[53], phosphorothioates[54], amine acylation[55, 56], and metal coordination complex formation[57, 58] (Figure 1.6). These approaches could proceed efficiently and sequence specifically by polymerization of DNA building blocks with the above chemical-based side chains at various positions. In this manner, enzyme-free DNA-templated polymerization can be efficiently performed using DNA building blocks with a wide range of side-chain structures at specific positions. Finally, the sequence-defined synthetic polymers can achieve functionalization densities.

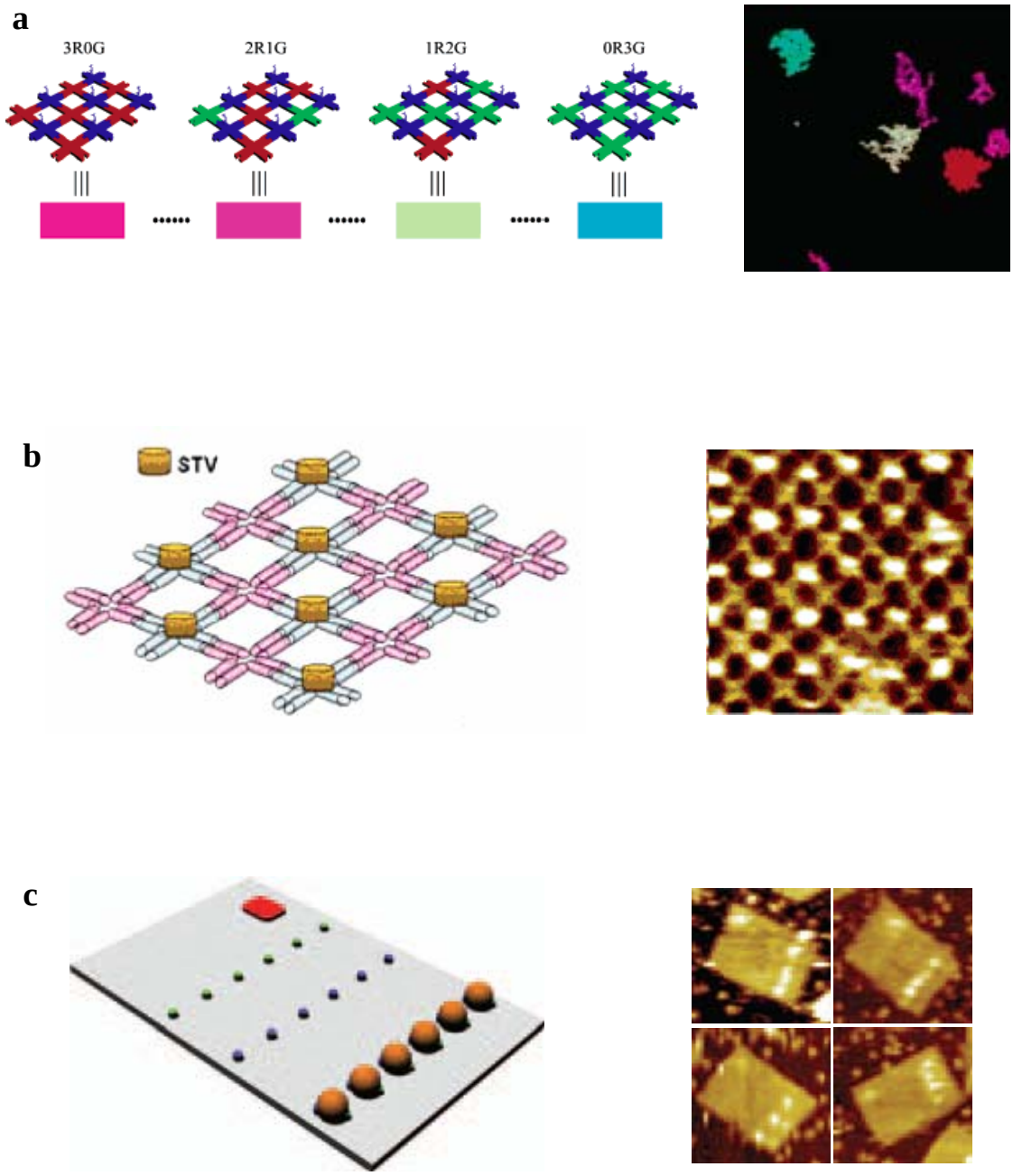

Figure 1.2. Fluorescence image of 2D DNA lattice for biosensing with fluorescence dyes (a) [39] and AFM images of 2D DNA lattices with streptavidins (b) [42] and thrombins (c) [43]. All images were adapted from the original references.

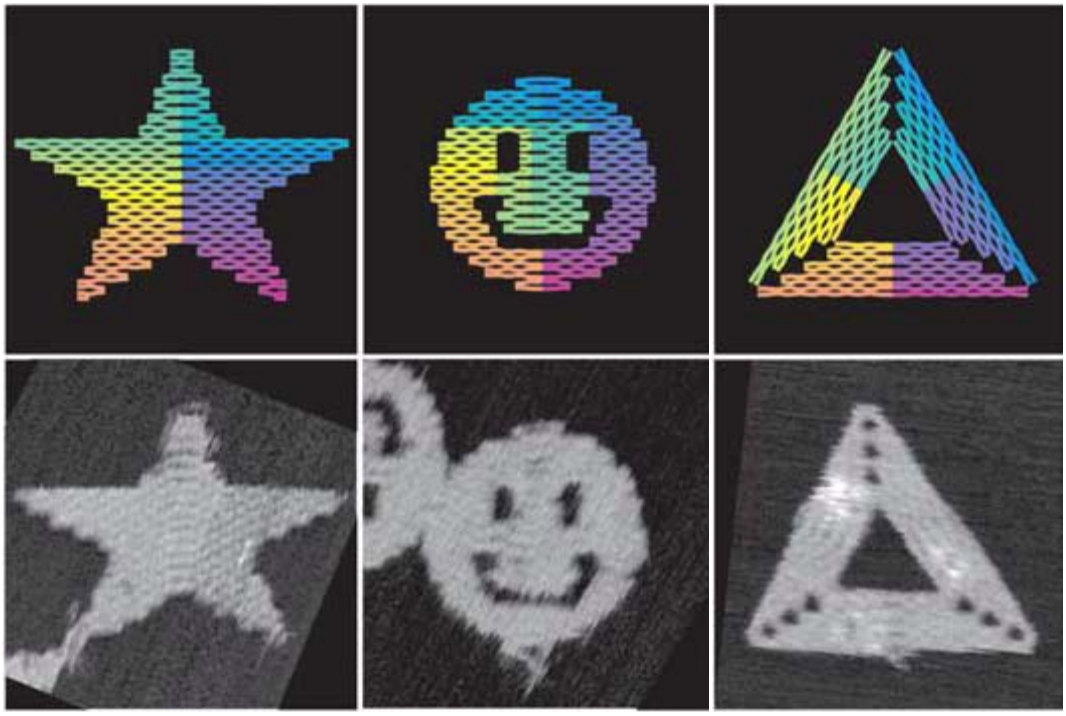

Figure 1.3. AFM images of DNA origami structures (images adapted from [45]).

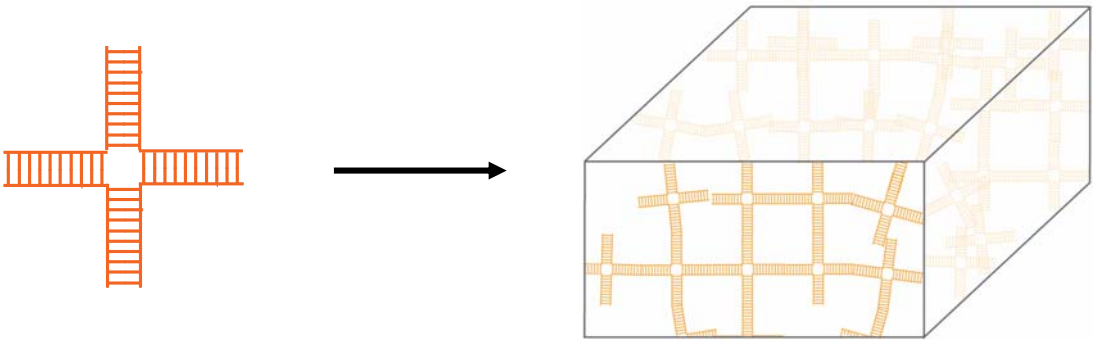

Figure 1.4. 3D DNA hydrogel from X-shaped DNA by T4 DNA ligation (image adapted from [34]).

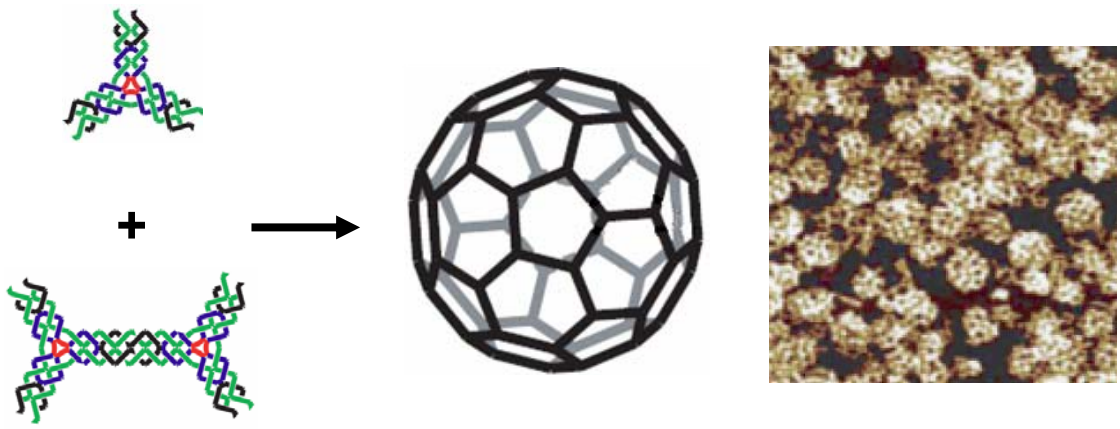

Figure 1.5. Design of DNA buckyball from three-point-star motifs and AFM image (image adapted from [49]).

1.4.2. DNA-templated enzymatic polymerization

DNA polymerizations can be done by a variety of enzymes like DNA polymerases and DNA ligases. The resultant DNA polymers were formed by creating a chain of repeated DNA monomers. Mao reported a strategy of enzymatic DNA polymerization by combination of DNA ligase and restriction endonuclease[59]. This paper showed that a polymerase was replaced by the combination of T4 DNA ligase and Bgl I restriction enzyme. T4 DNA ligase was used to link a DNA monomer to a growing chain and the Bg1 restriction enzyme was used to cut specific sequences of the DNA monomer and regenerate sticky ends which could be ligased with the next DNA monomer.

Rolling circle amplification (RCA) is another elegant method to polymerize DNA strands with a repeating sequence motif[60]. In this method, a single-stranded circular DNA is used as a template for a DNA polymerase. The polymerase produces complimentary copies of the circular DNA template. After one turn of polymerization, the polymerase continues to copy the template sequence with exceptional displacement of the earlier complimentary strands from the circular DNA template (Figure 1.7). This RCA approach has been applied on solid surfaces like gold nanoparticles[61] and microgels[62], resulting in DNA-templated polymer.

1.4.3. DNA-templated polymerization by hybridization chain reaction

Unlike typical DNA-templated polymerization, Pierce showed that polymerization could be achieved exclusively using the free energy of DNA hybridization without other additional synthetic methods[63]. In this article, metastable DNA hairpins were non-covalently polymerized by hybridization chain reaction when the hairpins encountered a target molecule.

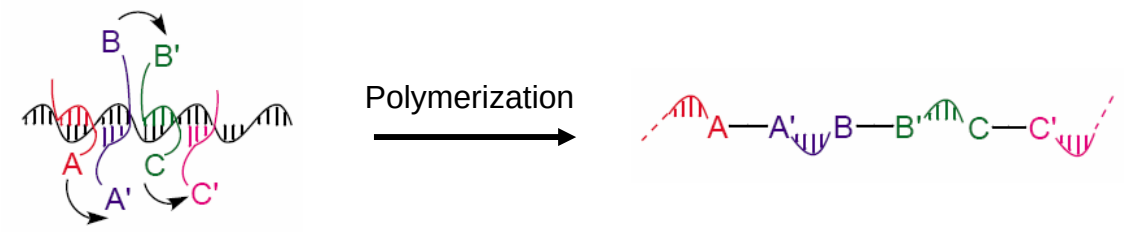

Figure 1.6. Nonenzymatic DNA-templated polymerization by recognizing the encoding DNA template before polymerization (image adapted from [52]).

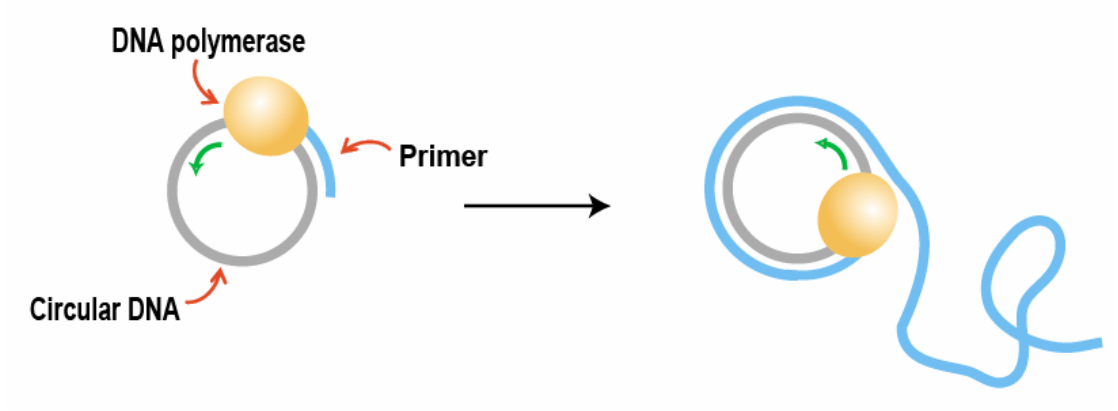

Figure 1.7. DNA-templated polymerization by rolling circle amplification (image adapted from [60]).

1.5 Significance of this dissertation

DNA's excellent programmability has allowed the building up of artificially engineered supramolecular structures and networks. A variety of approaches have been reported for synthesizing DNA-based structures and networks. However, there is lack of understanding about the stability and ways to employ controllability and multivalency to DNA-based structures or networks. The second chapter in this dissertation addresses the stability of DNA-based structures from simple branched DNA (Y- and X-DNA) to DNA hydrogel. In addition, the second chapter demonstrates the effect of junctions on the stability of DNA structures. The third chapter introduces a general approach to synthesizing multifunctional nanoarchitectures including nanoparticle-based DNA nanobarcodes based on the multivalancey and controllability of DNA structures. The chapter also introduces a new method to detect pathogen DNA by target-driven polymerization. The precise control of DNA assembly is also achieved through various enzymatic tools. The fourth chapter describes the new concept of DNA hydrogels synthesized by polymerase with repeated DNA sequences.

REFERENCE

1. Seeman, N.C. Nucleic acid junctions and lattices. J Theor Biol 99, 237-247 (1982).
2. Seeman, N.C. DNA nanotechnology: Novel DNA constructions. Annual Review of Biophysics and Biomolecular Structure 27, 225-248 (1998).
3. Fu, T.J. & Seeman, N.C. DNA double-crossover molecules. Biochemistry 32, 3211-3220 (1993).
4. Marky, L.A., Mcdonough, K.A., Kallenbach, N.R., Breslauer, K.J. & Seeman, N.C. Thermodynamics of a Nucleic-Acid Junction. Biophysical Journal 49, A49-A49 (1986).
5. Niemeyer, C.M., Boldt, L., Ceyhan, B. & Blohm, D. DNA-directed immobilization: Efficient, reversible, and site- selective surface binding of proteins by means of covalent DNA- streptavidin conjugates. Analytical Biochemistry 268, 54-63 (1999).
6. Xia, T. et al. Thermodynamic parameters for an expanded nearest-neighbor model for formation of RNA duplexes with Watson-Crick base pairs. Biochemistry 37, 14719-14735 (1998).
7. Bommarito, S., Peyret, N. & SantaLucia, J., Jr. Thermodynamic parameters for DNA sequences with dangling ends. Nucleic Acids Res 28, 1929-1934 (2000).
8. Peyret, N., Seneviratne, P.A., Allawi, H.T. & SantaLucia, J., Jr. Nearest-neighbor thermodynamics and NMR of DNA sequences with internal A.A, C.C, G.G, and T.T mismatches. Biochemistry 38, 3468-3477 (1999).
9. Allawi, H.T. & SantaLucia, J., Jr. Nearest neighbor thermodynamic parameters for internal G.A mismatches in DNA. Biochemistry 37, 2170-2179 (1998).

10. Smith, S.B., Cui, Y. & Bustamante, C. Overstretching B-DNA: the elastic response of individual double-stranded and single-stranded DNA molecules. Science 271, 795-799 (1996).
11. Vologodskaia, M. & Vologodskii, A. Contribution of the intrinsic curvature to measured DNA persistence length. J Mol Biol 317, 205-213 (2002).
12. Seeman, N.C. & Kallenbach, N.R. Design of immobile nucleic acid junctions. Biophys J 44, 201-209 (1983).
13. Luo, D. The road from biology to materials. Materials Today 6, 38-43 (2003).
14. Luo, D. in Handbook of Nanostructured Biomaterials and Their Applications, Vol. (invited author). (ed. H.S. Nalwa) (Academic Press, San Diego, 2004).
15. Glotzer, S.C. & Solomon, M.J. Anisotropy of building blocks and their assembly into complex structures. Nature Materials 6, 557-562 (2007).
16. Pol, S.V., Pol, V.G., Calderon-Moreno, J.M., Cheylan, S. & Gedanken, A. Facile synthesis of photoluminescent ZnS and ZnSe nanopowders. Langmuir 24, 10462-10466 (2008).
17. Danovitch, G.M., Cohen, B. & Smits, J.M. Waiting time or wasted time? The case for using time on dialysis to determine waiting time in the allocation of cadaveric kidneys. Am J Transplant 2, 891-893 (2002).
18. Mohamed, M.B., Tonti, D., Salman, A.A. & Chergui, M. Chemical synthesis and optical properties of size-selected CdSe tetrapod-shaped nanocrystals. Chemphyschem 6, 2505-2507 (2005).
19. Chen, S., Wang, Z.L., Ballato, J., Foulger, S.H. & Carroll, D.L. Monopod, bipod, tripod, and tetrapod gold nanocrystals. Journal of the American Chemical Society 125, 16186-16187 (2003).

20. Lee, S.M., Jun, Y.W., Cho, S.N. & Cheon, J. Single-crystalline star-shaped nanocrystals and their evolution: programming the geometry of nano-building blocks. Journal of the American Chemical Society 124, 11244-11245 (2002).

21. Tang, Z., Wang, Y., Shanbhag, S., Giersig, M. & Kotov, N.A. Spontaneous transformation of CdTe nanoparticles into angled Te nanocrystals: from particles and rods to checkmarks, X-marks, and other unusual shapes. Journal of the American Chemical Society 128, 6730-6736 (2006).

22. Mann, S., Shenton, W., Li, M., Connolly, S. & Fitzmaurice, D. Biologically programmed nanoparticle assembly. Advanced Materials 12, 147-150 (2000).

23. Alivisatos, A.P. et al. Organization of 'nanocrystal molecules' using DNA. Nature 382, 609-611 (1996).

24. Fu, A. et al. Discrete nanostructures of quantum dots/Au with DNA. Journal of the American Chemical Society 126, 10832-10833 (2004).

25. Loweth, C.J., Caldwell, W.B., Peng, X.G., Alivisatos, A.P. & Schultz, P.G. DNA-based assembly of gold nanocrystals. Angewandte Chemie-International Edition 38, 1808-1812 (1999).

26. Mirkin, C.A., Letsinger, R.L., Mucic, R.C. & Storhoff, J.J. A DNA-based method for rationally assembling nanoparticles into macroscopic materials. Nature 382, 607-609 (1996).

27. Elghanian, R., Storhoff, J.J., Mucic, R.C., Letsinger, R.L. & Mirkin, C.A. Selective colorimetric detection of polynucleotides based on the distance-dependent optical properties of gold nanoparticles. Science 277, 1078-1081. (1997).

28. Sun, W., Mao, C., Liu, F. & Seeman, N.C. Sequence dependence of branch migratory minima. J Mol Biol 282, 59-70 (1998).

29. Seeman, N.C. DNA in a material world. Nature 421, 427-431 (2003).

30. Chhabra, R., Sharma, J., Liu, Y. & Yan, H. Addressable molecular tweezers for DNA-templated coupling reactions. Nano Lett 6, 978-983 (2006).
31. Seeman, N.C. De novo design of sequences for nucleic acid structural engineering. J Biomol Struct Dyn 8, 573-581 (1990).
32. Barish, R.D., Rothemund, P.W. & Winfree, E. Two computational primitives for algorithmic self-assembly: copying and counting. Nano Lett 5, 2586-2592 (2005).
33. Li, Y. et al. Controlled assembly of dendrimer-like DNA. Nature Materials 3, 38-42 (2004).
34. Um, S.H. et al. Enzyme-catalysed assembly of DNA hydrogel. Nature Materials 5, 797-801 (2006).
35. Um, S., Lee, J., Kwon, S., Li, Y. & Luo, D. Dendrimer-Like DNA (DL-DNA) Based Fluorescence Nanobarcodes. Nature Protocols 1, 995-1000 (2006).
36. Aldaye, F.A., Palmer, A.L. & Sleiman, H.F. Assembling materials with DNA as the guide. Science 321, 1795-1799 (2008).
37. Pinto, Y.Y. et al. Sequence-encoded self-assembly of multiple-nanocomponent arrays by 2D DNA scaffolding. Nano Lett 5, 2399-2402 (2005).
38. Zheng, J. et al. Two-dimensional nanoparticle arrays show the organizational power of robust DNA motifs. Nano Lett 6, 1502-1504 (2006).
39. Lin, C., Liu, Y. & Yan, H. Self-assembled combinatorial encoding nanoarrays for multiplexed biosensing. Nano Lett 7, 507-512 (2007).
40. Lund, K., Liu, Y., Lindsay, S. & Yan, H. Self-assembling a molecular pegboard. Journal of the American Chemical Society 127, 17606-17607 (2005).
41. Liu, Y., Ke, Y. & Yan, H. Self-assembly of symmetric finite-size DNA nanoarrays. Journal of the American Chemical Society 127, 17140-17141 (2005).

42. Park, S.H. et al. Programmable DNA self-assemblies for nanoscale organization of ligands and proteins. Nano Lett 5, 729-733 (2005).

43. Rinker, S., Ke, Y., Liu, Y., Chhabra, R. & Yan, H. Self-assembled DNA nanostructures for distance-dependent multivalent ligand-protein binding. Nat Nanotechnol 3, 418-422 (2008).

44. He, Y., Chen, Y., Liu, H., Ribbe, A.E. & Mao, C. Self-assembly of hexagonal DNA two-dimensional (2D) arrays. Journal of the American Chemical Society 127, 12202-12203 (2005).

45. Rothemund, P.W. Folding DNA to create nanoscale shapes and patterns. Nature 440, 297-302 (2006).

46. Kamens, J.S., Ratnofsky, S.E. & Hirst, G.C. Lck inhibitors as a therapeutic approach to autoimmune disease and transplant rejection. Curr Opin Investig Drugs 2, 1213-1219 (2001).

47. Ebbe, S.A., Mingdong, D., Morten, M.N., Kasper, J., Allan, L., Wael, M., Kurt, V. G., Flemming, B., Jørgen, K. DNA Origami Design of Dolphin-Shaped Structures with Flexible Tails. ACS Nano 2, 1213-1218 (2008)

48. Yin, P. et al. Programming DNA tube circumferences. Science 321, 824-826 (2008).

49. He, Y. et al. Hierarchical self-assembly of DNA into symmetric supramolecular polyhedra. Nature 452, 198-201 (2008).

50. Goodman, R.P. et al. Rapid chiral assembly of rigid DNA building blocks for molecular nanofabrication. Science 310, 1661-1665 (2005).

51. Goodman, R.P. et al. Reconfigurable, braced, three-dimensional DNA nanostructures. Nat Nanotechnol 3, 93-96 (2008).

52. Li, X. & Liu, D.R. DNA-templated organic synthesis: nature's strategy for controlling chemical reactivity applied to synthetic molecules. Angewandte Chemie (International ed 43, 4848-4870 (2004).

53. Luther, A., Brandsch, R. & von Kiedrowski, G. Surface-promoted replication and exponential amplification of DNA analogues. Nature 396, 245-248 (1998).

54. Xu, Y., Karalkar, N.B. & Kool, E.T. Nonenzymatic autoligation in direct three-color detection of RNA and DNA point mutations. Nature biotechnology 19, 148-152 (2001).

55. Gartner, Z.J., Grubina, R., Calderone, C.T. & Liu, D.R. Two enabling architectures for DNA-templated organic synthesis. Angewandte Chemie (International ed 42, 1370-1375 (2003).

56. Gartner, Z.J. & Liu, D.R. The generality of DNA-templated synthesis as a basis for evolving non-natural small molecules. Journal of the American Chemical Society 123, 6961-6963 (2001).

57. Park, S.Y., Gibbs-Davis, J.M., Nguyen, S.T. & Schatz, G.C. Sharp melting in DNA-linked nanostructure systems: thermodynamic models of DNA-linked polymers. The journal of physical chemistry 111, 8785-8791 (2007).

58. Calderone, C.T. & Liu, D.R. Nucleic-acid-templated synthesis as a model system for ancient translation. Current opinion in chemical biology 8, 645-653 (2004).

59. Tian, Y. & Mao, C. Template-free, polymerase-free DNA polymerization. Chemical communications (Cambridge, England), 2669-2671 (2005).

60. Beyer, S., Nickels, P. & Simmel, F.C. Periodic DNA nanotemplates synthesized by rolling circle amplification. Nano Lett 5, 719-722 (2005).

61. Zhao, W., Gao, Y., Kandadai, S.A., Brook, M.A. & Li, Y. DNA polymerization on gold nanoparticles through rolling circle amplification:

towards novel scaffolds for three-dimensional periodic nanoassemblies. Angewandte Chemie (International ed 45, 2409-2413 (2006).

62. Ali, M.M., Su, S., Filipe, C.D., Pelton, R. & Li, Y. Enzymatic manipulations of DNA oligonucleotides on microgel: towards development of DNA-microgel bioassays. Chemical communications (Cambridge, England), 4459-4461 (2007).

63. Venkataraman, S., Dirks, R.M., Rothemund, P.W., Winfree, E. & Pierce, N.A. An autonomous polymerization motor powered by DNA hybridization. Nat Nanotechnol 2, 490-494 (2007).

CHAPTER 2

Study of the thermal stability of DNA nanostructures

Jong B. Lee, Adam S. Shai, Michael J. Campolongo, Nokyoung Park, Dan Luo*

"Study of the thermal stability of DNA nanostructures". Submitted (2009).

Department of Biological & Environmental Engineering, Cornell University, Ithaca, NY 14850, USA

2.1 Abstract

DNA nanostructures have been attracting much attention because of their well-controlled nanoarchitectural features. However, regulating the stability of DNA nanostructures is less well understood because of complexity. In this chapter, the stability of Y- and X-shaped DNA was studied first in the form of simple building blocks. Since these DNA building blocks have junctions on the center of the structures, the junctions were mainly investigated as a factor in the instability. In addition, regulation of the stability of complicated nanostructures based on these building blocks was achieved. Förster resonance energy transfer (FRET) and nanosurface energy transfer (NSET) methods were employed to monitor the conformation change with nano-scale sensitivity. The junction effect on dendrimer-like DNA (DL-DNA) was monitored with labeling FRET pairs at various positions. DNA hydrogel was also thoroughly studied with various types of FRET pair labeled X-DNA.

2.2 Introduction

Nucleic acids have received much attention as nanoscale building materials because of their sequence-specific programmability and their compatibility with other biological molecules[1, 2]. Inspired by branched junctions that exist transiently in cells, a variety of branched DNA motifs have been engineered, enabling bottom-up assembly of highly ordered nanostructures[3, 4]. Controlled design of branched DNA has facilitated the formation of lattices[5-9] and nanotubes[10-13], which have served as scaffolds for periodic arrays of nanoparticles and proteins. In addition, highly complex honeycomb[14, 15] and buckyball[16, 17] structures, which require delicate tuning of the mechanical properties, have been demonstrated. To this end, consideration must be given to conformational flexibility and stability. DNA junctions govern the flexibility

of the structure as well as the stability. Therefore, thorough investigations of DNA junctions are necessary for engineering stable DNA nanostructures.

Numerous characterization techniques have already been utilized to study the properties of simple three- and four-way DNA junctions. The conformation of engineered DNA containing one three-way junction (Y-DNA), the simplest branched DNA molecule, has been investigated with NMR to study the destabilization by unpaired bases[18]. Four-way Holliday junctions (X-DNA), one of the major building blocks for DNA nanostructures, have been extensively studied using X-ray[19], UV absorption[20], and fluorescence methodologies[21-24]. In addition to spectroscopic methods, direct monitoring of the geometry and dynamics of three-way junctions has been achieved with atomic force microscopy (AFM)[25]. Optical tweezers have been used to successfully observe dynamic structural changes caused by metal ions and enzymatic forces[24, 26]. Although simple three- and four-way junctions have been successfully investigated, more complex DNA nanostructures containing multiple junctions, blunt ends, sticky ends, loops, and bulges have not been studied as thoroughly. In particular, it is not well understood how multiple junctions, which are necessary for the construction of complex DNA nanostructures, affect the stability of the overall structure. Therefore, direct monitoring of denaturation at specific positions close to and far from the junctions is of great importance. However, traditional spectroscopic techniques based on UV measurement are not location specific.

Förster resonance energy transfer is a unique way to monitor denaturation at specific positions of interest on DNA motifs. FRET has been applied to observe the conformational change of DNA because of the high sensitivity to the change of distance between donor and acceptor[27-32]. In addition, nanosurface energy transfer (NSET) has been used as an optical ruler to measure DNA distance with extended detectable distance[33-35]. FRET and NSET are efficient for separation distances 1-

10nm and 5-25nm, respectively[36, 37]. Both methods allow for distance information during conformational change to be calculated. Applying these two methods enables sensitive study of the effect of multiple junctions within DNA nanostructures. As the first step in understanding the stability of complex nanostructures, we focus our study on the effects of multiple junctions on thermal stability. Here, we report thermal behavior of diverse DNA nanostructures and the effect of junctions on the stability of these structures studied by nanometer resolution monitoring with FRET and NSET methods. The distance as a function of temperature at a particular region was calculated by converting the fluorescence intensity to the distance between FRET pairs. In particular, denaturation distance was measured for both dendrimer-like DNA (DL-DNA)[38], which consists of four junctions, and macroscopic DNA hydrogel[39], which was assembled from X-DNA building blocks while gradually increasing temperature.

2.3 Materials and Methods

2.3.1. Synthesis of DNA nanostructures

2.3.1.1. Synthesis of Y-DNA and X-DNA

Y-DN and X-DNA were fabricated according to previously published methods from our group[38, 39]. The Y-DNA was synthesized by mixing the equal molar amount of three corresponding oligonucleotide strands whose nomenclature is as follows: Y_{01}, Y_{02} and Y_{03}. Hybridization was performed by heating the mixture at 95°C for 2min and then cooling it to desired temperature by the following protocol: 2 min at 65°C, 5 min 60°C, 30 sec of incubation every -1°C decrease from 60°C to 20°C. The resultant solution was then held at 4°C. Similarly, the four corresponding single oligonucleotides, X_{01}, X_{02}, X_{03} and X_{04}, were mixed and then annealed by the above annealing protocol to form an X-DNA. To form FRET or NSET pair tagged Y- or X-DNA, commercially synthesized Alexa488, dabcyl, or thiol tagged oligonucleotide

strands were used instead of one of the oligonucleotides. All strands including modified strands were purchased from IDT (Integrated DNA Technologies, Coralville, Iowa).

2.3.1.2. Conjugation of gold nanoparticles on Y-DNA and X-DNA

For labeling 1.4nm gold nanoparticles (AuNP) on the thiol-modified DNA nanostructures, thiol modified oligonucleotide strands were first deprotected with dithiothreitol (DTT) according to literature procedures[31]. The deprotected strands were then assembled with Alexa488 tagged strands to form NSET pairs tagged Y- and X-DNA. Monomaleimido-modified 1.4nm gold nanoprticles, which was purchased from Nanoprobes (Yaphank, NY), was incubated with the deprotected thiol modified Y- or X-DNA overnight at 4ºC.

2.3.1.3. Synthesis of FRET pair labeled Dendrimer-like DNA

A dendrimer-like DNA (DL-DNA) was assembled with four Y-DNA by the complementary sticky ends using T4 DNA ligase (Promega, Madison, WI) according to literature procedures[38]. The positions of FRET pairs on the DL-DNA were determined by controlling sticky ends and position of FRET pairs on Y-DNA (Figrue 2.1a). DL-DNA were separately labeled with a FRET pair at one of four different positions [end (E), junction1 (J1), junction2 (J2), and middle (M) of DNA nanostructures] (Figrue 2.1b).

2.3.1.4. Synthesis of FRET pair labeled DNA hydrogel

Similar to DL-DNA, DNA hydrogel was also enzymatically assembled with X-DNA using T4 DNA ligase[39]. By labeling a FRET pair on the junction of each X-DNA, four palindromic sticky ends of X-DNA were used to be ligased (Figure 2.1c).

2.3.2. Melting temperature (T_m) measurement

Thermal denaturizing transitions were monitored to evaluate the stability of the DNA nanostructures using by an SLM model 8000 fluorescence spectrometer (SLM Instruments, Inc.). The pairs of fluorescence dye and dabcyl or fluorescence dye and gold nanoparticle labeled DNA nanostructures were denatured by heating every 0.5°C / 30sec. Thermal denaturation of DNA nanostructures were monitored by the fluorescence intensity changes at 530nm (for Alexa 488, an excitation wavelength of 488nm and emission wavelength of 530nm were used).

2.3.3. Distance calculations from melting transition

Distances were calculated from $R = R_0 [F_{DA}/(F_D-F_{DA})]^{1/6}$, where R_0 is the Förster radius corresponding to 50% energy transfer efficiency, and R is the distance between the donor and the acceptor. The fluorescence intensities, F_D and $F_{DA,}$ are experimentally determined from the melting transition of each sample.

2.3.4. Gel electrophoresis

DNA nanostructures were run in a 3% agarose gel at 90V at 25°C in Tris-acetate-EDTA (TAE) buffer (40nM Tris, 20nM acetic acid and 1mM EDTA, pH 8.0, Bio-Rad). The fluorescence gel image was taken using a digital camera under UV illumination. The gel was then stained with 0.5 μg/ml of ethidium bromide in TAE buffer.

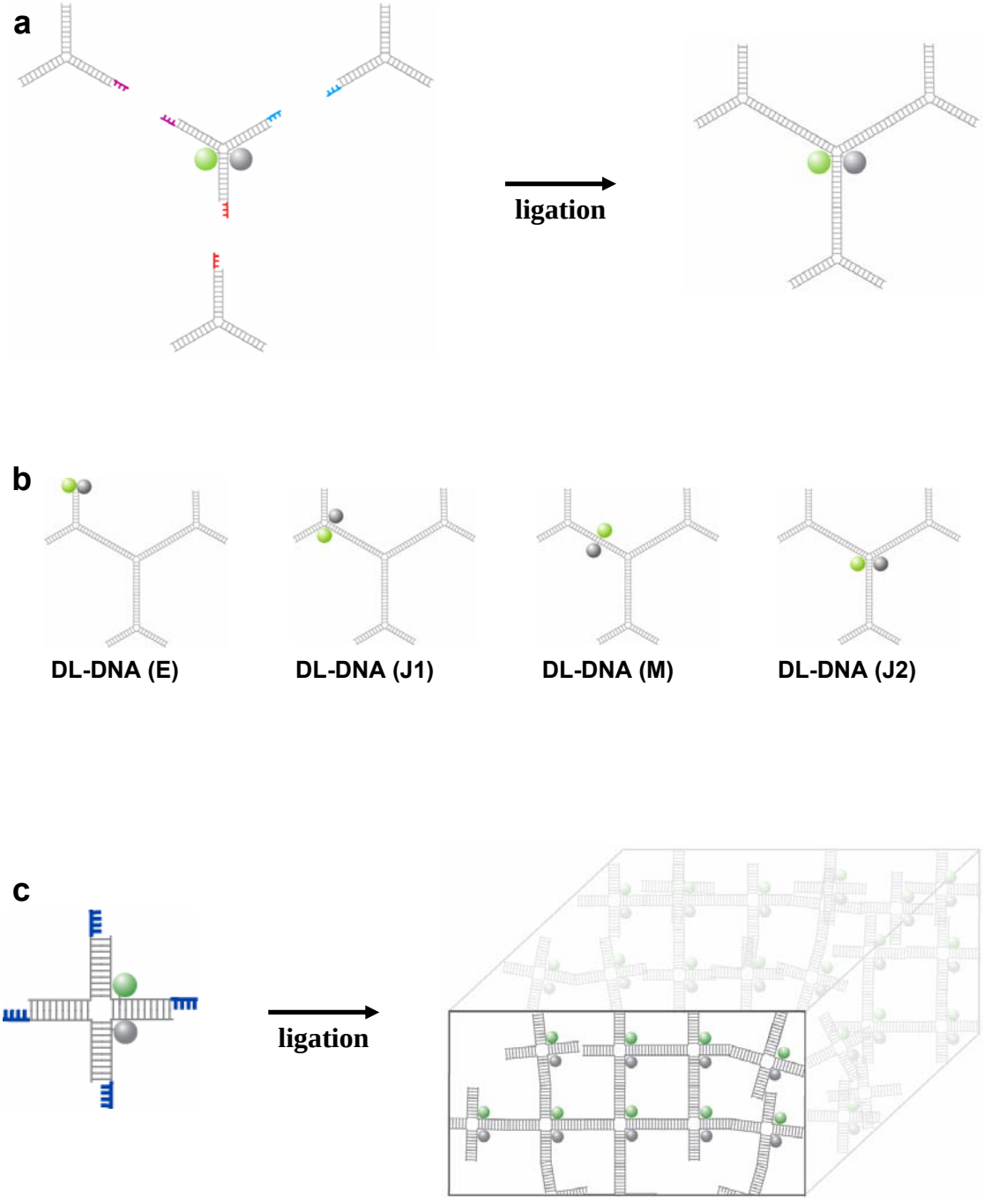

Figure 2.1. Schematic drawing of FRET pair labeled dendrimer-like DNA and DNA hydrogel.

2.4 Results and Discussions

2.4.1 Design the strategy for denaturation studies

FRET was used to monitor thermal response at specific locations within the DNA nanostructure. Specific base pairs on the DNA nanostructure were labeled with a donor, Alexa488, and an acceptor, Dabcyl. When in close proximity, energy transfer between FRET pairs prevents emission of fluorescence from the donor. As the labeled bases separate with increasing temperature, less energy transfer occurs between the donor and acceptor, resulting in an increase in fluorescence intensity (as shown in Figure 2.2). Hence, direct monitoring of the fluorescence intensity translates to the relative distance between the two bases. The FRET efficiency is given by

$$E_{FRET} = 1 - F_{DA}/F_D \quad (1)$$

where F_{DA} is the fluorescence intensity measured when the donor-acceptor pair are within proximity, and F_D is the maximum intensity corresponding to complete separation. FRET efficiency can also be expressed as a function of the relative donor-to-acceptor separation

$$E_{FRET} = 1/[1+(R/R_0)^6] \quad (2)$$

where R is the donor-to-acceptor distance, R_0 is the Förster distance, which was determined to be 49Å for the Alexa488 and Dabcyl pair. The relationship between distance and fluorescence can be obtained from Eqs. (1) and (2):

$$R = R_0 [F_{DA}/(F_D-F_{DA})]^{1/6} \quad (3)$$

In this strategy, the red dot and the light purple dash line in scheme 1 are taken as F_D and F_{DA}, respectively.

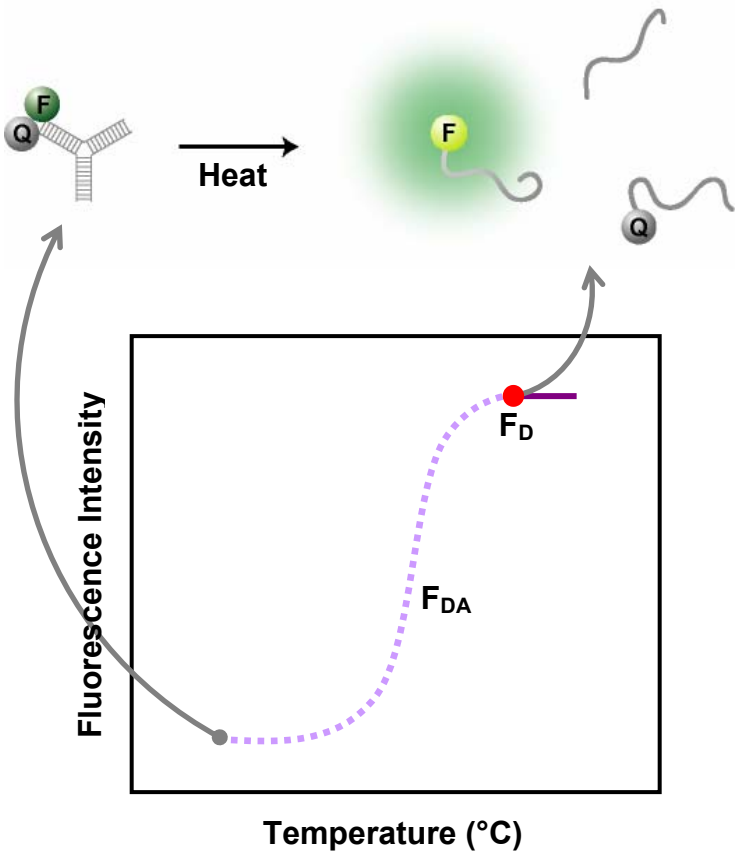

Figure 2.2. Schematic drawing of thermal denature of DNA nanostructure with FRET. Where F is the relative donor fluorescence intensity in the absence (F_D) and presence (F_{DA}) of the acceptor. Here, when an increase in temperature no longer results in an increase in fluorescence, the relative fluorescence can be taken as F_D (red dot) because the denatured distance between donor and acceptor does not allow for any energy transfer. The relative fluorescence from when an increase in temperature begins to result in an increase in fluorescence to right before F_D can be taken as an F_{DA} (light purple dash) because the D/A pair are in their closest proximity for energy transfer.

2.4.2 Thermal denaturation of simple DNA nanostructures

Before investigating more complicated DNA nanostructures, the melting transition was monitored for Y-DNA with 39 total base pairs, Y-DNA (39). Each of the three arms was labeled with FRET pairs in order to observe the uniformity of the denaturation. Prior to the thermal denaturation experiments, gel electrophoresis was performed to verify both the formation of Y-DNA and energy transfer of FRET pairs (Figure 2.3a). Fig.1a shows the observed colors resulting from UV illumination for Y-DNA before (top) and after (bottom) staining with ethidium bromide (EtBr). Lanes 1, 3, and 5 contain Y-DNA labeled with only the donor, and lanes 2, 4, and 6 contain Y-DNA labeled with both the donor and the acceptor. Bands without an acceptor clearly fluoresce under UV light, while bands with both the donor and the acceptor are not visible due to the quenching effect of Dabcyl in close proximity to Alexa488. After EtBr staining, all six Y-DNA bands appear under UV light.

The differently labeled Y-DNA show very similar melting transitions during a steady temperature increase from 25˚C to 55˚C (Figure 2.3b). Moreover, the minimum temperatures for complete denaturation (T_{CD}) of all three Y-DNA were overlapped at 45.3˚C. This result indicates that the Y-DNA are fully denatured to single stranded DNA at this temperature. The melting temperatures of all three Y-DNA, which were determined by taking the maximum of the first derivative of each spectra, were also matched at around 43.0˚C (Figure 2.3c). From Eq. (3) the transition of distance change between donor and acceptor at each temperature was determined as shown in Figure 2.3d. The initial distance between the D/A pair was subtracted from the found distances between the D/A pair to show the real denatured distance resulting from thermal energy. As can be seen in Figure 2.3d, the denatured distances of the three Y-DNA were almost identical. Interestingly, the denatured distance of Y-DNA increased slightly to 43°C but from 43°C until full denaturation the denatured distance increased

at a rapid rate. These results indicate that most parts of Y-DNA become denatured within a range of 2°C.

2.4.3 Confirmation of the complete denaturation of DNA nanostructures by FRET and NSET measurement

Although, FRET is a very sensitive method of determining intermolecular distance due to the inverse-sixth-power separation dependency, it is limited to distances less than 100Å. Therefore, confirmation of the validity of F_D in our strategy was needed to ensure that F_D was caused by complete denaturation rather than by experimental limitations of FRET. The nanosurface energy transfer (NSET) method allows for energy transfer up to 250Å, which is much greater than the theoretical maximum base separation within the DNA nanostructures used in these studies.

For our experiment, Alexa488 and 1.4nm gold nanoparticle (AuNP) were used as the donor and acceptor pair. Since NSET consists of energy transfer from a single dipole to a metallic surface, it has an inverse fourth power distance dependence[33,34]. The efficiency of NSET is given as

$$E_{NSET} = 1/[1+(R/R_0)^4] \quad (4)$$

To confirm the complete denaturation on DNA nanostructures, Y- and X- DNA were selected here as a simple DNA nanostructure. By comparing the results of FRET and NSET of Y- and X-DNA, the temperatures at F_D were almost identical in both Y- and X-DNA at around 45°C and 52°C, respectively (Figure 2.4a and 2.4b). When total denaturation was reached, the donor and acceptor pairs move to distances apart outside the limits of both FRET and NSET techniques (at least 250Å). In other words, the FRET efficiency became zero by complete denaturation. The results confirm that these flat portions of the melting transition found by FRET methods were caused by the complete denaturation of DNA nanostructures to single stranded DNA. It was

observed that both FRET and NSET methods result in the same T_{CD}, confirming that the FRET method was sufficient for our studies (Figure 2.4).

2.4.5 Investigation of junction effect on DNA nanostructures

In order to better understand the destabilizing role of junctions, we measured melting transitions at the junctions and compared them to those acquired for the ends. In a similar fashion to the ends of Y-DNA, FRET pairs were used to label Y-DNA near the junction as well as specific locations on the arms of X-DNA. To compare the thermal denaturation at the junction and end of these DNA nanostructures in more detail, denatured distance graphs were derived from melting transitions (Figure 2.5a and 2.5b). The results show that, in both X- and Y-DNA nanostructures, the denatured distance of the junctions and ends matched very closely. However, it appeared that the middle of the X-DNA arm began to denature about 10°C later than either the junction or ends (Figure 2.5b). These results suggest that denaturation of DNA nanostructures begins from the junction and ends and then propagates inward towards the middle of each arm until the nanostructures are completely denatured. This feature, which adds to the overall structural instability, is referred to as the junction penalty. The junction penalty suggests that each arm of the DNA nanostructures is denatured like a single linear double stranded DNA (dsDNA) which denatures inwards from each end. Thus, this junction in the center greatly influences the stability of DNA nanostructures.

To obtain more insight into the junction effect, measuring melting temperature of various DNA nanostructures was carried out. As can be seen in Figure 2.6, T_m of Y-DNA(39), which had three 13bp arms, was about 3°C higher than a single 13bp linear DNA, although the entire Y-DNA structure consisted of a total of 39bp. For

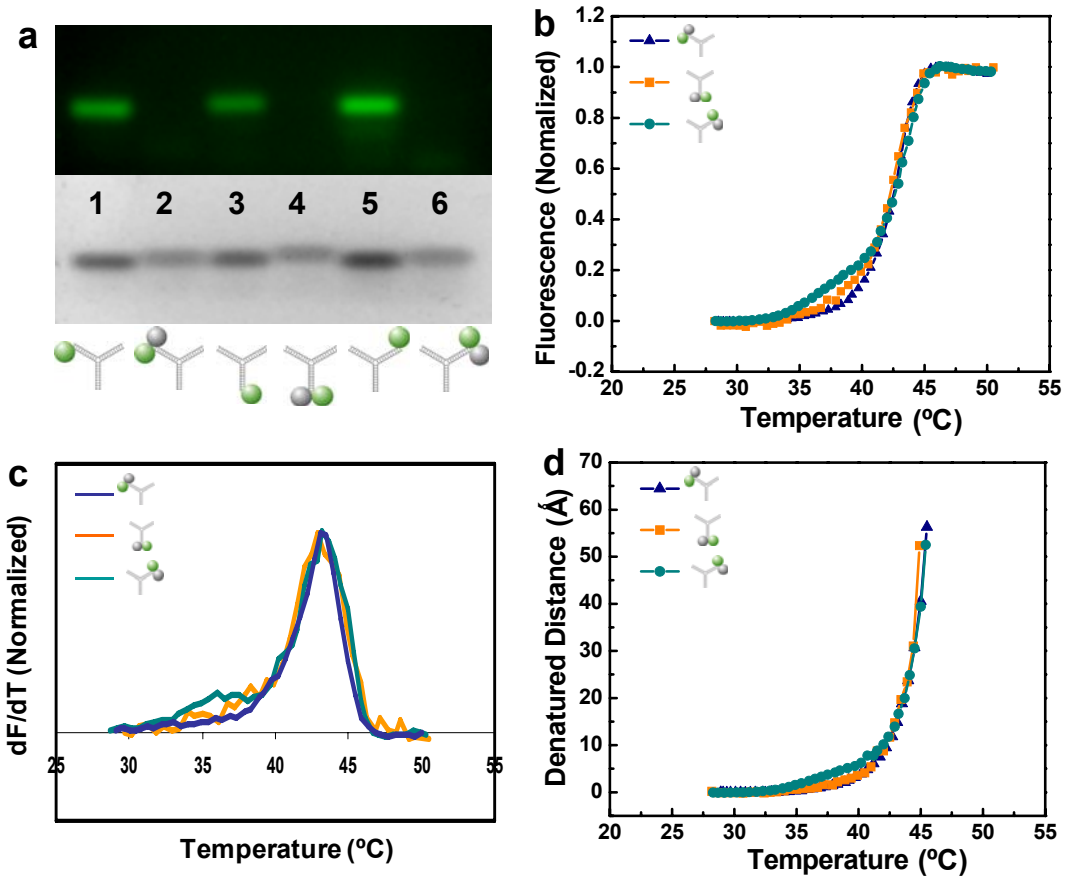

Figure 2.3. Gel electrophoresis image of Y-DNA with different position labeling with fluorescence and EB staining under UV light (a), normalized melting transition (b), normalized derivative curve (c) and thermally denatured distance of Y-DNA (d).

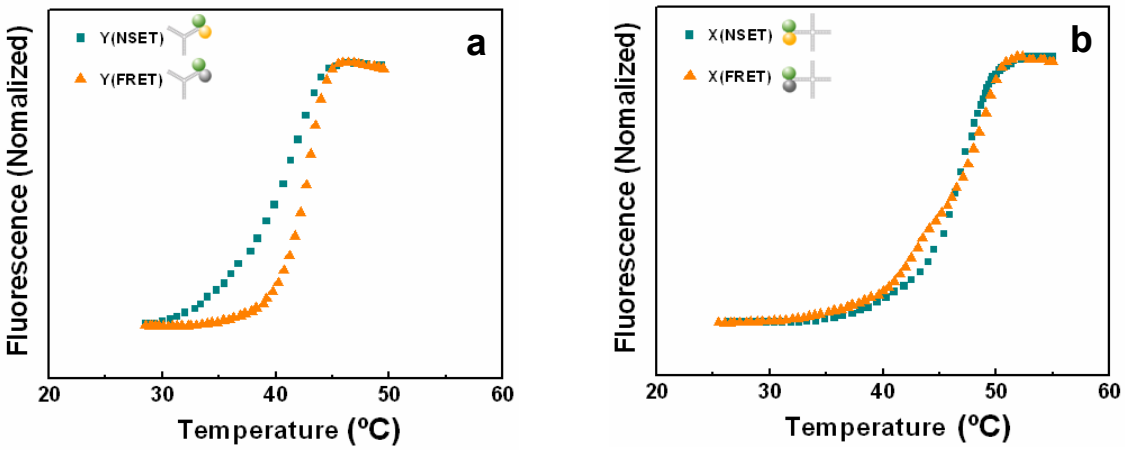

Figure 2.4. Normalized melting transition measured with Alexa488 and AuNP pair (NSET) of Y-DNA (a) and X-DNA (b).

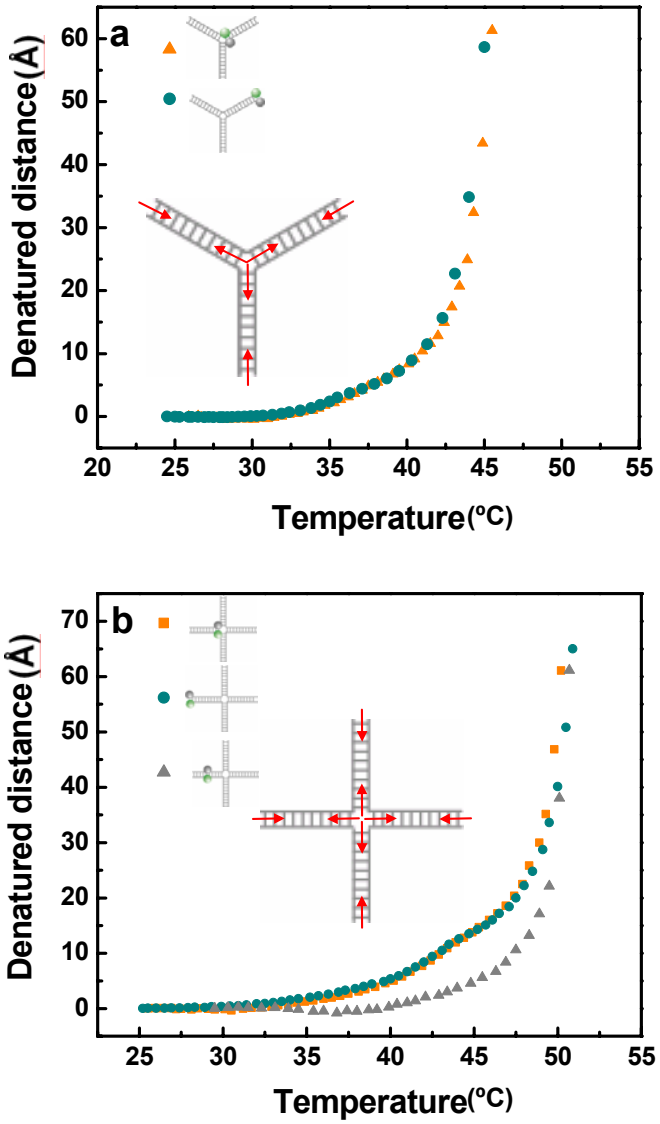

Figure 2.5. Thermally denatured distance of Y-DNA (a) and X-DNA (b) with Alexa488 and Dabcyl labeling on the junction (■), end (●), and middle of arm (▲). The red arrows indicate the direction of denature.

comparison, Y-DNA(39) was observed to denature at a temperature 27°C lower than 40bp linear DNA. Additionally, Y-DNA(54) and X-DNA(72), which had three and four 18bp arms, respectively, showed only a 4°C difference between T_m. Also, T_m of Y-DNA(54) was about 2°C higher than a single 18bp linear DNA. These results show that individual arms of DNA nanostructures behave similarly to their linear DNA analogs, suggesting that the junction has an isolating effect on the branched arms.

2.4.6 Determination of thermodynamic parameters for DNA nanostructures

To determine the thermal stability of branched DNA experimentally, thermodynamic information was derived from the concentration dependence of melting transitions. The thermodynamic data provides the stability, free energy ($\Delta G°$), and thermal melting behavior, enthalpy ($\Delta H°$), of samples. The relationship between $1/T_m$ and $\ln C_T$ were plotted using melting temperatures found in the manner previously used and varying concentration in experiments. The following equation was derived by Marky and Breslauer[40].

$$1/T_m = [(n-1)R/\Delta H°]\ln C_T + [\Delta S° - (n-1)R\ln 2n]/\Delta H° \quad (5)$$

where T_m is the melting temperature, n is molecularity, R is the gas constant, and C_T is the total concentration; the equation describes the linear relation of $1/T_m$ and $\ln C_T$. Plotting data and finding a best fit linear model allow the calculation of parameters for $\Delta H°$, $\Delta S°$, and then $\Delta G°$ using the familiar equation:

$$\Delta G° = \Delta H° - T\Delta S° \quad (6)$$

Molecularity of Y- and X-DNA is 3 and 4 respectively because Y-DNA consists of three ssDNA and X-DNA consists of four ssDNA. When the individual strands in a random coil state form into a branched DNA, a negative change in free energy is expected because branched DNA spontaneously forms at a certain temperature. A negative change in enthalpy is also expected because of base pairing.

The change in entropy is also expected to be negative since forming a nanostructure is a transition to a more ordered system. Figure 2.7 shows the $1/T_m$ versus $\ln C_T$ relation for Y- and X-DNA from the experiments along with best fit linear models. The slopes and intercepts of these lines were used to calculate $\Delta S°$ and $\Delta H°$ from the experimentally-determined concentration-dependent melting data, $\Delta G°$ was calculated using eq(6) at T=298K. These thermodynamic paremeters are provided in Table 1. The free energy values of linear DNA were predicted via mFold software developed by Rensselaer Polytechnic Institute (RPI) and compared with the experimentally determined values of branched DNA given in Table 1. $\Delta G°_{exp}$ (298K) of Y-DNA, which was composed of 39bp, was -44.2 kcal/mol but $\Delta G°_{pred}$ (298K) of 39bp linear DNA was -81.5 kcal/mol. $\Delta G°_{exp}$ (298K) of 72bp X-DNA was -93.9 kcal/mol but $\Delta G°_{pred}$ (298K) of 72bp linear DNA was -145.6 kcal/mol. Branched DNA in the experimentally-derived free energy is less stable than the predicted value of the same base paired linear DNA because of instability factors like the junction penalty. In addition, linear DNA has only two ends, while branched DNA has more ends, result in depending on the number of arms and junctions, which cause unstable structures. These instability factors account for the fact that Y- and X-DNA were approximately 37.3 kcal/mol and 51.7 kcal/mol less stable than linear DNA, respectively.

2.4.7 Thermal denaturation of dendrimer-like DNA

To explore the melting behavior of more complex DNA nanostructures, we investigated DL-DNA which consisted of four Y-DNA (39). Figure 2.8 shows the denatured distance from melting transitions of DL-DNA with four different FRET pair labelings. DL-DNA(E), which had the FRET pair at the end (Figure 2.1b), was denatured at a much lower temperature than the other locations. Interestingly, the melting behavior of DL-DNA(E) followed a melting transition that is nearly identical

to the one observed for Y-DNA(39). The outer ssDNA was denatured first due to limited interaction with the inner stem of DNA dendrimer structure (inset of Figure 2.8). At the temperatures higher than 45°C, the regions between E and J1 remain as ssDNA overhangs. Further denaturation did not occur until 60°C. At about 60°C, positions (J1) and (J2) began to separate prior to (M), displaying the same inward propagation that was observed for the arms of X-DNA. We believe that the shoulder observed on the (J1) curve between 60°C and 70°C can be attributed to the destabilizing effect of the ssDNA dangling ends. Position (M) in DL-DNA began to be denatured at about 70°C which is about 10°C higher than for junctions on DL-DNA. Most of the denaturation of the central region of DL-DNA occurred between 73°C and 76°C, resulting in complete denaturation at around 76°C. As mentioned previously, the denatured distances suggest that melting behavior is dependent on the relative instability of free ends and junctions to position (M). The movies can be generated to illustrate the ensembles' average denaturation based on the melting transition curves. These results demonstrate the destabilizing effects of the junctions on the DNA nanostructures. In addition, the stability of structures could be regulated by controlling the position of junction. Furthermore, our findings suggest that denaturation of more complex DNA nanostructures can be predicted based on the observed behavior of junction-separated individual components.

2.4.8 Thermal behavior of DNA hydrogel

To further examine the denaturation of three dimensional DNA nanostructures, four different types of DNA nanostructures made by ligation of X-DNA (72) were investigated. Interestingly, the DNA structures assembled by ligation of X-DNA bearing one, two, or three sticky ends showed relatively low T_m at around 62°C compared to that of DNA hydrogel formed with X-DNA bearing four sticky ends

Table 2.1. Predicted values of the standard free energy of linear DNA, $\Delta G°_{pred}$, were determined by mFold software of IDT based on nearest-neighbor model. Thermodynamic parameters for linear (13), Y- (39) and X-DNA (72), were calculated from the plot of $1/T_m$ vs ln C_T.

	$\Delta H°_{exp}$ (kcal/mol)	$\Delta S°_{exp}$ (kcal/K·mol)	$\Delta G°_{exp}$(298K) (kcal/mol)	$\Delta G°_{pred}$(310K) (kcal/mol)
Y-DNA (39)	-397.4	-1.19	-44.2	-81.5
X-DNA (72)	-851.6	-2.54	-93.9	-145.6

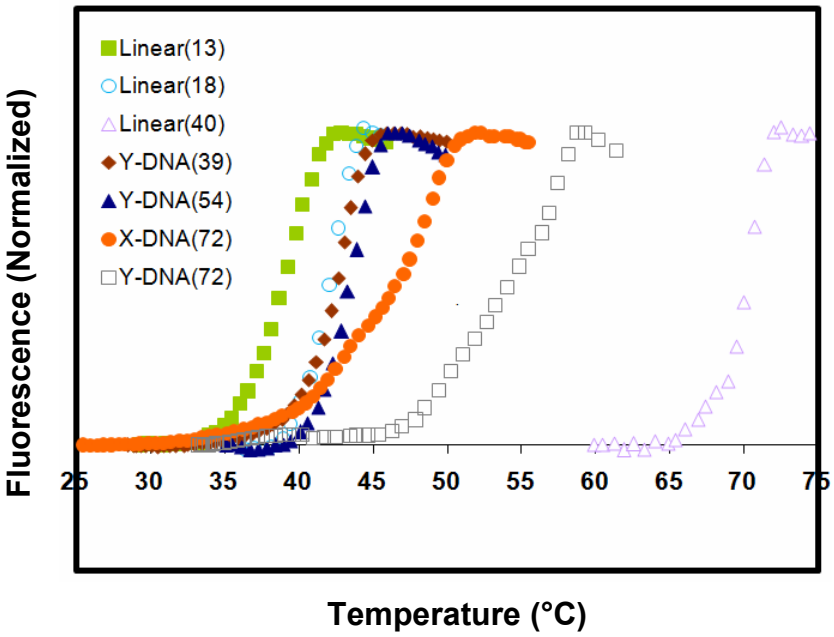

Figure 2.6. Melting temperatures and normalized melting transitions of 13bp, 18bp, and 40bp linear DNA; 39bp, 54bp, and 72bp Y-DNA, which have three 13bp, 18bp, and 24bp, respectively; and 72bp X-DNA, which has four 18bp.

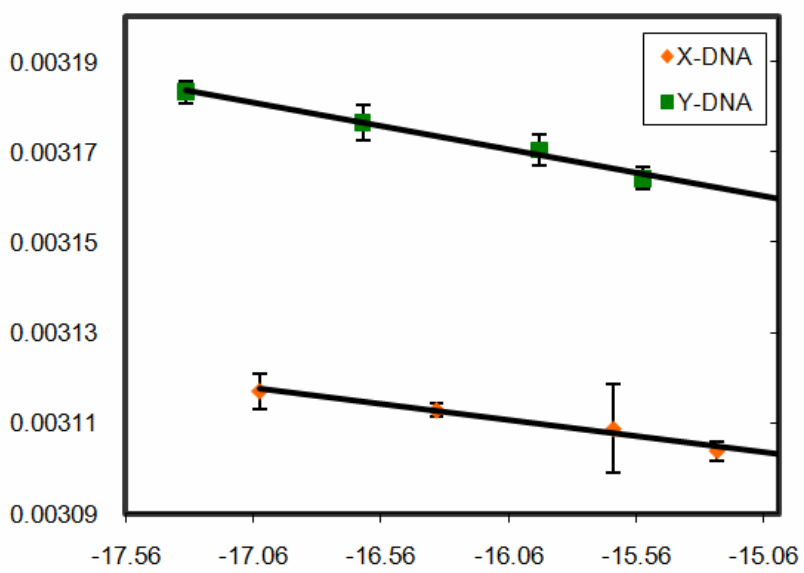

Figure 2.7. The concentration dependence of the melting temperature for Y-DNA and X-DNA. The slope is inversely proportional to the enthalpy and the X-axis intercept is proportional to the entropy

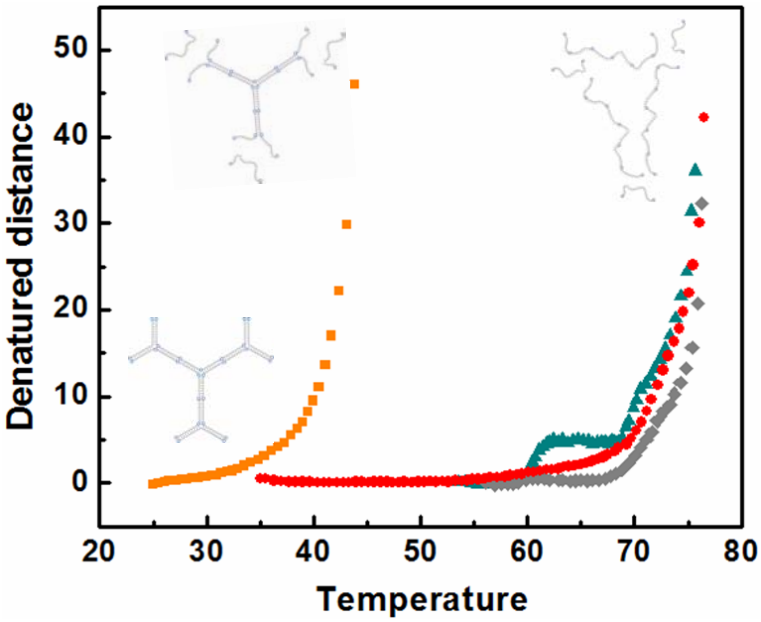

Figure 2.8. Thermally denatured distance of DL-DNA with four different position labelings of FRET pairs with schematic illustration of thermal denaturation of DL-DNA based on the thermally denatured distance. FRET pairs are labeled on junction 1(▲), Junction 2(●), end (■), and middle of stem (◆).

(Figure 2.9a). This is due to the breathing of ends on DNA nanostructures, which is also significant to the stability of complex DNA nanostructures[65]. DNA hydrogel contain less free ends due to the ligation of most ends. This reduction in free ends resulted in relatively high T_m. Therefore, DNA hydrogel showed high stability at high temperature until it totally denatured into the entire solution at about 77.6°C. As can be seen in Figure 2.9b and c, the FRET pairs attached on the DNA hydrogel were locally concentrated. The fluorescence of DNA gel was very weak because of the high efficiency of FRET (Figure 2.9c). To check for reversibility, the solution was cooled down to room temperature but the gel was not reformed (Figure 2.9d and e).

In order to investigate the junction effect on DNA hydrogel, X-DNA (160) which consisted of four 40bp arms was introduced. As can be seen in the schematic drawing of Figure 2.10, DNA hydrogel was formed by ligation of four 18bp-armed X-DNA. After ligation of X-DNA, the distance between junctions in DNA hydrogel was 40bp because four base sticky ends were used. Interestingly, from the melting transition of DNA hydrogel in Figure 2.10, most denaturation of DNA gel occurred within a 2 to 3°C range. This result shows that DNA gel is a thermally stable material under a temperature of 70°C, unlike a single X-DNA (72) which is the component of DNA hydrogel. The comparison of DNA hydrogel and X-DNA (160) shows their similarity in melting transitions. This data clearly demonstrates that denaturing effects from junctions play a significant role in the stability of 3D nanostructures and are similar to the effect of the end. Also, this result suggests that the thermal behavior of complicated DNA nanostructures can be anticipated by a consideration of the building block components of nanostructures.

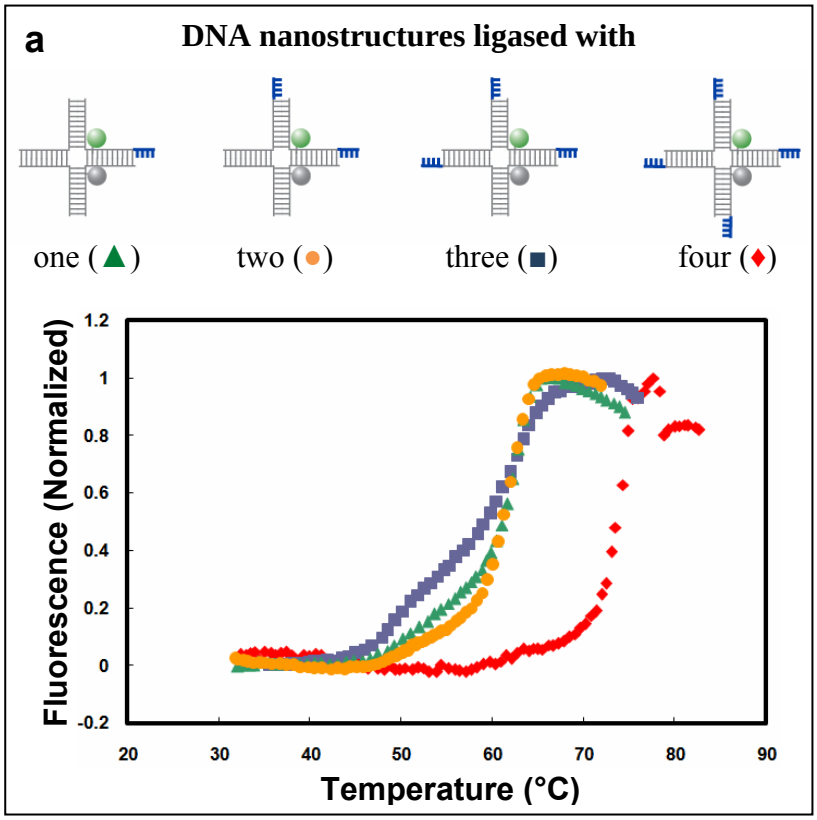

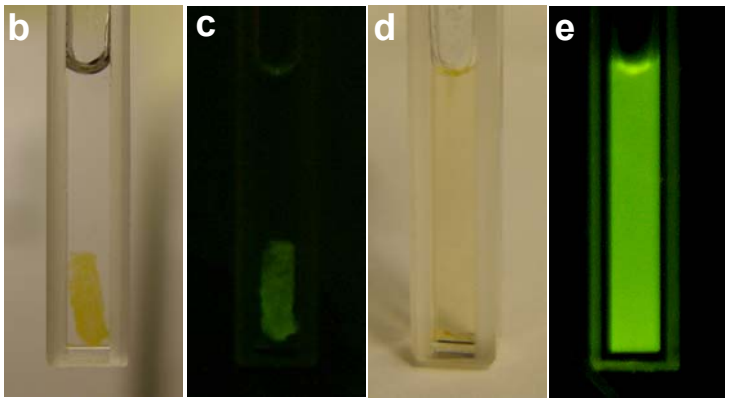

Figure 2.9. Melting transition of DNA nanostructures ligased with X-DNA (72) which is bearing one (▲), two (●), and three (■), and DNA hydrogel with four (♦) sticky ends (a). Digital camera images of DNA hydrogel before (b) and after heating at 90 °C (d), and fluorescence images of DNA gel before (c) and after heating (e) under UV light.

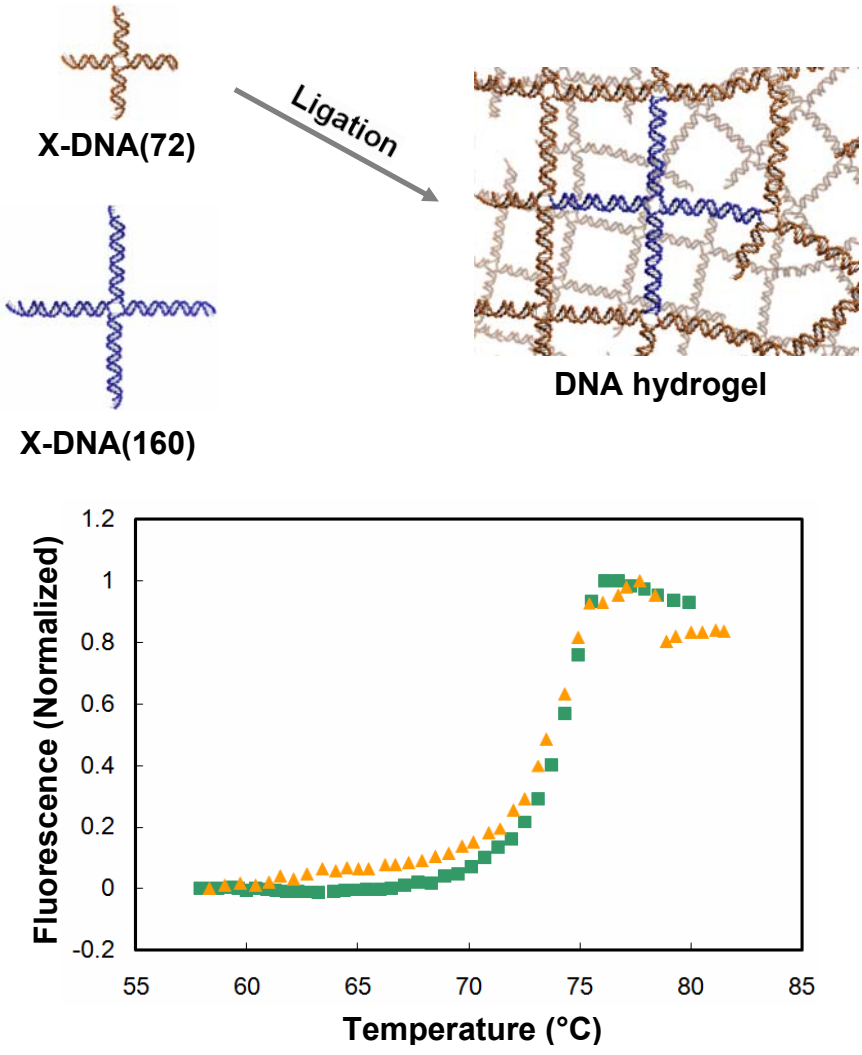

Figure 2.10. Denatured distance of DNA hydrogel and X-DNA (160) which has four 40bp arms. Melting transition of DNA hydrogel (▲) and X-DNA (160) (■).

Conclusions

In summary, we have investigated thermal behaviors of DNA nanostructures with FRET and NSET based measurement showing the effect of junctions and multi-ends on structural stability. In this research, we successfully achieved precise monitoring of nanostructural denaturation on the order of angstroms and found real time denatured distance. To the best of our knowledge, this is first time to show the denatured distance versus temperature and simulate the denaturation of nanostructures. With the advent of engineered DNA, building of two and three dimensional structures has been achieved. To anticipate the thermal behaviors and stability of complex DNA nanostructures, it is obvious that length, junctions, and multi-ends all will serve an important role in any analysis. The results presented here make it clear that the structural change and instability factors of complicated DNA nanostructures during heating can be understood through various FRET and NSET pair labelings. The melting temperature of nanostructures was found to be considerably lower than linear DNA with the same number of base pairs. It was also found that the thermodynamic behavior of complex DNA structures was governed by the behavior of the individual components separated by DNA junctions. Therefore, the results suggest that stability of complex DNA nanostructures can be predicted based on the observed behavior of individual building blocks. We expect that further studies will result in a new model that is able to anticipate the various parameters of the stability of DNA nanostructures.

REFERENCE

1. Mao, C.D., Sun, W.Q., Shen, Z.Y. & Seeman, N.C. A nanomechanical device based on the B-Z transition of DNA. Nature 397, 144-146 (1999).
2. Yan, H., Zhang, X.P., Shen, Z.Y. & Seeman, N.C. A robust DNA mechanical device controlled by hybridization topology. Nature 415, 62-65 (2002).
3. Seeman, N.C. DNA in a material world. Nature 421, 427-431 (2003).
4. Rothemund, P.W. Folding DNA to create nanoscale shapes and patterns. Nature 440, 297-302 (2006).
5. Winfree, E., Liu, F.R., Wenzler, L.A. & Seeman, N.C. Design and self-assembly of two-dimensional DNA crystals. Nature 394, 539-544 (1998).
6. Park, S.H. et al. Programmable DNA self-assemblies for nanoscale organization of ligands and proteins. Nano letters 5, 729-733 (2005).
7. Pinto, Y.Y. et al. Sequence-encoded self-assembly of multiple-nanocomponent arrays by 2D DNA scaffolding. Nano letters 5, 2399-2402 (2005).
8. Zheng, J. et al. Two-dimensional nanoparticle arrays show the organizational power of robust DNA motifs. Nano letters 6, 1502-1504 (2006).
9. Rinker, S., Ke, Y., Liu, Y., Chhabra, R. & Yan, H. Self-assembled DNA nanostructures for distance-dependent multivalent ligand-protein binding. Nat Nanotechnol 3, 418-422 (2008).
10. Liu, D., Park, S.H., Reif, J.H. & LaBean, T.H. DNA nanotubes self-assembled from triple-crossover tiles as templates for conductive nanowires. Proceedings of the National Academy of Sciences of the United States of America 101, 717-722 (2004).
11. Endo, M., Seeman, N.C. & Majima, T. DNA tube structures controlled by a four-way-branched DNA connector. Angew Chem Int Ed Engl 44, 6074-6077 (2005).

12. Ke, Y., Liu, Y., Zhang, J. & Yan, H. A study of DNA tube formation mechanisms using 4-, 8-, and 12-helix DNA nanostructures. J Am Chem Soc 128, 4414-4421 (2006).
13. Yin, P. et al. Programming DNA tube circumferences. Science 321, 824-826 (2008).
14. May, S. & Ben-Shaul, A. DNA-lipid complexes: stability of honeycomb-like and spaghetti-like structures. Biophysical journal 73, 2427-2440 (1997).
15. Ewert, K.K. et al. A columnar phase of dendritic lipid-based cationic liposome-DNA complexes for gene delivery: hexagonally ordered cylindrical micelles embedded in a DNA honeycomb lattice. J Am Chem Soc 128, 3998-4006 (2006).
16. Park, S.H. et al. Finite-size, fully addressable DNA tile lattices formed by hierarchical assembly procedures. Angew Chem Int Ed Engl 45, 735-739 (2006).
17. He, Y. et al. Hierarchical self-assembly of DNA into symmetric supramolecular polyhedra. Nature 452, 198-U141 (2008).
18. Ouporov, I.V. & Leontis, N.B. Refinement of the solution structure of a branched DNA three-way junction. Biophysical journal 68, 266-274 (1995).
19. Eichman, B.F., Ortiz-Lombardia, M., Aymami, J., Coll, M. & Ho, P.S. The inherent properties of DNA four-way junctions: comparing the crystal structures of holliday junctions. Journal of molecular biology 320, 1037-1051 (2002).
20. Kadrmas, J.L., Ravin, A.J. & Leontis, N.B. Relative stabilities of DNA three-way, four-way and five-way junctions (multi-helix junction loops): unpaired nucleotides can be stabilizing or destabilizing. Nucleic acids research 23, 2212-2222 (1995).

21. McKinney, S.A. et al. Single-molecule studies of DNA and RNA four-way junctions. Biochemical Society transactions 32, 41-45 (2004).

22. Buranachai, C., McKinney, S.A. & Ha, T. Single molecule nanometronome. Nano letters 6, 496-500 (2006).

23. Benvin, A.L. et al. Fluorescent DNA nanotags: supramolecular fluorescent labels based on intercalating dye arrays assembled on nanostructured DNA templates. J Am Chem Soc 129, 2025-2034 (2007).

24. Hohng, S. et al. Fluorescence-force spectroscopy maps two-dimensional reaction landscape of the holliday junction. Science 318, 279-283 (2007).

25. Shlyakhtenko, L.S., Potaman, V.N., Sinden, R.R., Gall, A.A. & Lyubchenko, Y.L. Structure and dynamics of three-way DNA junctions: atomic force microscopy studies. Nucleic acids research 28, 3472-3477 (2000).

26. Johnson, D.S., Bai, L., Smith, B.Y., Patel, S.S. & Wang, M.D. Single-molecule studies reveal dynamics of DNA unwinding by the ring-shaped T7 helicase. Cell 129, 1299-1309 (2007).

27. Stryer, L. Fluorescence energy transfer as a spectroscopic ruler. Annual review of biochemistry 47, 819-846 (1978).

28. Clegg, R.M. Fluorescence resonance energy transfer and nucleic acids. Methods in enzymology 211, 353-388 (1992).

29. Selvin, P.R. Fluorescence resonance energy transfer. Methods in enzymology 246, 300-334 (1995).

30. Weiss, S. Measuring conformational dynamics of biomolecules by single molecule fluorescence spectroscopy. Nature structural biology 7, 724-729 (2000).

31. Lytton-Jean, A.K. & Mirkin, C.A. A thermodynamic investigation into the binding properties of DNA functionalized gold nanoparticle probes and molecular fluorophore probes. J Am Chem Soc 127, 12754-12755 (2005).

32. Sacca, B., Meyer, R., Feldkamp, U., Schroeder, H. & Niemeyer, C.M. High-throughput, real-time monitoring of the self-assembly of DNA nanostructures by FRET spectroscopy. Angew Chem Int Ed Engl 47, 2135-2137 (2008).

33. Jennings, T.L., Schlatterer, J.C., Singh, M.P., Greenbaum, N.L. & Strouse, G.F. NSET molecular beacon analysis of hammerhead RNA substrate binding and catalysis. Nano letters 6, 1318-1324 (2006).

34. Jennings, T.L., Singh, M.P. & Strouse, G.F. Fluorescent lifetime quenching near d = 1.5 nm gold nanoparticles: probing NSET validity. J Am Chem Soc 128, 5462-5467 (2006).

35. Pons, T. et al. On the quenching of semiconductor quantum dot photoluminescence by proximal gold nanoparticles. Nano letters 7, 3157-3164 (2007).

36. Yun, C.S. et al. Nanometal surface energy transfer in optical rulers, breaking the FRET barrier. J Am Chem Soc 127, 3115-3119 (2005).

37. Lu, H., Schops, O., Woggon, U. & Niemeyer, C.M. Self-assembled donor comprising quantum dots and fluorescent proteins for long-range fluorescence resonance energy transfer. J Am Chem Soc 130, 4815-4827 (2008).

38. Li, Y. et al. Controlled assembly of dendrimer-like DNA. Nature Materials 3, 38-42 (2004).

39. Um, S.H. et al. Enzyme-catalysed assembly of DNA hydrogel. Nature Materials 5, 797-801 (2006).

40. Marky, L.A. & Breslauer, K.J. Calculating thermodynamic data for transitions of any molecularity from equilibrium melting curves. Biopolymers 26, 1601-1620 (1987).

CHAPTER 3

A General Approach to Generating Multifunctional Nano-architectures from DNA-based ABC Monomers

---

Jong B. Lee[1], Young H. Roh[1], Soong H. Um[1], Hisakage Funabashi[1], Wenlong Cheng[1], Judy J. Cha[2], Pichamon Kiatwuthinon[1], David A. Muller[2], Dan Luo[1.] "Multifunctional nano-architectures from DNA-based ABC Monomers". Submitted *Nature Nanotechnology*. Accepted (2009).

[1]Department of Biological & Environmental Engineering and [2]Department of Applied & Engineering Physics, Cornell University, Ithaca, NY 14850, USA

3.1 Abstract

From a branched DNA labeled with quantum dots, gold nanoparticles, and polyethylene glycol monoacrylate, **a**nisotropic, **b**ranched, and **c**rosslinkable monomers (ABC monomers) were created. These multifunctional nano-architectures were used for detecting pathogen DNA as DNA nanobarcodes and encoded spherical polymers. Importantly, the spherical polymers were generated only in the presence of a specific DNA molecule, enabling highly-sensitive pathogen detection. Using this momomer system, we also designed a biocompatible multi-drug delivery vector that delivered both drugs and tracers simultaneously.

3.2 Introduction

Nano-architectures bearing different molecular and nanoparticular building blocks can perform multitasks at small scale and can also possibly provide synergistic functionalities that are not available from the simple combination of individual moieties[1, 2]. The multifunctional nano-architectures can have applications ranging from nanoelectronics[3] and nanophotonics4 to intelligent sensing[5] and drug-delivery systems[6, 7]. Anisotropy of molecules is required to control multifunctionality, and many anisotropic building blocks, including nanoparticles, micro-crystals and dendrimers, have been created that can provide some capabilities to tether multiple molecular moieties together[1, 8-14]. However, it remains challenging to attach multiple moieties onto a single core molecule with nanometer precision. Also lacking is a general approach to generating such multi-functional nano-architectures. State-of-the-art DNA nanotechnology on the other hand provides precise and versatile controls over micro-and nanostructures[15-19]. In particular, recent progress in positioning different molecular moieties through DNA self-assembly have been indicated[20-28]. Our previous studies have also demonstrated that DNA can provide simultaneously the

multivalencies and anisotropicities with nanometer precision[29-32], suggesting that DNA might serve as an ideal base for building multifunctional nano-architectures. Here we report a general and precise approach for the creation of an anisotropic, branched, and crosslinkable monomer (ABC monomer) that is DNA-based and that can be further polymerized to form multifunctional nano-architectures. Each single ABC monomer consists entirely of DNA whose ends can be designed to precisely tether multi-moieties including QDs, gold nanoparticles (AuNP), fluorescence dyes, photoresponsive chemicals, etc. Importantly, novel properties were obtained from these DNA-based multifunctional nano-architectures. In particular, we achieved a target-driven (pathogen-DNA-driven) polymerization that was successfully employed in signal amplification for pathogen detection. In addition, a multi-drug delivery vector was devised and taken up by mammalian cells. Overall, our DNA-based, ABC monomer is a platform technology beyond most DNA-based materials and particle-based nanostructures. Its "plug-and-play" flexibility in design enables precise control over functionalities. Compared with most synthetic polymers, the DNA components also enable easier interface with biological systems. Our approach provides a general yet versatile route towards creating a range of multifunctional nano-architectures.

3.3 Materials and Methods

3.3.1. A general approach for synthesis of multifunctional nanoarchitectures

In this work, we developed a modular ("plug-and-play") approach to constructing a multifunctional nano-architecture from an ABC monomer building block. To create the ABC monomer, branched, Y-shaped DNA (Y-DNA) conjugated with different moeities served as the modular donor, while X-shaped DNA (X-DNA) was used as the core acceptor molecule (Figure 3.1). Anisotropy was achieved by designing unique DNA sequences at the end of each branch of the core X-DNA.

Because of the freedom in synthesizing any desired DNA sequence at any position, the capacity of anisotropy (from different sequences) is practically unlimited. Multi-functionality was realized by the specific connections of different donor Y-DNA onto the same acceptor X-DNA. Single-stranded bridge DNA whose sequence was complementary to both acceptor and donor sequences, was used to connect the Y to the X. To simplify the notation, we named each unique end-sequence as *West*, *North*, and *East* based on the branch orientation (designated as *W*, *N*, and *E* for Y-DNA and *W'*, *N'*, and *E'* for X-DNA; subscript *i* is used sometimes to distinguish different sequences; Fig. 1). The bridge DNAs were notated correspondingly (*w*, *n*, and *e* in lower case letters).

3.3.2. Conjugation of PEGA onto Y-DNA

Acrylate-(polyethylene glycol)-succinimidyl carboxy methyl ester is a set of compounds having polyethylene glycol (PEG) spacers with monoacrylate (PEGA) and amine-reactive *N*-hydroxysuccinimide (NHS) -ester groups at opposite ends (Figure 3.2). The NHS-ester is spontaneously reactive with primary amines ($-NH_2$) of Y-DNA, providing an efficient route for conjugation. To tether the PEGA to Y-DNA, 0.5 μM PEGA-NHS (3,400 Da) was added to the solution containing 0.2 μM 5' amine-modified Y-DNA (NH_2-Y-DNA). The reaction was carried out overnight at room temperature. PEGA-Y-DNA was separated from non-reacted NH_2-Y-DNA and PEGA by an HPLC XBridge C18 column equipped with a photo-diode array detector (Waters).

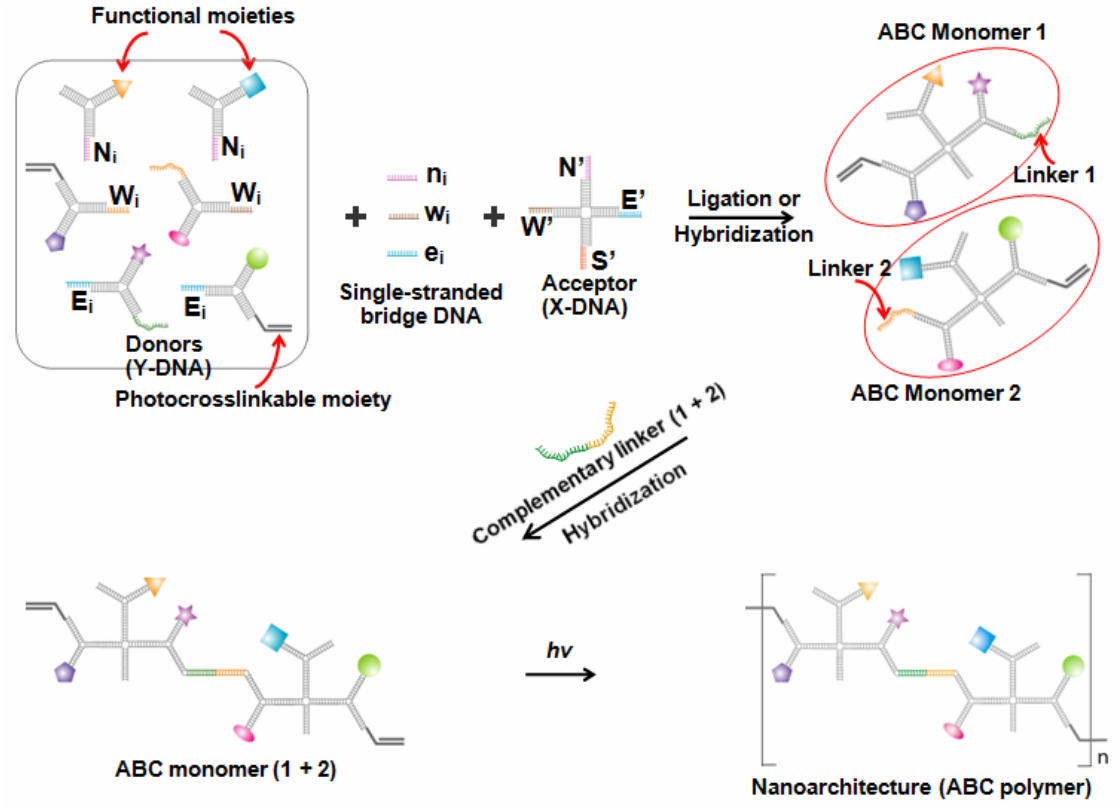

Figure 3.1. Schematic illustration of a general approach of assembly of ABC monomer and target-driven photo-polymerization. Multiple moieties are conjugated on Y-DNA donors. The functionalized Y-DNAs are then connected to corresponding end-sequences of acceptor X-DNA to form ABC monomer. The bridge DNA glues donor and acceptor together. To perform photo-polymerization, ABC monomers 1 and 2 are linked together through hybridization with a complementary linker DNA. These ABC monomers (1 + 2) are then photo-polymerized.

Figure 3.2. Synthesis of PEGA modified Y-DNA.

3.3.3. Synthesis of ABC monomer (nanobarcodes) with fluorescence dyes

First, 1.5μM X-DNA and three different types of 1.5μM Y-DNA (one green (1G), two reds (2R), and one green and one red (1G1R)) were incubated (Figure 3.3). Second, specific Y-DNA was connected to X-DNA by adding 1.5μM specific bridge DNA which was complementary to the sticky ends of both X- and Y-DNA. Without bridge DNA, X- and Y-DNA could not link. For example, only 1G Y-DNA were connected to X-DNA by adding *w* bridge DNA. Both 1G and 2R Y-DNA were liked to one X-DNA by adding *w* and *n* bridge DNA.

3.3.4. Synthesis of ABC monomers with nanoparticles

3.3.4.1. Conjugation of gold nanoparticles with oligonucleotide

AuNPs with a diameter of 5 nm were purchased from Ted. Pella. Inc. and functionalized following literature procedures. Oligonucleotides having an alkanedisulfide covalently bonded to 3' ends were deprotected and incubated with 4.5nM gold nanoparticles. The mixture was allowed to stand for 12 hours at room temperature. Then, sodium chloride was added to the mixture with a final concentration of 0.2M. The mixture was aged at room temperature for another 12 hours. The purpose of this procedure was also to increase surface number density of oligonucleotides on gold nanoparticle surfaces. Then, the mixture was centrifuged and exchanged into Milli-Q water. According to the O.D. of released oligonucleotides by DTT, a 150 number density of ssDNA/particle was achieved. The as-prepared oligonucleotide modified gold nanoparticles were ready to be attached with donor Y-DNA.

Figure 3.3. Schematic drawing of synthesizing ABC monomers by controlling multi-moieties onto a single anisotropic X-DNA. We first prepared three different types of Y-DNA (designated as *W*, *N*, and *E*) that carried three different configurations of fluorescence dyes: one green (1G), two reds (2R), and one green and one red (1G1R). In addition, three single stranded DNAs (designated as *w*, *n*, and *e* in lower case letters) were uniquely designed in such a way that half of the sequence was complementary to the corresponding Y-DNA's sticky end, and the other half was complementary to one of the X-DNA's end-sequence (*W'*, *N'*, and *E'*). Thus, these three single stranded DNA served as "bridge DNA" that linked X and Y together in an anisotropic and specific manner: *w*, *n*, and *e* only linked *W'*-*w*-*W*, *N'*-*n*-*N*, and *E'*-*e*-*E*, respectively. By simply adding a specific bridge DNA, different fluorescence dyes were donated onto the corresponding branches of a single X-DNA with nanometer precision.

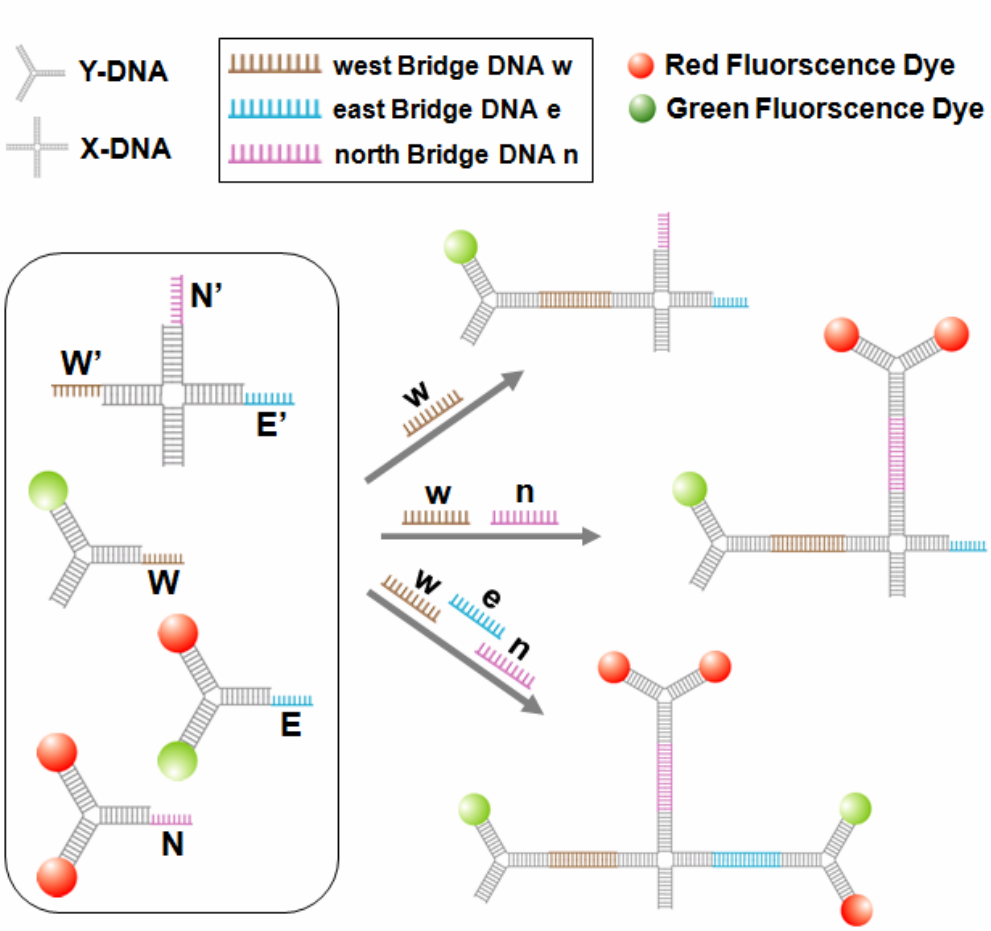
Y-DNA
X-DNA
west Bridge DNA w
east Bridge DNA e
north Bridge DNA n
Red Fluorscence Dye
Green Fluorscence Dye
N'
W'
E'
W
E
N
w
w
n
w
e
n

3.3.4.2. Conjugation of quantum dots (QDs) with Y-DNA

QDs, from Invitrogen (Carlsbad, CA), were commercially coated with streptavidin. The emission wavelengths of the green QD (Qdot® 525 streptavidin conjugate) and the red QD (Qdot® 655streptavidin conjugate) were 525nm and 655 nm, respectively. In the structure of the QD, the CdSe core is encapsulated in a shell of ZnS and the polymer shell and the outside was covalently conjugated with streptavidin. The QD and Y-DNA conjugation was performed by direct association of biotinylated Y-DNA to streptavidin-coated QDs. Because of the highly specific interaction between streptavidin and biotin, the yield of conjugation is high. 20 pmole of Y-DNA was reacted with 10 μl of 1 μM QD solution in 10 mM PBS overnight at room temperature. Non-reacted biotinylated Y-DNA was removed by a streptavidin affinity column (Promega, Madison, WI).

3.3.4.3. Synthesis of ABC monomers with QDs and AuNP

To synthesize ABC monomer with QDs and AuNP, the South branch of the X-DNA is first anchored onto a solid bead **1** (Figure 3.4). Both west and east end-sequences of X-DNA are then connected with Y-DNA donor tethering quantum dots **2A**. The north end-sequence of X-DNA is connected with another Y-DNA **2B**. Then, AuNP functionalized with ssDNA **4** are hybridized onto **3** to achieve a QD-AuNP labeled ABC monomer. The ABC monomers attached to the beads **5** are released by restriction enzyme Dde I digestion and the isolated ABC monomers **6** are collected. Aggregates were prevented by blocking the non-reacted strands of **3**.

3.3.4.4. Synthesize ABC monomers (QD nanobarcodes)

To synthesize ABC monomers (QD nanobarcodes) with three quantum dots, the south branch of the X-DNA was first anchored onto a solid bead **1** (Figure 3.5).

Both *west* and *east* end-sequences of X-DNA were then connected with Y-DNA donor tethering green quantum dots. The end-sequence at the *north* of an X-DNA was connected with a red QD Y-DNA. Then, the ABC monomers attached to the beads **3** were released by restriction enzyme *Dde* I digestion and the isolated ABC monomers **4** were collected. This solid phase synthesis was modified according to previously reported methods from our group[31].

3.3.5. Preparation of ABC dimer

The ABC dimer was assembled by mixing equimolar quantities of each ABC monomer with pathogen DNA in a solution containing 15 mM $MgCl_2$ and 10 mM Tris buffer (pH 8) (Figure 3.1). The mixture was incubated at 30 °C for 30 min.

3.3.6. Formation of ABC polymer by Photo-polymerization

ABC dimers were photo-polymerized at 265 nm UV light (8 mW/cm^2) in the presence of an initiator (Irgacure, Ciba Geigy, Ardsley, NY) using a UV crosslinker (Spectronics Corporation, XL-1000) (Figure 3.1).

3.3.7. Gel electrophoresis

The ABC monomers were run in a 3% agarose gel at 90 volts at room temperature in Tris-acetate-EDTA, pH 8.0, Bio-Rad, Hercules, CA). A true color picture of the gel was taken using a digital camera under strong UV illumination. The gel was stained with 0.5 µl/ml of ethidium bromide in TAE buffer.

3.3.8. Atomic Force Microscopy (AFM) Imaging

A 5 µl sample was placed onto the surface of freshly cleaved mica (Ted Pella, Redding, CA) functionalized with aminopropyltriethoxysilane (APTES, Aldrich, St.

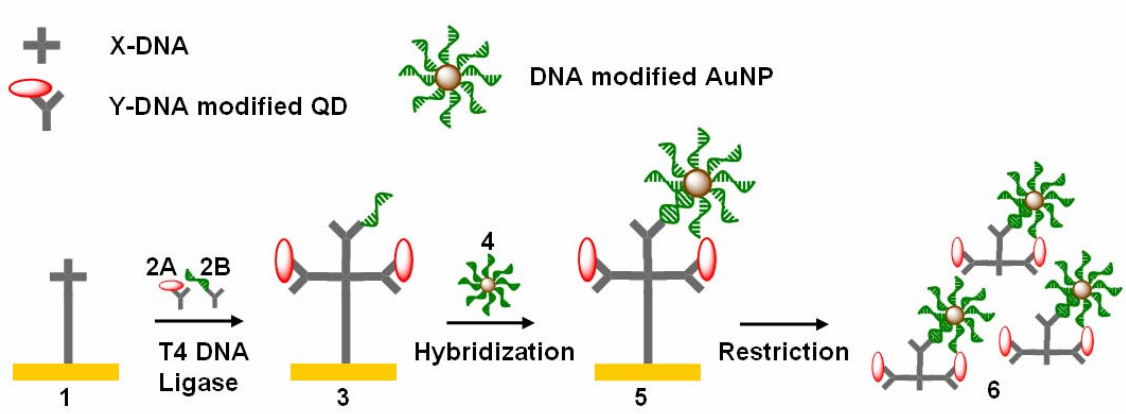

Figure 3.4. Schematic drawing of synthesis of ABC monomer with QD and AuNP.

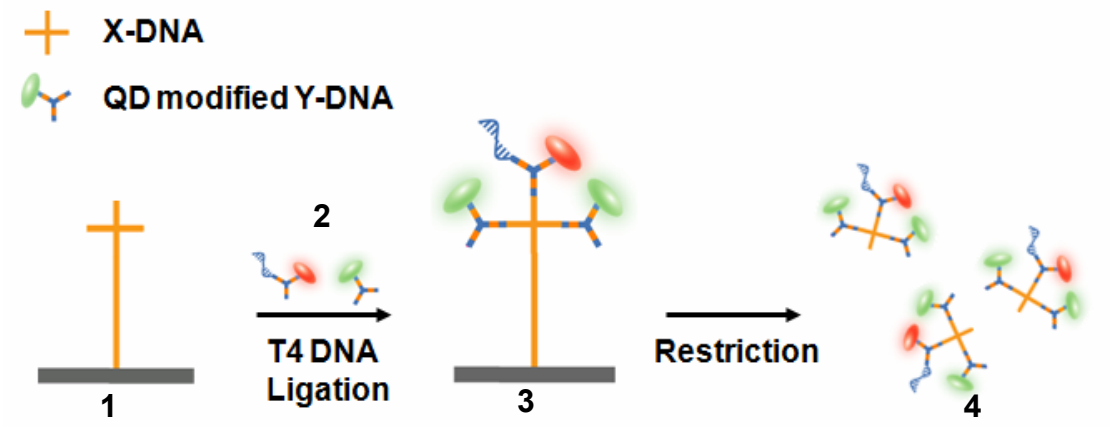

Figure 3.5. Schematic drawing of synthesis of ABC monomer with QDs.

Louis, MO) and allowed to adsorb to the mica surface for approximately 20 min. The mica was then rinsed in Milli-Q water. Tapping-mode AFM images were taken in air using a Dimension 3100 AFM (Digital Instruments, Santa Barbara, California).

3.3.9. Microscopy of Nano-architectures (ABC polymers)

A 10 μl sample was placed onto the microscope glass and then covered by cover glass (22 × 22 mm^2). The DNA nano-architectures were observed with a microscope (Olympus IX70) equipped with an 100x (high magnification) oil-immersion objective. Images were acquired with MetaMorph image acquisition software. All observations were performed at room temperature.

3.3.10. Scanning Transmission Electron Microscopy (STEM) Imaging

Samples were prepared by placing a 10 μl drop of the ABC monomer solution onto a copper grid coated with an ultra-thin carbon film and allowed to evaporate. Once the solution was completely evaporated, the sample was exposed to UV light for approximately 40 minutes to prevent contamination build-up during microscopy. STEM images were obtained on a 200 keV Tecnai F20 microscope with 1.6 Å resolution in annular dark-field STEM mode.

3.3.11. Cell culture

HeLa cells were cultured at 37 °C with 5% CO_2 in Dulbecco's Minimum Essential Medium (DMEM, Mediatech, Inc. Manassas, VA) supplemented with 10% fetal bovine serum (FBS, Hyclone, Logan, UT) and 2% penicillin/streptomycin (P/S, Mediatech, Inc, Manassas, VA).

3.3.12. Fluorescence labeling and imaging of cell

Cells (3 x 10^4) were cultured in each well on Lab-Tek chamber slides (8 wells, Permanox slide, Nunc) for one day. Cells were further cultured in the presence of 20 µl polymeric spheres (2.9 pM) overnight at 37°C, at 4°C, or 10 min at 37°C. Cells were washed three times with PBS, then fixed with 4% paraformaldehyde. Actin filaments and nuclei were stained with Allexa Fluor®488 phalloidin (Invitrogen, Carlsbad, CA) and DAPI (4',6-diamidino-2-phenylindole) with an antifade reagent (Invitrogen, Carlsbad, CA) according to the supplier's protocol. Cross-sectional images of the cell were obtained by confocal microscopy (Zeiss LSM 510 Meta Confocal Microscope).

3.3.13. Cell cytotoxicity evaluation

The cytotoxicity of the polymer spheres (with ABC monomer from 10 pM to 5 nM) was determined after a 36-hour incubation with HeLa cells (1 x 10^4 cell) by measuring the release of lactate dehydrogenase (LDH) from a damaged membrane of cells using CytoTox-One™ Homogeneous Membrane Integrity Assay (Promega, Madison, WI).

3.3.14. Investigation of the endocytosis mechanism of the polymeric spheres uptake

To investigate the cellular endocytosis mechanism of the polymeric spheres, HeLa cells (5 x 10^4) were cultured in each well on a Lab-Tek chamber slide (8 wells, Permanox slide, Nunc) overnight. Cells were pre-incubated with endocytosis inhibitors for 30 min with 10 µg/mL of chlorpromazine hydrochloride (sigma) and 5 µg/mL of filipin complex (sigma), and for 1 hr with 0.5 µg/mL of Cytochalasin B and 0.1% of DMSO as a positive control. Cells were then cultured with 20 µL of

polymeric spheres (2.9 pM) and each inhibitor for 3 hrs. The number of cells uptaking the spheres was counted from fluorescent microscope images after staining with the same method described previously.

3.4 Results and discussions

3.4.1. Synthesis of ABC monomers

Because of the built-in modularity, the type of moiety that can be linked to the core is virtually unrestricted. To build up a multifunctional polymer from ABC monomers, we designed different modules separately, including DNA capture probes, fluorescent dyes, quantum dots (QDs), and gold nanoparticles (AuNPs) (for DNA sequences see Tables 3.1 and 3.2). In addition, by incorporating a polyethylene glycol monoacrylate (PEGA) moiety onto the Y-DNA (Figures 3.6 and 3.7), we further introduced a new capability for photo-crosslinking (for sequences, see Table 3.3). The resulting ABC monomers, now with multiple and varying functional groups, can thus be photo-polymerized using the built-in photo-reactive groups.

3.4.1.1. Evaluation of Conjugation of PEGA onto Y-DNA

The HPLC chromatogram was obtained (Figure 3.6a) from a gradient elution of 0–50% acetonitrile in 0.1 M triethylammonium acetate (TEAA, pH 7.0) as the mobile phase within 40 min at a flow rate of 0.5 mL/min with UV detection (260 nm). The conjugation of PEGA to Y-DNA was confirmed by gel electrophoresis (Figure 3.6b). Lane 1 indicates NH_2-Y-DNA (from HPLC fraction B) and lane 2 indicates PEGA-Y-DNA (from HPLC fractions C1-C2). Compared to NH_2-Y-DNA, the gel electrophoretic mobility of PEGA-Y-DNA was retarded, as expected, because of the increase of molecular weight.

Table 3.1. Oligonucleotide sequences of the DNA building blocks for ABC monomers with fluorescent dyes.

Strand		Sequence
X-DNA	X_{01}	5'-CGACCGATGAATAGCGGTCAGATCCGTACCTACTCGCTCA-3'
	$X_{02}(W')$	5'-CGAGACCATACGTACAGCACCGCTATTCATCGGTCGTGGTGGGTTATAAT-3'
	$X_{03}(N')$	5'-CGAGTCGTTCGCAATACGGCTGTACGTATGGTCTCGCGTCTCTACCTGAT-3'
	$X_{04}(E')$	5'-/Phos/-CGAGTAGGTACGGATCTGCGTATTGCGAACGACTCGGCTGTGAACCAAG-3'
Bridge DNA (*w*)		5'-CATGTCAGTGATTATTATAACCCACCA-3'
Bridge DNA (*n*)		5'-AGATGCAATAGTAATCAGGTAGAGACG-3'
Bridge DNA (*e*)		5'-ATAATACTGCGTCTTGGTTCACAGC-3'
Y-DNA (*W*)	$Y_{01}(W)$	5'-AATCACTGACATGTGGATCCGCATGACATTCGCCGTAAG-3'
	Y_{02}(●)	5'-Alexa Fluor488●-CTTACGGCGAATGACCGAATCAGCCT-3'
	Y_{03}	5'-AGGCTGATTCGGTTCATGCGGATCCA-3'
Y-DNA (*N*)	$Y_{01}(N)$	5'-TACTATTGCATCTTGGATCCGCATGACATTCGCCGTAAG-3'
	Y_{02}(●)	5'-BODIPY630/650●-CTTACGGCGAATGACCGAATCAGCCT-3'
	Y_{03}(●)	5'-BODIPY630/650●-AGGCTGATTCGGTTCATGCGGATCCA-3'
Y-DNA (*E*)	$Y_{01}(E)$	5'-ACGCAGTATTATTGGATCCGCATGACATTCGCCGTAAG-3'
	Y_{02}(●)	5'-Alexa Fluor488●-CTTACGGCGAATGACCGAATCAGCCT-3'
	Y_{03}(●)	5'-BODIPY630/650●-AGGCTGATTCGGTTCATGCGGATCCA-3'
SP-DNA	SP_{01}	5'-Biotin-C_6-CCGGATAAGGCGCAGCGGTCGGCTGAATTCAGGGTTCGTGGCAGGCCAGCACACTTGGAGACCGAAGCTTACCGGACTCCTAACTGAG-3'
	SP_{02}	5'-/Phos/-GTTAGGAGTCCGGTAAGCTTCGGTCTCCAAGTGTGCTGGCCTGCCACGAACCCTGAATTCAGCCGACCGCTGCGCCTTATCCGG-3'

Note that /phos/ represents the phosphorylation on the 5' end of the oligonucleotide. The labeled fluorescent dye is represented by a dot with the same color. The same colored sequences represent complementary pairs.

Table 3.2. Oligonucleotide sequences of the DNA building blocks for ABC monomers with nanoparticles.

Strand		Sequence
X-DNA	X_{01}	5'-/Phos/- TGAGCACCGATGAATAGCGGTCAGATCCGTACCTACTCG-3'
	X_{02}	5'-/Phos/-ATCCCGAGTAGGTACGGATCTGCGTATTGCGAACGACTCG-3'
	X_{03}	5'-/Phos/-GCAACGAGTCGTTCGCAATACGGCTGTACGTATGGTCTCG-3'
	X_{04}	5'-/Phos/-GAGTCGAGACCATACGTACAGCACCGCTATTCATCGGTGC-3'
Template DNA		5'-TTACGGAGGTGGTTGTGGCA-A_{10}-C_3-SH - 3'
Y-DNA (QD)	Y_{01}	5'-GCCACTGGATCCGCATGAGGTAGGACGACATTCGCCGTAAGCACAC-3'
	Y_{02} (Biotin)	5'-Biotin-C_6-GTGTGCTTACGGCGAATGTCGTCACAGCACCGAATCAGCCTGTCG A-3'
	Y_{03}	5'-/Phos/-GGAT TCGACAGGCTGATTCGGTGCTGTCTACCTCATGCGGATCCAGT 5'-/Phos/-ACTC GGC-3'
Y-DNA (AuNP)	Y_{01}	5'-GCCACAACCACCTCCGTAAGCCACTGGATCCGCATGAGGTAGGACGACAT TCGCCGTAAGCACAC-3'
	Y_{02}	5'-GTGTGCTTACGGCGAATGTCGTCACAGCACCGAATCAGCCTGTCGA-3'
	Y_{03}	5'-/Phos/-TTGCTCGACAGGCTGATTCGGTGCTGTCTACCTCATGCGGATCCAGTG GC-3'
SP-DNA	SP_{01}	5'-Biotin- C_6-CCGGATAAGGCGCAGCGGTCGGCTGAATTCAGGGTTCGTGGCAG GCCAGCACACTTGGAGACCGAAGCTTACCGGACTCCTAAC-3'
	SP_{02}	5'-/Phos/-TCAGTTAGGAGTCCGGTAAGCTTCGGTCTCCAAGTGTGCTGGCCTGC CAC GAACCCTGAATTCAGCCGACCGCTGCGCCTTATCCGG-3'

Table 3.3. Oligonucleotide sequences of pathogen DNA and DNA building blocks for target-driven polymerization (Ban = Anthrax, Ebo = Ebola, Sars = SARS)

Strand		Sequence	
Target (Ban) DNA		5'-GGATTATTGTTAAATATTGATAAGGAT-3'	
Target (Ebo) DNA		5'-CATGTCAGTGATTATTATAACCCACCA-3'	
Target (Sars) DNA		5'- ATAATACTGCGTCTTGGTTCACAGC-3'	
Unrelated DNA		5'- AGATGCAATAGTAATCAGGTAGAGACG-3'	
Y-DNA (Probe1)	Y_{01}(Ban)	5'-TTAACAATAATCC	GCCACTGGATCCGCATGAGGTAGGACGACATTCG CCGTAAGCACAC-3'
	Y_{01}(Ebo)	5'-AATCACTGACATG	
	Y_{01}(Sars)	5'-GACGCAGTATTAT	
	Y_{02} (Biotin)	5'-Biotin-C_6-GTGTGCTTACGGCGAATGTCGTCACAGCACCGAATCAGCCTGT CGA-3'	
	Y_{03}	5'-/Phos/-GGATTCGACAGGCTGATTCGGTGCTGTCTACCTCATGCGGATCCAGT GGC-3'	
Y-DNA (probe2)	Y_{01}	5'-GCCACTGGATCCGCATGAGGTAGGACGACATTCGCCGTAAGCACAC-3'	
	Y_{02} (Biotin)	5'-Biotin-C_6-GTGTGCTTACGGCGAATGTCGTCACAGCACCGAATCAGCCTG TCGA-3'	
	Y_{03}(Ban)	5'-/Phos/-GGATTCGACAGGCTGATTCGGTGCTGTCT ACCTCATGCGGATCCAGTGGC	ATCCTTATCAATAT-3'
	Y_{03}(Ebo)		TGGTGGGTTATAAT-3'
	Y_{03}(Sars)		GCTGTGAACCAA-3'
Y-DNA (NH_2)	Y_{01}	5'-GCCACTGGATCCGCATGAGGTAGGACGACAT TCGCCGTAAGCACAC-3'	
	Y_{02}	5'-/NH_2/GTGTGCTTACGGCGAATGTCGTCACAGCACCGAATCAGCCTGTCGA-3'	
	Y_{03}	5'-/Phos/-TTGCTCGACAGGCTGATTCGGTGCTGTCTACCTCATGCGGATCCAGT GGC-3'	

The FTIR spectrum of PEGA-Y-DNA (Figure 3.7) revealed several transmission bands from an amide bond, PEG, and DNA. Two characteristic bands of C=O and N-H groups were observed at 1672 and 1620 cm^{-1} for amide bonds. The transmission bands at higher wavenumbers were assigned to the amide I band and the bands at lower wavenumbers to the amide II band, which is typical of primary amides. Another transmission band at 2881 cm^{-1} was assigned to the CH_2 group of PEG. The transmission bands at 1080 and 1252 cm^{-1} were assigned to the PO_2 group of DNA. The appearance of a new amide bond confirmed the formation of PEGA-Y-DNA.

3.4.1.2. Evaluation of Conjugation of AuNPs with Oligonucleotides

To evaluate the conjugation of DNA on AuNPs, UV-visible absorbance spectra were measured with bare AuNPs (solid line) and DNA modified AuNPs (dash line) (Figure. 3.8). After DNA modification, the UV-visible absorbance spectrum was changed from 517nm to 524nm and the peak at 260nm appeared after DNA binding.

3.4.2. Evaluation of ABC monomers with fluorescence dyes using electrophoresis

To demonstrate the precision of our approach, we created ABC monomers that carried different fluorescence dyes at a pre-determined ratio within a single monomer (Figure 3.3). The monomers were characterized using gel electrophoresis (Figure 3.9a and 9b), which revealed that the fluorescence colors of the ABC monomers corresponded to the various combinations of donor Y-DNAs. Without adding the bridge DNA, only unconnected green donor Y-DNAs were appeared (Figure. 3.9b, lane 1). Un-reacted acceptor X-DNAs, which carried no fluorescence dyes, were dark and undetectable but could be seen upon staining with a DNA-specific dye, ethidium bromide (Figure 3.9c). After the *w* bridge DNA was added to the reaction, a single green band whose electrophoretic mobility was retarded could be observed (Figure

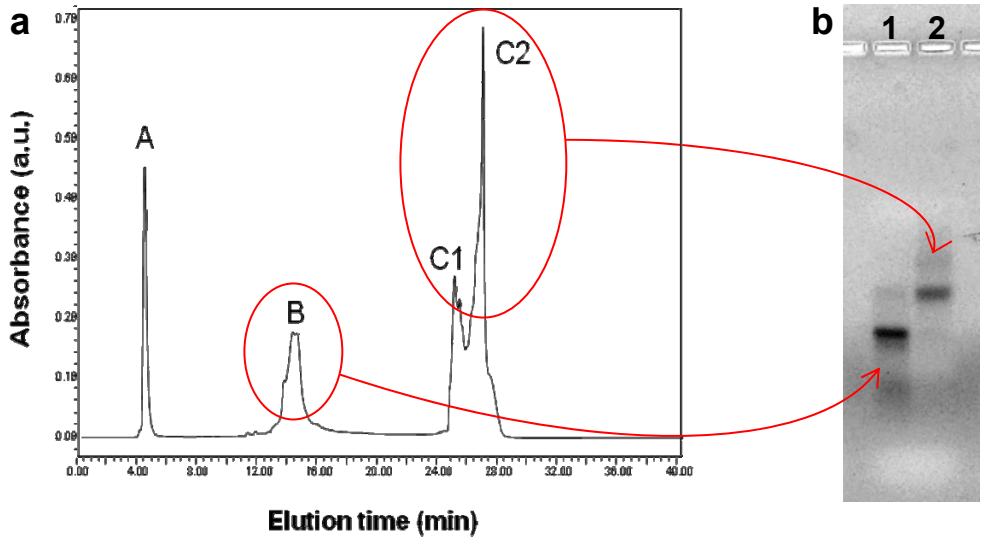

Figure 3.6. a, HPLC chromatogram of PEGA and Y-DNA conjugation reaction. The separation of PEGA-NHS (**A)**, NH_2-Y-DNA (**B)**, and PEGA-Y-DNA (**C1, C2)** were achieved by a gradient elution. **b**, Gel electrophoresis (3% agarose gel, EtBr staining) of HPLC fractions. Lanes 1 and 2 indicate NH_2-Y-DNA and PEGA-Y-DNA, respectively.

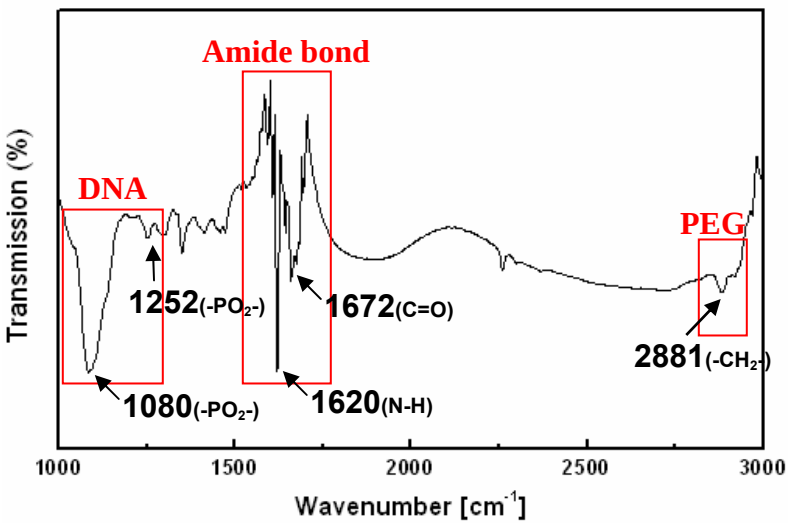

Figure 3.7. FTIR spectra (KBr) of PEGA-Y-DNA in the region of 3000 to 1000 cm^{-1}. [transmittance bands at 1080 and 1252 cm^{-1} in both spectra belong to PO_2 of DNA; 1620 cm^{-1} belongs to N-H of amide bond (amide II) and 1672 cm^{-1} belongs to C=O of amide bond (amide I). 2881 cm^{-1} belongs to CH_2 of PEG].

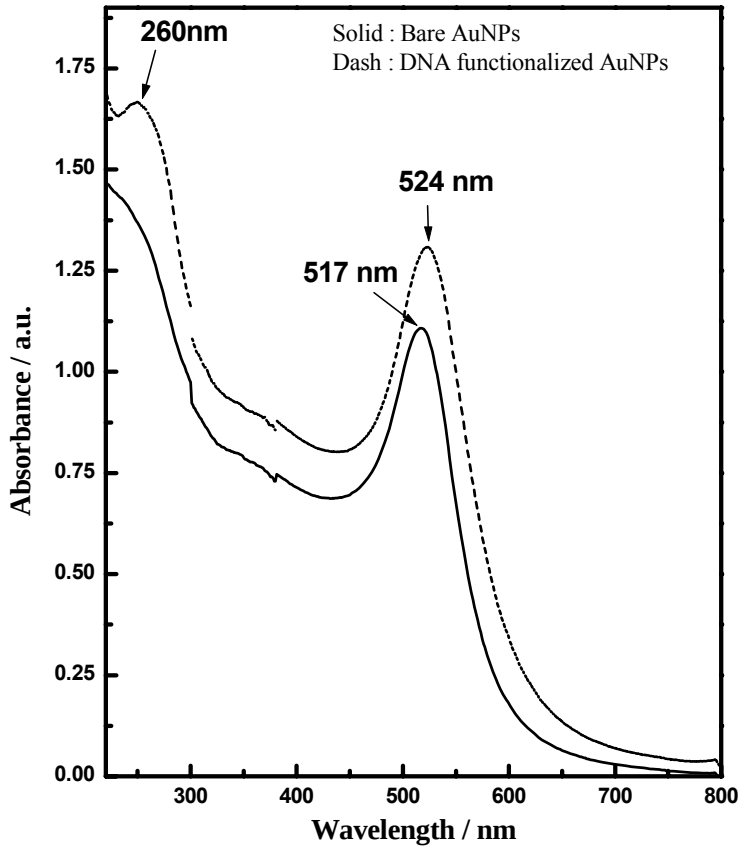

Figure 3.8. UV-visible absorbance spectra of aqueous gold nanoparticles before (solid line) and after (dash line) DNA attachment. Note that plasmon resonance peak shifts to red and the peak at 260nm appears after DNA binding.

3.9b, lane 2), suggesting that 1) the green fluorescence dye was exclusively attached to the *West* branch of the X-DNA (X-*W'*) and 2) the product was monodispersed. Similar results were obtained with fluorescence dye attached to the *East* and *North* branches of the X-DNA after adding *n* and *e* bridge DNA (Figure 3.9, lanes 3 and 4, respectively). To link two different configurations of fluorescence dyes simultaneously onto two different branches of a single X-DNA, we added two bridge DNAs simultaneously (Figure 3.9, lanes 5, 6, and 7). By adding all three bridge DNAs, all three different donor Y-DNAs were anisotropically linked onto the X-DNA simultaneously (Figure 3.9, lane 8) in a controlled fashion. This approach is robust and efficient; the estimated yield of ABC monomers is close to 90%, as estimated by densitometry.

3.4.3. Evaluation of ABC monomers with AuNP and QD using STEM

To characterize the ABC monomer at the individual molecule level, we generated donor Y-DNAs tethered with two different types of nanoparticles: AuNP and QDs. Both nanoparticles were individually visible via scanning transmission electron microscopy (STEM) (Figure 3.10a). A High magnification image is shown with an imaginary DNA molecule superimposed at scale bar = 25 nm (inset). The multi-moieties within one ABC monomer were obvious where two 15 nm rod-shaped QDs and one 5 nm round-shaped AuNP appear to be tethered together and are within the expected distance (Figure 3.10b). Although DNA molecules themselves were not visible in STEM, the distance between two QDs should be close to the distance of the DNA in between them, which was about 41 nm (considering a rigid DNA model with 0.34 nm per base pair; for the detailed calculation see Figure 3.10b). From STEM images, considering the center to center distance based on the assumption that the biotin-streptavidin conjugation occurs at the center of QDs, the average measured

Figure 3.9. a, Gel electrophoresis image of three donor Y-DNAs conjugated with one green fluorescence dye (1G), two red fluorescence dyes (2R), and one green and one red fluorescence dye (1G1R). **b,** Gel electrophoresis image of ABC monomers with different configurations. The resulting ABC monomers show different color bands determined by donor Y-DNAs which are connected to X-DNA by a specific bridge DNA. Unrelated donors, if any, are shown at the bottom because they can not be connected to acceptor X-DNA without presence of a corresponding bridge DNA (Lane 1). Lanes 5, 6 and 7 represent *w* + *n* (1G + 2R), *w* + *e* (1G + 1G1R), and *n* + *e* (2R + 1G1R), respectively. **c,** Gel electrophoresis migration pattern of ABC monomers after Ethidium Bromide (EtBr) staining. Lane 1 corresponds to X-DNA (top) and non-reacted Y-DNA (bottom). Note that X-DNA itself is not shown in gel electrophoresis images before EB staining. Lanes 2, 3, and 4 correspond to X-DNA connected with one Y-DNA (top). Lanes 5, 6, and 7 correspond to X-DNA connected with two Y-DNA (top). Lane 8 indicates that all three Y-DNA are connected onto X-DNA with all three bridge DNA.

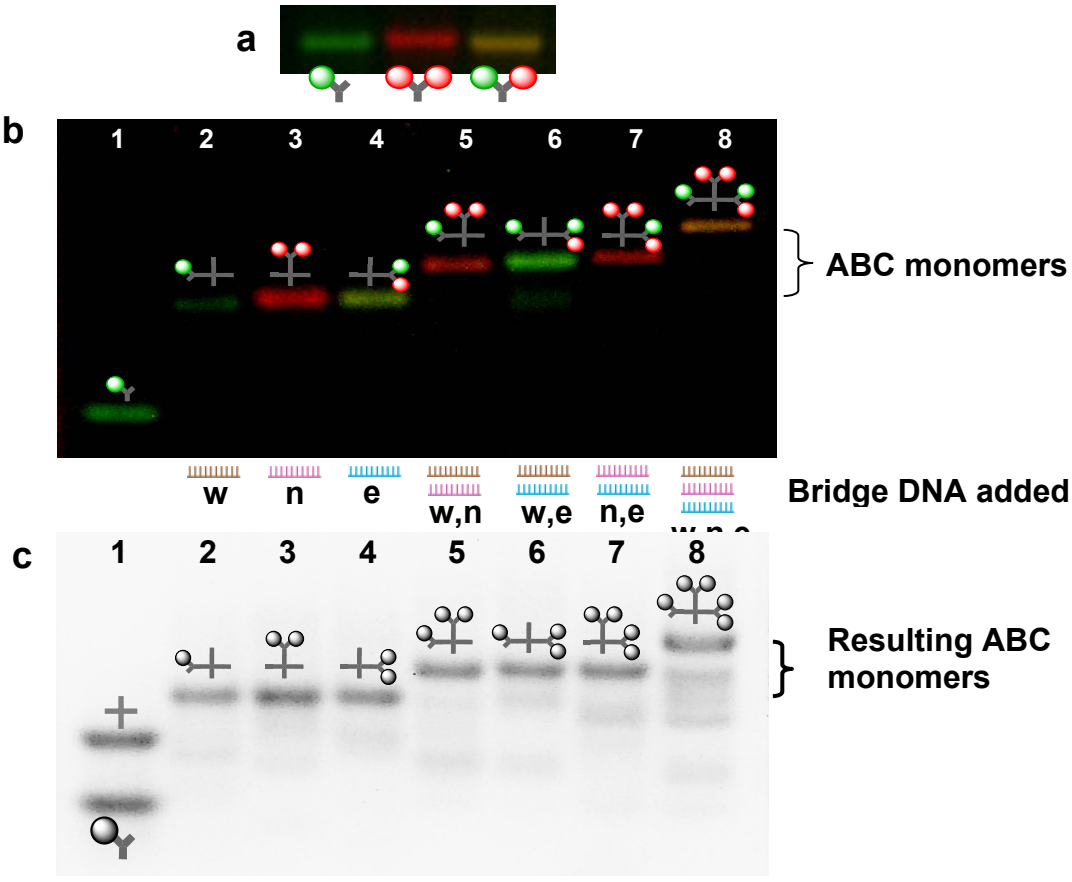
a
b
1
2
3
4
5
6
7
8
ABC monomers
w
n
e
w,n
w,e
n,e
Bridge DNA added
c
1
2
3
4
5
6
7
8
Resulting ABC monomers

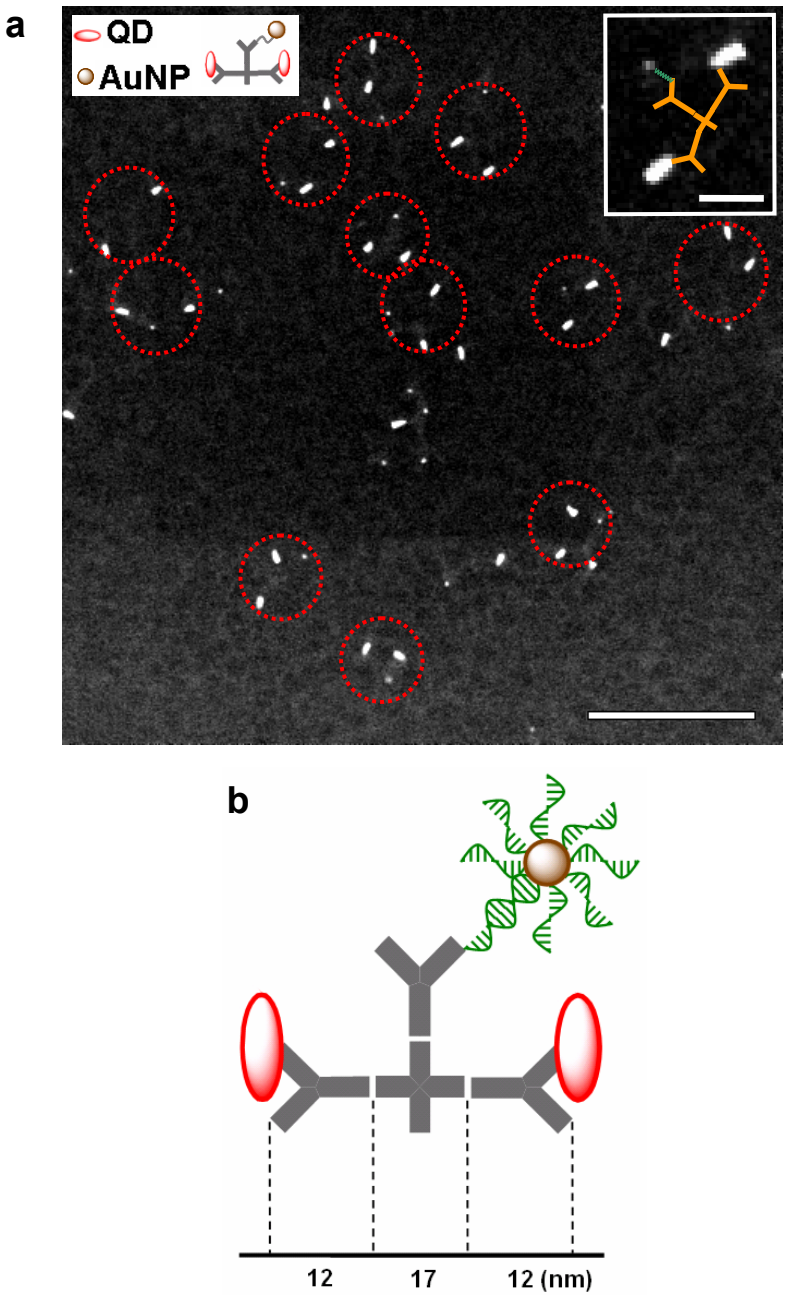

Figure 3.10. a, Annular dark-field STEM image of ABC monomers with nanoparticles (QD and AuNP). **b,** The distance between two QDs could be close about 41 nm which is calculated by considering a rigid DNA model with 0.34 nm per base pair.

distance between two QDs (with a AuNP in between) is obtained. The measured distance based on STEM images was 43.5 ± 8.5 nm. Because AuNP was bridged through a single-stranded DNA with extra poly A, whose persistence length is shorter than 1 nm, the position of the AuNP was, as expected, variable relative to the rest of the complex. These images revealed that different multi-moieties were individually and anisotropically placed at the accurate position within one ABC monomer.

3.4.4. Evaluation of ABC monomers with QD (QD DNA nanobarcodes)

We also generated quantum dot based ABC monomers (QD DNA nanobarcodes). The QDs of ABC monomers were individually detected via scanning transmission electron microscopy (STEM) (Figure 3.11). The three QDs within one DNA nanobarcode were obviously tethered together and were within the expected distance. In addition, QDs were also visible at both the bulk and solution scales through their intrinsic fluorescence (Figure 3.12). Before exposing the nanobarcode solution under UV-light, the solution did not show their fluorescence (Figure 3.12a). After the solution was exposed with a near-UV lamp, five distinguishable colors of QD-labeled DNA nanobarcodes excited (Figure 3.12b). From left to right (green to red), the ratios were 3G1R, 2G1R, 1G1R, 1G2R and 1G3R. These images revealed that different multi-moieties were individually and anisotropically placed accurately within one ABC monomer.

The resultant QD-labeled DNA nanobarcodes were first evaluated by attaching them on microbeads following literature procedures[30,31]. The overlay color (pseudocolor) images by fluorescence microscopy are shown in Figure 3.13a. The quantitative decoding fluorescent intensity ratios were obtained From the fluorescence microscope images of QD-nanobarcodes embedded microbeads emitting multiple-color signals depending on the ratio of red and green QDs (Figure 3.13b). Using a

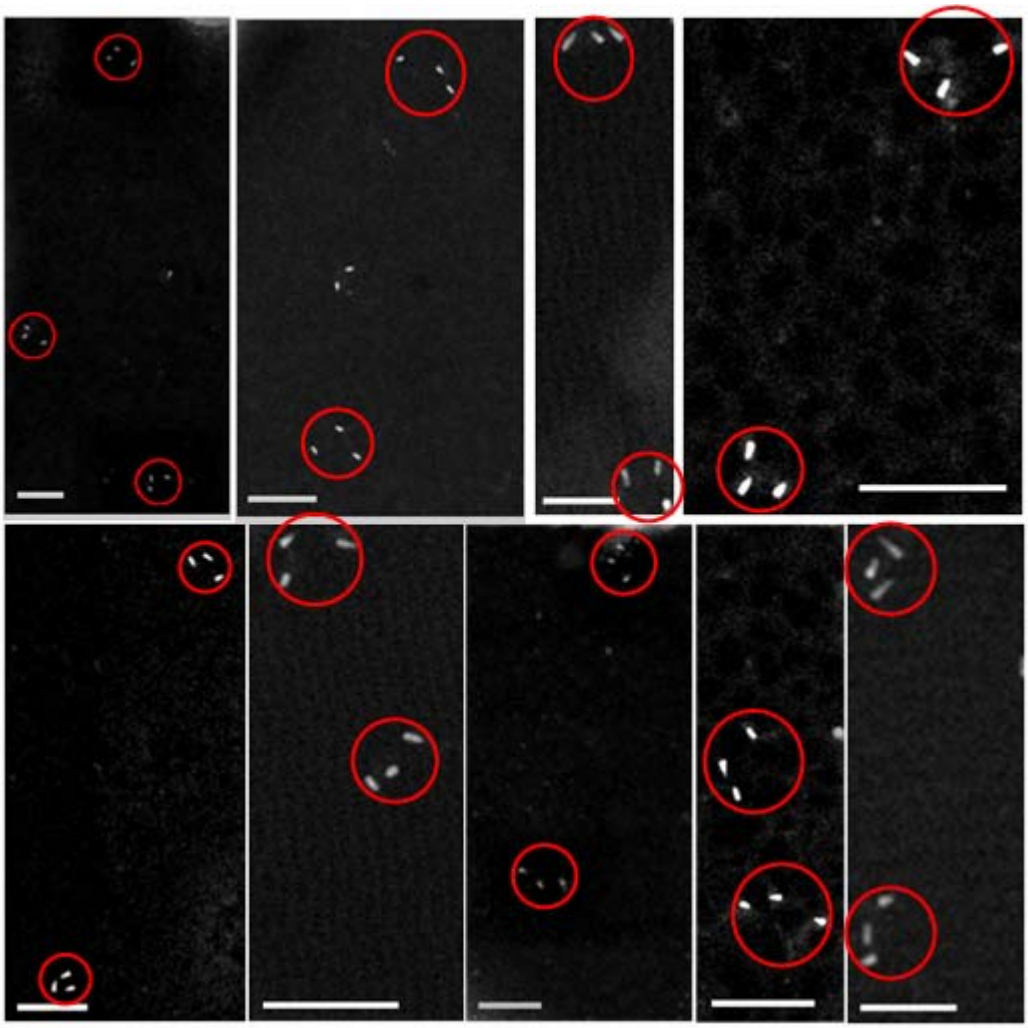

Figure 3.11. Annular dark-field STEM images of ABC monomers with three QDs at scale bar = 100 nm. Although DNA molecules themselves were not visible in STEM, the distance between QDs should be close to the distance of the DNA in between them, which was about 41 nm (considering a rigid DNA model with 0.34 nm per base pair). The measured distance based on STEM annular dark-field images was 44.8 ± 7.3 nm.

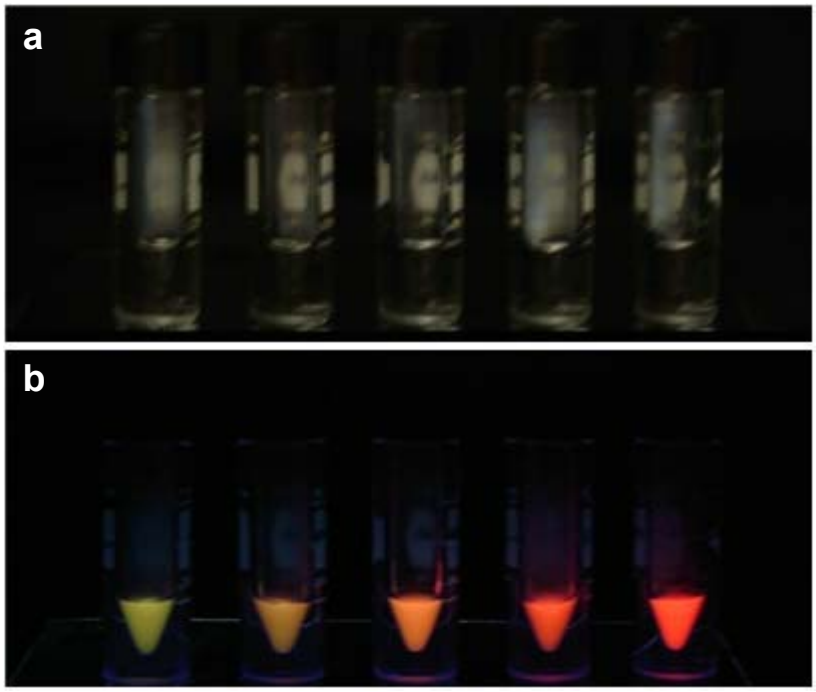

Figure 3.12. a, Digital camera image of five distinguishable colors of QD-labeled nanobarcodes before exposing the nanobarcodes solution under UV-light. **b,** After exposing the solution under UV-light, multiple nanobarcodes are shown with the ratios 3G1R, 2G1R, 1G1R, 1G2R and 1G3R from left to right (green to red).

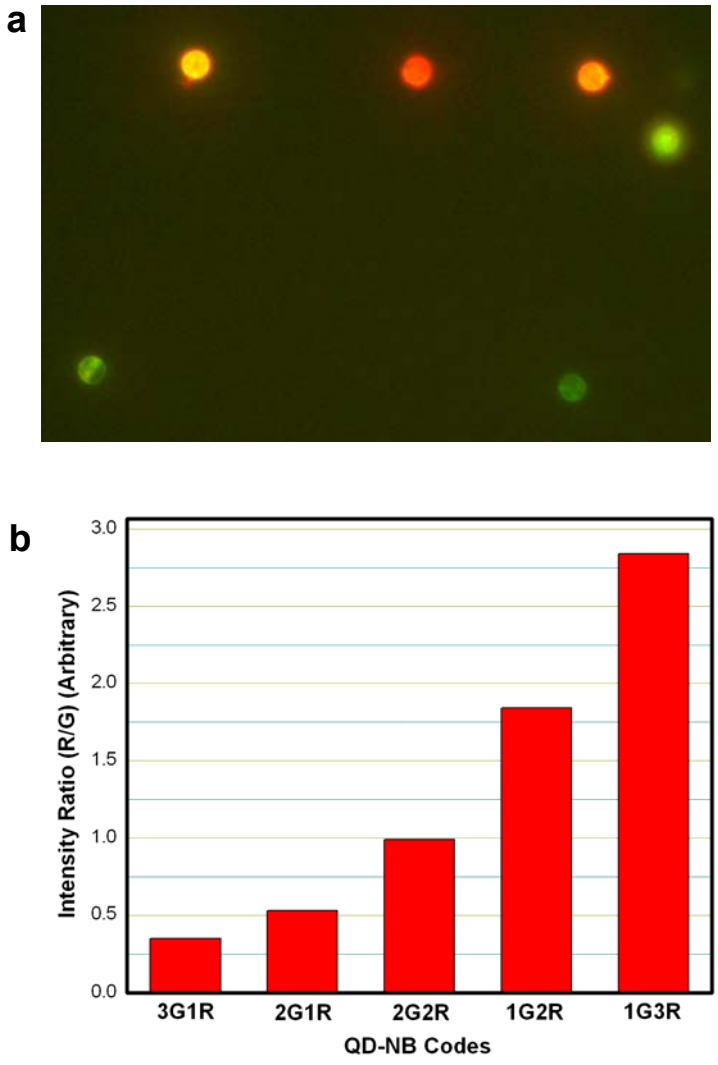

Figure 3.13. a, Fluorescence microscope image of a mixture of a variety of QD-nanobarcode immobilized microbeads emitting multiple-color signals depending on the ratio of red and green QDs**. b,** DNA nanobarcode quantitative decoding based on fluorescence intensity of microbeads.

2G2R nanobarcode as reference, the other four QD nanobarcodes can be easily decoded. Therefore, these DNA nanobarcodes and ABC monomers can be applied for multiplexed DNA detection.

3.4.5. Target-driven polymerization for pathogen DNA detection

3.4.5.1. Design of target-driven polymerization

To synthesize multifunctional nano-architectures from an ABC monomer, we designed each ABC monomer to possess two QDs with three different color configurations (2G, 1G1R, or 2R), one photo-responsive PEGA moiety, and one single-stranded oligonucleotide probe that is complementary to a specific pathogen DNA such as *SARS coronavirus*, *Ebola* virus, or *Bacillus anthracis* (this unique DNA is termed "capture probe", see **1A** and **1B** in Figure 3.14, and Table 3.3). Consequently, an ABC dimer formed only in the presence of a targeted pathogen DNA because the pathogen DNA now served as a complementary linker DNA to link the two ABC monomers **1A** and **1B** together (see **2** in Figure 3.14). Upon a short UV illumination (10 min), photo-crosslinking occurred with the dimers but not with the monomers (Figure 3.14, species **3**). With unrelated DNA, polymerization was not observed (see **4** and **5** in Figure 3.14). In other words, we have successfully developed a "target-driven" polymerization where polymers (diblock co-polymers in this case) can only be synthesized in the presence of a specific target DNA. To the best of our knowledge, this is the first time that a polymerization process has been designed to be dependent on the presence of a pathogen DNA. This novel polymerization approach can be utilized to generate detectable polymers for pathogen sensing.

3.4.5.2. Evaluation of target-driven polymerization

We employed atomic force microscopy (AFM) to image the morphology of the pathogen-target-driven polymer. The image in Figure 3.15a shows that the polymerized ABC monomers are nearly spherical in shape. Because each monomer contained two specific QDs with a pre-determined ratio (1G1R), the formation of the target-driven polymers was further evaluated by both bright-field and epi-fluorescence optical microscopy (Figure 3.15b and c). The overlay of bright-field and fluorescence images confirmed again that the polymeric spheres were generated from ABC monomers due to the unique 1G1R fluorescence ratio (Figure 3.15c). Dynamic light scattering (DLS) measurement revealed that the average diameter was 410 ± 70 nm (Figure 3.16a). Interestingly, the polymerization efficiency was very high as shown by the lack of a monomer peak post-polymerization (Figure 3.16a). In addition, the diameters of resulting polymeric spheres can be further controlled by varying the concentrations of the initial ABC monomer (Figure 3.16b).

3.4.5.3. Evaluation of DNA Pathogen detection by Target-driven polymerization

Aside from being able to link several hundred QDs together and thus effectively amplify signals from a single target-binding event, each target-driven polymer also contains a unique fluorescence code with a specific ratio of green and red; this feature makes it possible to detect multiple targets simultaneously. Here, three different pathogen DNAs (*SARS*, *Ebola*, and *Anthrax*) were used as target DNAs (for sequences see Supplementary Information, Table S3). We first added an "unknown" DNA and after the target-driven photo-polymerization the resultant spheres possessed a color ratio of 1G1R (Figure 3.17a). By referring to the pre-assigned fluorescence codes (Table 3.4), this result indicated that the "unknown" DNA

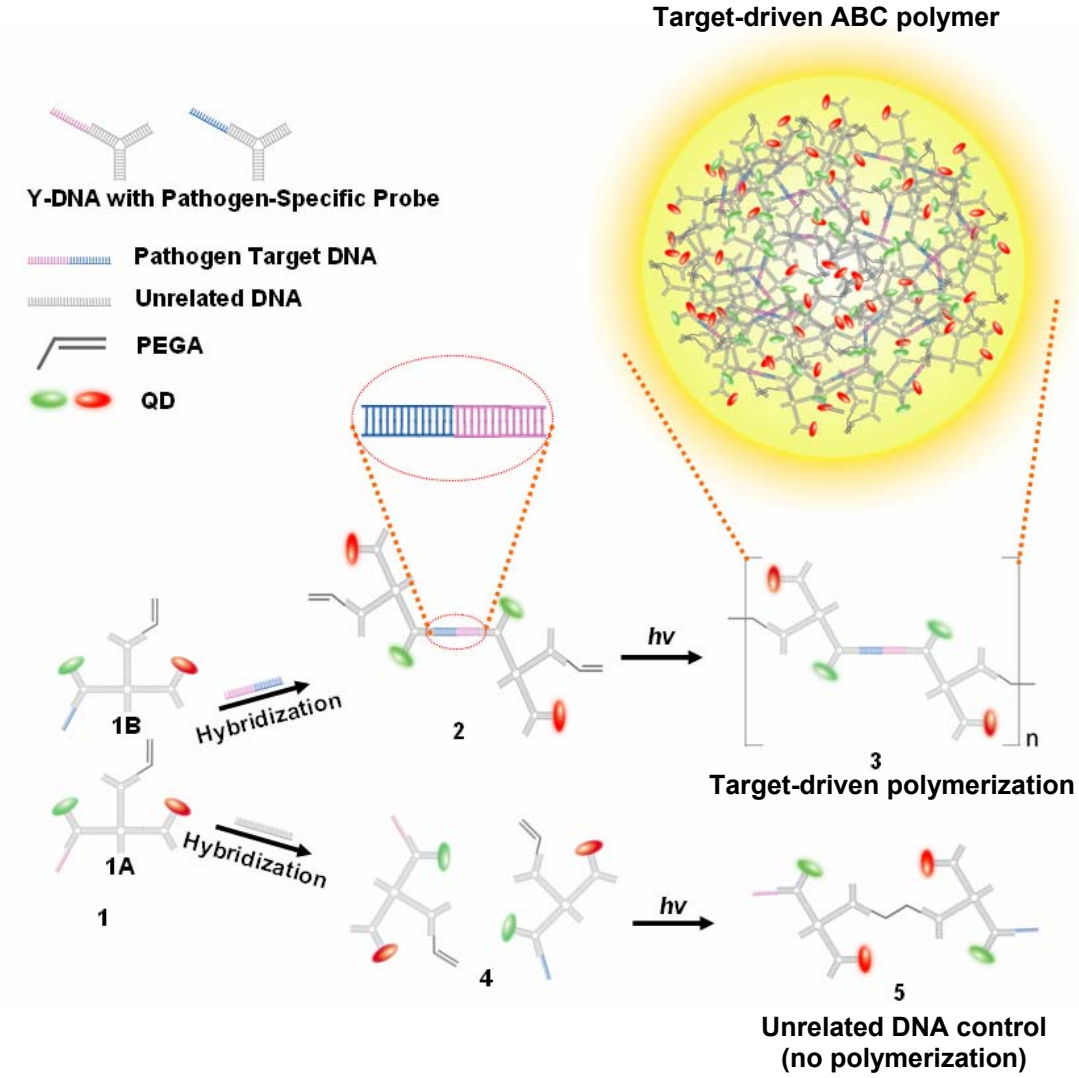

Figure 3.14. Schematic drawing of target-driven polymerization.

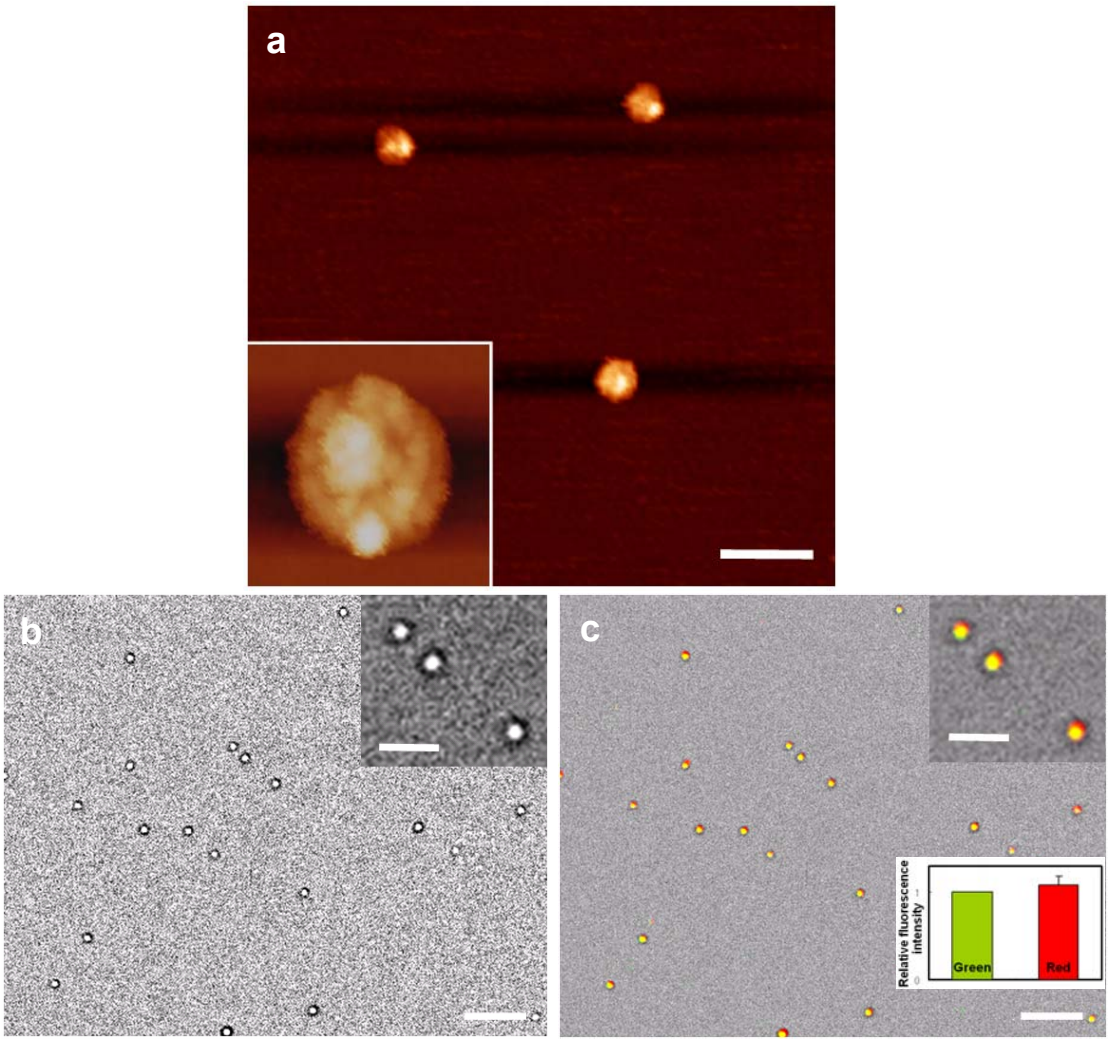

Figure 3.15. a, Atomic force microscopy (AFM) image of polymeric spheres and with a higher magnification (inset). Scale bar indicates 1 μm. **b**, Bright-field optical microscopy images after photo-crosslinking and **c**, overlay image of with bright-field and fluorescence. The scale bar indicates 5 μm (inset, 2 μm).

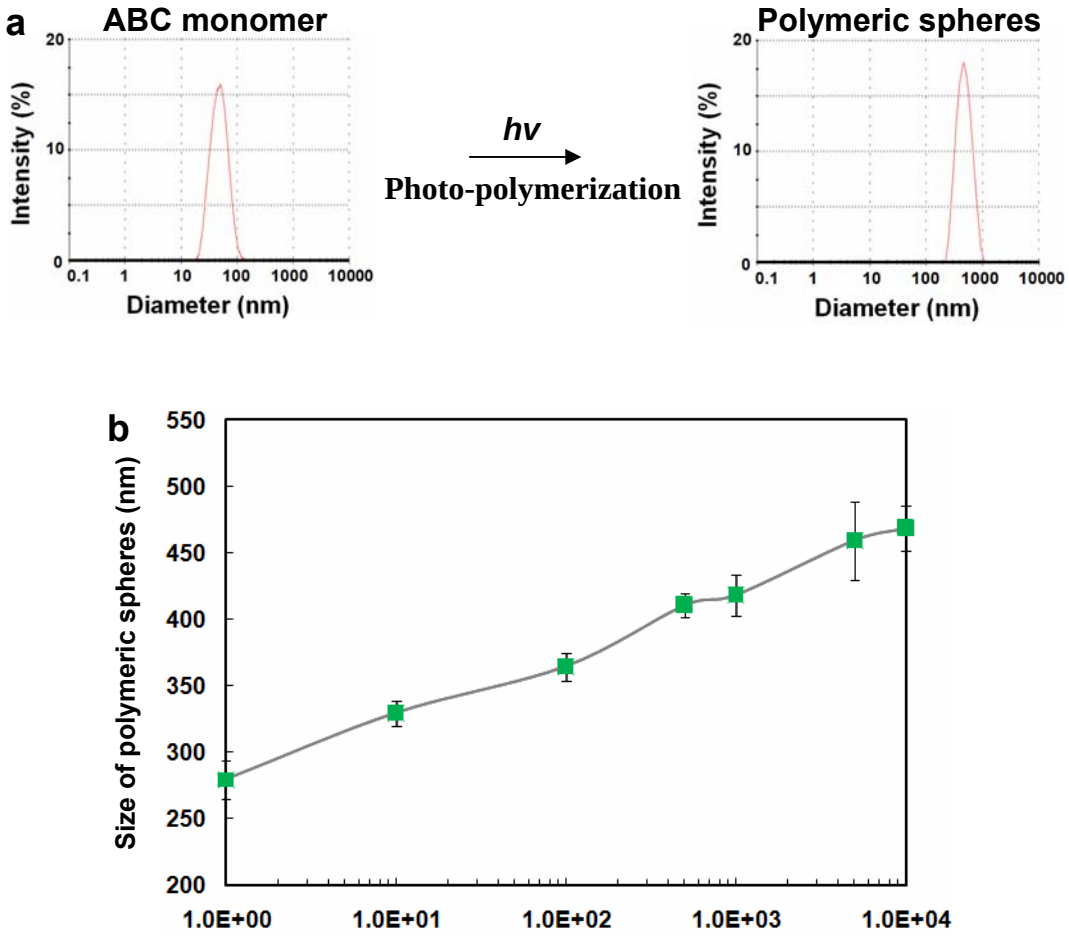

Figure 3.16. Dynamic light scattering data of the ABC monomers and polymeric spheres. **a**, The increase of size of the polymeric spheres after photo-polymerization. **b**, Changes of polymeric sphere sizes with different concentrations of ABC monomers.

Table 3.4. Pre-assigned fluorescence code library of nano-architectures

Polymeric sphere	ABC monomer 1	ABC monomer 2	Target DNA
1G3R	2R	1G1R	Bacillus anthracis
4G0R	2G	2G	Ebola virus
2G2R	1G1R	1G1R	SARS Coronavirus
(No polymer formation)	1G1R	1G1R	Unrelated DNA

To experimentally decode the color signal of polymeric spheres, the signal intensity is counted as photon counts per pixel area with a pixel in the microscope image.

Figure 3.17. Detection of pathogen DNA via target-driven polymerization of ABC monomers. **a, b, c**, Fluorescence microscopic images of target-driven polymers with pathogen DNAs including *SARS*, *Bacillus anthracis*, and *Ebola*, respectively. Orange colored (1G1R) polymeric spheres were generated from ABC monomers which were dimerized by *SARS* DNA in **a**. 1G3R and 4G coded polymeric spheres were produced by Bacillus anthracis and Ebola pathogen DNA in **b** and **c**, respectively. **d**, By incubating 1G1R ABC monomers with an unrelated pathogen DNA, no polymerized DNA materials were observed. All scale bars are 5μm. **e**, Relationship between the number of polymerized spheres per 140 × 180 μm^2 and the concentration of pathogen DNA for determining the sensitivity of detection through target-driven polymerization. The coefficient of variation (CV) of the assay ranged from 5.6% to 10.4%, depending on the concentration of the target pathogen DNA (for more details see Supplementary Information, Table 5).

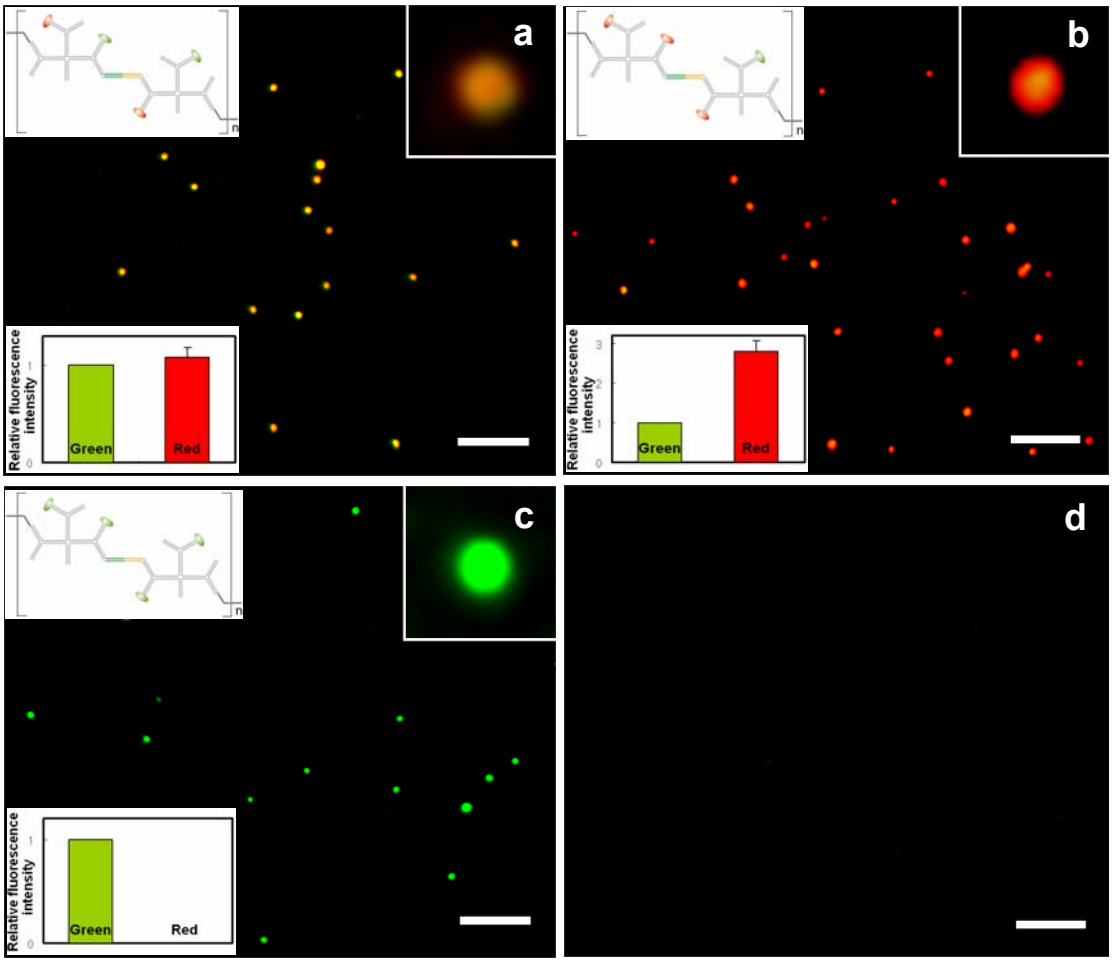
a
b
c
d
Relative fluorescence intensity
Green
Red

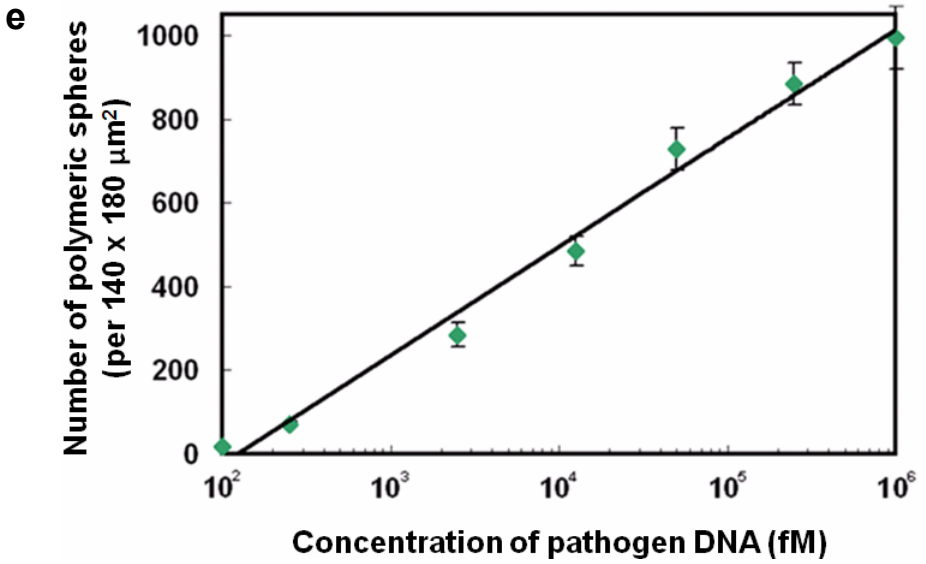
e
Number of polymeric spheres (per 140 x 180 μm²)
1000
800
600
400
200
0
10²
10³
10⁴
10⁵
10⁶
Concentration of pathogen DNA (fM)

was the *SARS* DNA. Similarly, Anthrax and Ebola DNA were detected with 1G3R and 4G0R, respectively (Figure 3.17b and c). The detection was highly specific: in the presence of an unrelated DNA, no polymerized spheres were observed (Figure 3.17d) because polymerization could not occur with only mono-PEGA-ABC monomers. Interestingly, we found that the concentrations of polymeric spheres (i.e, number per unit area from microscopy images) were linearly proportional to the log of concentrations of target DNA (Figure 3.17e). Thus we can easily detect the presence and approximate concentration of the pathogen DNA by simply counting the polymeric spheres under the microscope. The estimated detection limit was 100 fM at the current conditions (Figure 3.17e). Moreover, this method allows for a wide dynamic range (4 orders of magnitude) of detection.

3.4.6. Evaluation of ABC polymer as multi-drug delivery vector

In addition to detecting pathogen DNA, the ABC polymeric spheres can also serve as multi-drug delivery vectors due to their intrinsic multivalency and anisotropicity. The built-in DNA scaffolds also provide an ideal interface for nucleic acid-based drugs (Figure 3.18). Here, polymerized spheres were delivered to cells with both model drugs [oligonucleotide (ODN) and siRNA] and tracers (QDs). Microscopy images revealed that similar-sized spheres were internalized by HeLa cells (Figure 3.19a-c). The cellular uptake was attributed to endocytosis because no fluorescence was observed inside cells when endocytosis was inhibited (Figure 3.20a and b). These results suggest that the cells can internalize these multi-drug carriers without any additional treatment with a transfection reagent. To further understand the uptake mechanisms, we evaluated the cellular uptake in the presence of various endocytosis-specific inhibitors. Internalization of polymeric spheres was severely reduced in cells treated with inhibitor Cytochalasin B, suggesting that actin-dependent

endocytosis such as phagocytosis and macropinocytosis was the main mechanism (Figure 3.21).

3.4.7. Cytotoxicity of ABC polymer

It is noteworthy that these ABC polymers exhibit little cytotoxicity. After a 36-hour treatment with ABC monomers, HeLa cells showed more than 90% cell viability [or less than 10% cytotoxicity was observed (Figure 3.22)]. Using the conditions reported here, we were able to obtain a delivery efficiency of 25% (data not shown). Although further investigations are needed to optimize the delivery efficiency, we have demonstrated that our ABC polymers provide a general route to carry different moieties within one entity for both delivery and tracing.

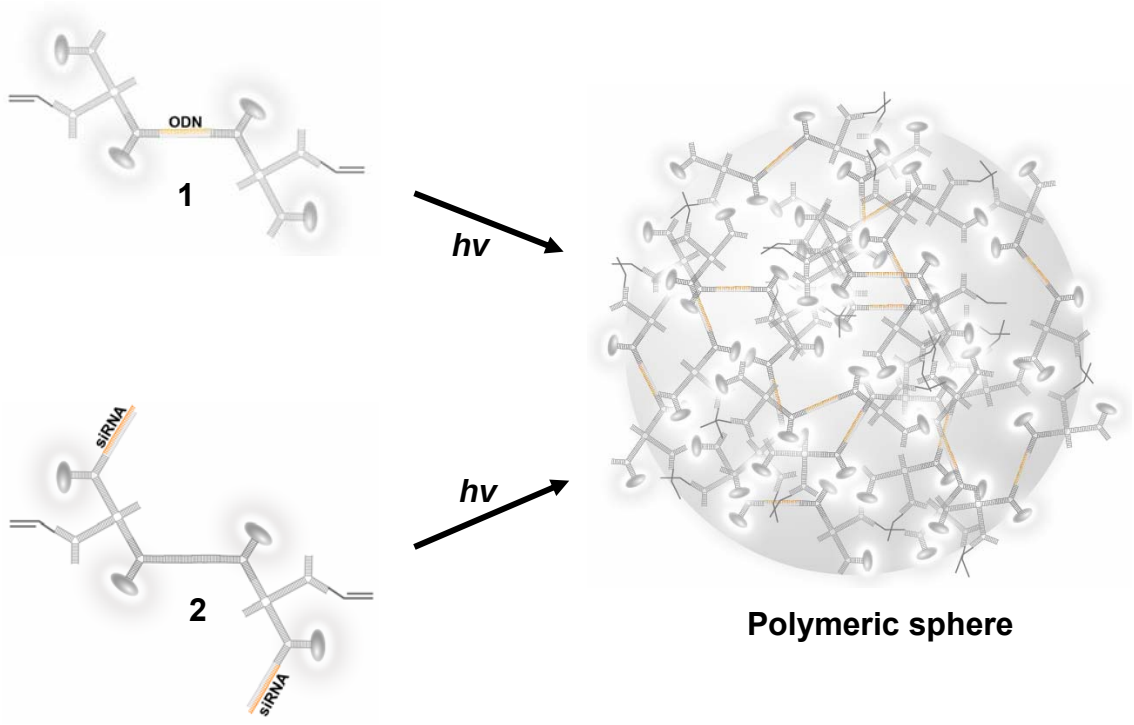

Figure 3.18. Schematic drawing of nucleic-acid-based drug loading into polymeric spheres with ODN **1** or siRNA **2**. Both ODN and siRNA can be loaded in the sphere by hybridization.

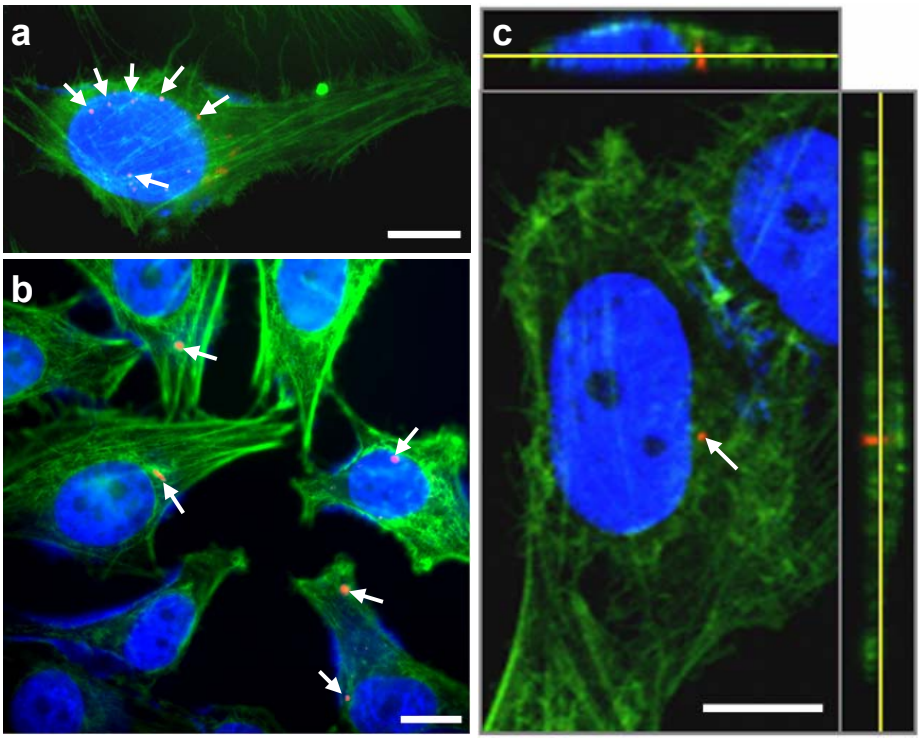

Figure 3.19. Microscopic images of HeLa cell treated with polymeric spheres at 37°C overnight and cytotoxicity studies. **a** and **b,** Fluorescence microscopic images (blue: nuclei, green: actin, red :polymeric spheres). All scale bars are 10 µm. **c**, Confocal microscopy image with resliced regions of interest. The resliced image shows that polymeric spheres are uptaken by HeLa cells.

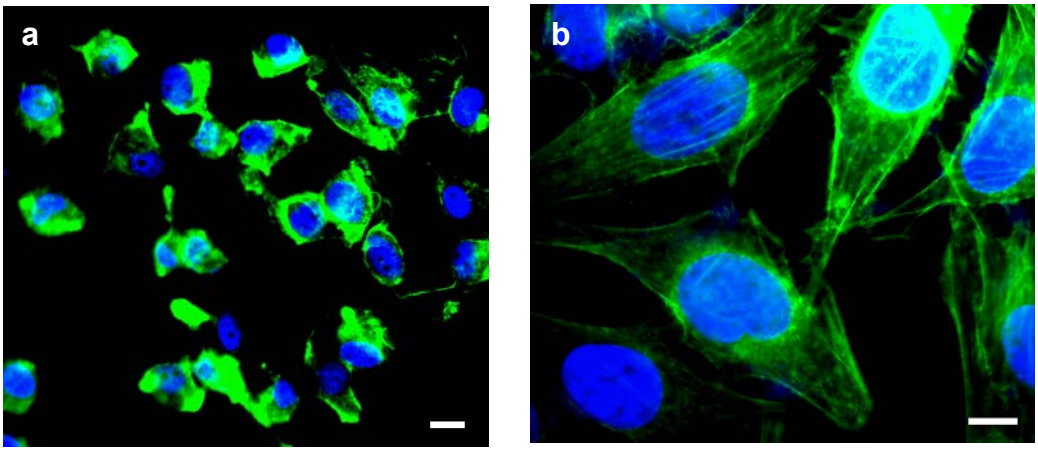

Figure 3.20. Fluorescence microscopic images of HeLa cell treated with polymeric spheres (blue: nuclei, green: actin), **a**, at 4°C overnight, and **b**, at 37°C for 10min. Scale bar is 10 μm.

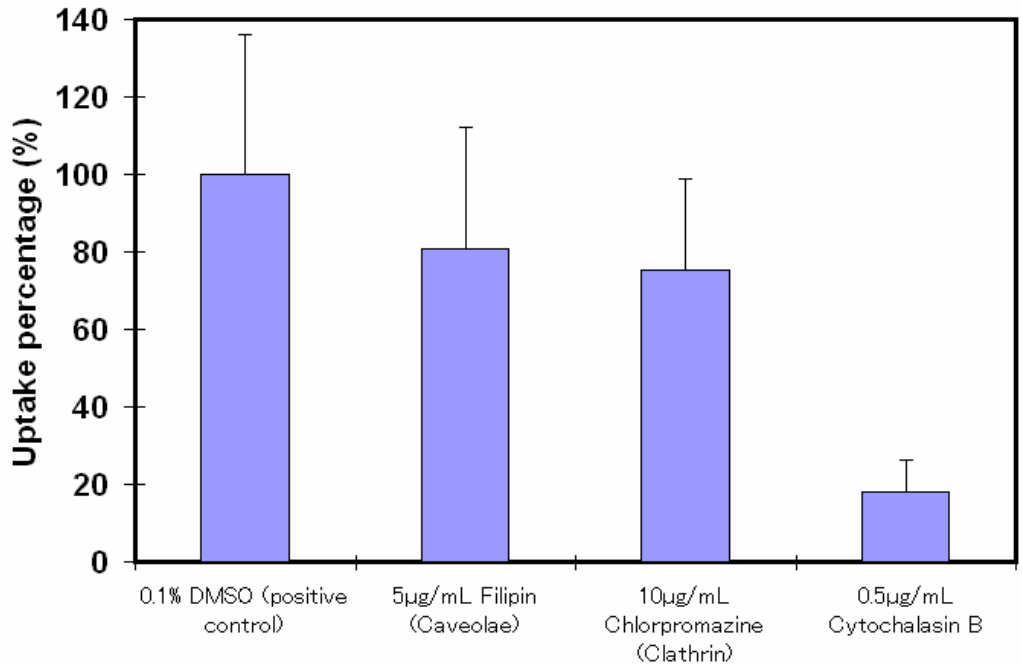

Figure 3.21. Cellular uptake of polymeric spheres in the presence of various endocytosis-specific inhibitors.

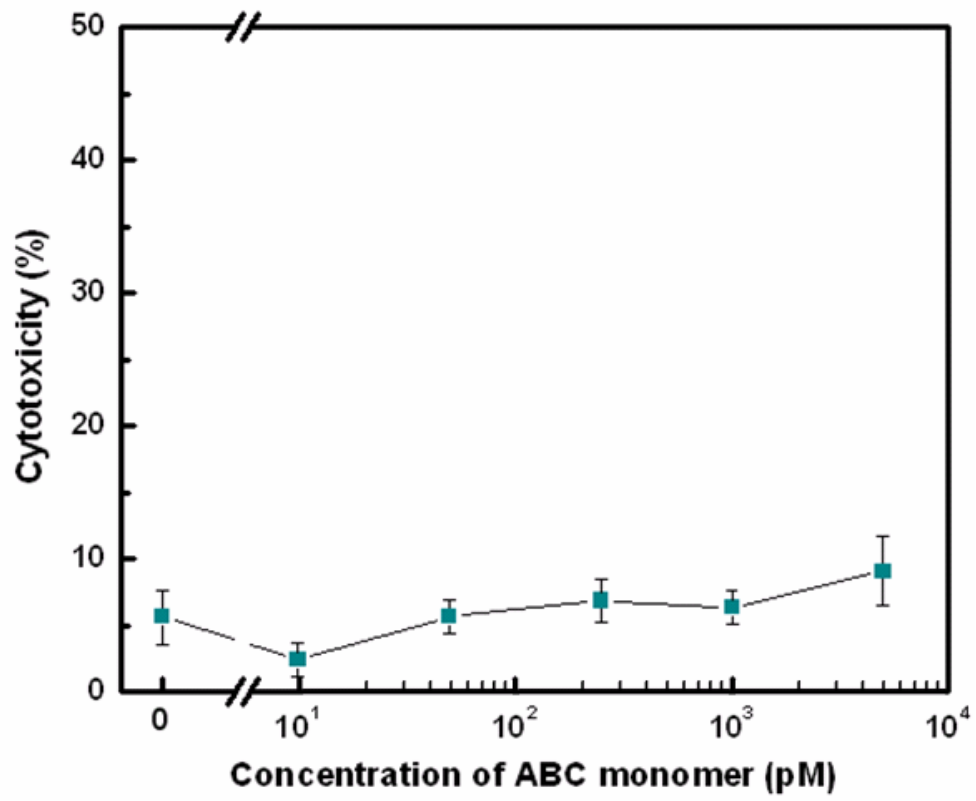

Figure 3.22. Cytotoxicity studies of polymeric spheres. The assay shows cytotoxicity after 36 hour exposures of cells to 0.01, 0.05, 0.25, 1, and 5 nM ABC monomers.

3.5 Conclusion

In summary, we have created anisotropic, branched, and crosslinkable monomers that are DNA-based and can be precisely manipulated. Using these ABC monomers, we have also developed a general approach to generate multifunctional nano-architectures that cannot be achieved with the current building blocks. In particular, we demonstrated, for the first time, a target-driven polymerization that can be used to rapidly amplify signals to detect pathogens with high specificity and sensitivity. In addition, we showed that these nano-architectures can be utilized as multi-drug carriers which are readily internalized by cells without any other chemical reagents. It is important to note that our ABC monomer system is designed to be modular. The built-in "plug-and-play" feature coupled with the "mix-and-match" flexibility makes the ABC monomer a versatile platform technology – any other functional groups, both organic and inorganic, that can be conjugated with DNA (or RNA), can be incorporated into the final nano-architectures. Thus, we anticipate that our ABC monomers will open myriad possibilities for creating more novel nanostructures and nanomaterials with multiple functionalities.

REFERENCE

1. Glotzer, S.C. & Solomon, M.J. Anisotropy of building blocks and their assembly into complex structures. *Nat. Mater.* **6**, 557-562 (2007).
2. Grill, L. et al. Nano-architectures by covalent assembly of molecular building blocks. *Nat. Nanotech.* **2**, 687-691 (2007).
3. Javey, A., Nam, S., Friedman, R.S., Yan, H. & Lieber, C.M. Layer-by-layer assembly of nanowires for three-dimensional, multifunctional electronics. *Nano Lett.* **7**, 773-777 (2007).
4. Slocik, J.M., Tam, F., Halas, N.J. & Naik, R.R. Peptide-assembled optically responsive nanoparticle complexes. *Nano Lett.* **7**, 1054-1058 (2007).
5. Pregibon, D.C., Toner, M. & Doyle, P.S. Multifunctional encoded particles for high-throughput biomolecule analysis. *Science* **315**, 1393-1396 (2007).
6. Torchilin, V.P. Multifunctional nanocarriers. *Adv. Drug Del. Rev.* **58**, 1532-1555 (2006).
7. Salem, A.K., Searson, P.C. & Leong, K.W. Multifunctional nanorods for gene delivery. *Nat. Mater.* **2**, 668-671 (2003).
8. Alivisatos, P. The use of nanocrystals in biological detection. *Nat. Biotechnol.* **22**, 47-52 (2004).
9. Busby, M., Kerschbaumer, H., Calzaferri, G. & De Cola, L. Orthogonally bifunctional fluorescent zeolite-L microcrystals. *Adv. Mater.* **20**, 1614-+ (2008).
10. Popovic, Z., Busby, M., Huber, S., Calzaferri, G. & De Cola, L. Assembling micro crystals through cooperative coordinative interactions. *Angew. Chem. Int. Edn* **46**, 8898-8902 (2007).

11. Popovic, Z., Otter, M., Calzaferri, G. & De Cola, L. Self-assembling living systems with functional nanomaterials. *Angew. Chem. Int. Edn* **46**, 6188-6191 (2007).

12. Lee, C.C. et al. A single dose of doxorubicin-functionalized bow-tie dendrimer cures mice bearing C-26 colon carcinomas. *Proc. Natl Acad. Sci. USA* **103**, 16649-16654 (2006).

13. Lee, C.C., Mackay, J.A., Frechet, J.M. & Szoka, F.C. Designing dendrimers for biological applications. *Nat. Biotechnol.* **23**, 1517-1526 (2005).

14. Guillaudeu, S.J. et al. PEGylated dendrimers with core functionality for biological applications. *Bioconjug. Chem.* **19**, 461-469 (2008).

15. Goodman, R.P. et al. Reconfigurable, braced, three-dimensional DNA nanostructures. *Nat. Nanotech.* **3**, 93-96 (2008).

16. Venkataraman, S., Dirks, R.M., Rothemund, P.W., Winfree, E. & Pierce, N.A. An autonomous polymerization motor powered by DNA hybridization. *Nat. Nanotech.* **2**, 490-494 (2007).

17. Rothemund, P.W. Folding DNA to create nanoscale shapes and patterns. *Nature* **440**, 297-302 (2006).

18. Seeman, N.C. DNA in a material world. *Nature* **421**, 427-431 (2003).

19. He, Y. et al. Hierarchical self-assembly of DNA into symmetric supramolecular polyhedra. *Nature* **452**, 198-U141 (2008).

20. Xu, X., Rosi, N.L., Wang, Y., Huo, F. & Mirkin, C.A. Asymmetric functionalization of gold nanoparticles with oligonucleotides. *J. Am. Chem. Soc.* **128**, 9286-9287 (2006).

21. Fu, A. et al. Discrete nanostructures of quantum dots/Au with DNA. *J. Am. Chem. Soc.* **126**, 10832-10833 (2004).

22. Feldkamp, U. & Niemeyer, C.M. Rational design of DNA nanoarchitectures. *Angew. Chem. Int. Edn* **45**, 1856-1876 (2006).

23. Zheng, J. et al. Two-dimensional nanoparticle arrays show the organizational power of robust DNA motifs. *Nano Lett.* **6**, 1502-1504 (2006).

24. Lin, C., Liu, Y. & Yan, H. Self-assembled combinatorial encoding nanoarrays for multiplexed biosensing. *Nano Lett.* **7**, 507-512 (2007).

25. Park, S.H. et al. Programmable DNA self-assemblies for nanoscale organization of ligands and proteins. *Nano Lett.* **5**, 729-733 (2005).

26. Pinto, Y.Y. et al. Sequence-encoded self-assembly of multiple-nanocomponent arrays by 2D DNA scaffolding. *Nano Lett.* **5**, 2399-2402 (2005).

27. Rinker, S., Ke, Y., Liu, Y., Chhabra, R. & Yan, H. Self-assembled DNA nanostructures for distance-dependent multivalent ligand-protein binding. *Nat. Nanotech.* **3**, 418-422 (2008).

28. Claridge, S.A., Liang, H.W., Basu, S.R., Frechet, J.M. & Alivisatos, A.P. Isolation of discrete nanoparticle-DNA conjugates for plasmonic applications. *Nano Lett.* **8**, 1202-1206 (2008).

29. Li, Y. et al. Controlled assembly of dendrimer-like DNA. *Nat. Mater.* **3**, 38-42 (2004).

30. Li, Y., Cu, Y.T. & Luo, D. Multiplexed detection of pathogen DNA with DNA-based fluorescence nanobarcodes. *Nat. Biotechnol.* **23**, 885-889 (2005).

31. Um, S., Lee, J., Kwon, S., Li, Y. & Luo, D. Dendrimer-Like DNA (DL-DNA) Based Fluorescence Nanobarcodes. *Nat. Prot.* **1**, 995-1000 (2006).

32. Um, S.H. et al. Enzyme-catalysed assembly of DNA hydrogel. *Nat. Mater.* **5**, 797-801 (2006).

CHAPTER 4

Liquid-like DNA hydrogel by rolling circle chain reaction (RCCR)

4.1 Abstract

A remarkable hydrogel made entirely from DNA that was elongated by a rolling circle chain reaction (RCCR) was successfully synthesized. The gelling process was based on the physical interactions of long DNA strands as opposed to base pairing. To the best of our knowledge, this gel is the first DNA hydrogel which is not based on base pairing. These biocompatible and biodegradable DNA hydrogels were almost fluid-like but still held a specific shape and gel properties. They were easily transformed back and forth to any shape depending on the mold. In addition, the hydrogels exibited thermoplastic behavior, remembering the mold shape in water after being extracted from the mold. Inspired by these characteristics of liquid-like DNA hydrogels, we have developed an injectable extracellular matrix for tissue engineering.

4.2 Introduction

Hydrogels have recently been developed as attractive biomaterials for applications in the biomedical and pharmaceutical fields[1]. The most commonly studied properties of hydrogels are their sensitivities in physiological or biological environment[2, 3]. Hydrogels environmentally responsive to pH[4], temperature[5], ionic strength[6], light[7, 8], antigens[9, 10], or DNA[11] have been often applied toward controlled drug delivery via swelling changes. In addition, much research attention has been paid to three dimensional hydrogel that can provide suitable environments for cell culture, because significant differences in behavior of cells exist between 2D and 3D culture[12-14]. For the purpose of cell culturing, the properties of hydrogel need to be similar to the microenvironment of native tissues[15].

To benefit from the programmability of DNA, hydrogels based on DNA-polymer conjugates in semi-interpenetrating networks (semi-IPN) have been synthesized[16, 17].

A sol-gel transition of hydrogels by DNA-strand displacement has been achieved with chemically crosslinking of DNA and polyacryamide[18]. However, chemically crosslinked hydrogels could be unsafe to use in biological systems because of potentially adverse side effects[19-21]. Previously we synthesized a DNA hydrogel entirely from branched DNA via ligase, based on our early achievements such as syntheses of dendrimer-like DNA and DNA nanobarcodes[22-24]. This pure DNA hydrogel is extremely biocompatible and biodegradable. Herein we report the extremely simple preparation of a remarkable liquid-like hydrogel entirely from DNA that was produced by a rolling circle chain reaction (RCCR), a modification of rolling circle amplification (RCA) and polymerase chain reaction (PCR). This gelling process was totally based on the physical entanglement of the elongated DNA strands as opposed to base pairing. The advantages are that the gelling processes are achieved under physiological conditions, and the physical properties of these hydrogels are easily tuned to provide suitable environments for the proliferation of cells.

RCA is a simple enzymatic method that can produce long single-stranded DNA (ssDNA) with a desired repeating sequence unit via Ø29 DNA polymerase[25-27]. Because of Ø29 DNA polymerase's strong ability to displace newly synthesized DNA strands, DNA polymerase produces continuous nucleotide additions to growing DNA strands over the circular DNA templates under isothermal conditions[28, 29]. With the strand-displacement activity of Ø29 DNA, PCR is performed by simply adding two different primers without adjusting the temperature for annealing. Since no other chemicals are used, the resultant DNA hydrogel retains general DNA properties such as biocompatibility and biodegradability. Mechanically, it is very robust but can easily change its shape depending on the mold.

4.3 Materials and Methods

4.3.1. Chemicals and DNA sequences

Ø29 DNA polymerase was purchased from New England Biolabs (Beverly, MA) in pure form at a concentration of 10,000 units / ml. Oligonucleotides were commercially synthesized and PAGE purified (Integrated DNA Technologies, Coralville, Iowa). Sequences of the oligonucleotides are listed in Table 4.1.

4.3.2 Preparation of circular DNA templates

0.5 μM of phosphorylated linear ssDNA was treated with 5 unit/μL of CircLigase ssDNA Ligase (Epicentre Biotechnologies, Madison, WI) overnight at 65ºC in 200 μL of commercially provided reaction buffer (50 μM of ATP, 2.5 mM of $MnCl_2$). The resultant solution was incubated at 80ºC for 10 min to inactivate the CircLigase, then gradually cooled down to 4ºC. To remove the non-circularized linear ssDNA template, 300U of Exonuclease I and 3,000U of Exonuclease III (New England Biolabs, Beverly, MA) were added to the solution. This solution was incubated at 37ºC for 3hrs and was then incubated at 80ºC for 40min followed by gradual cooling down to inactivate the exonucleases.

4.3.3 Hybridization of circular templates with primer1

The hybridization was carried out at room temperature for 2 hours by incubating an equimolar solution of primer1 and circular DNA in TE buffer [10mM Tris, 1mM EDTA (pH8.0)].

4.3.4 Synthesis of DNA hydrogel by DNA polymerization

10nM of circular templates hybridized with primer1 were incubated with Ø29 DNA polymerase (1 unit/μL) at 30°C for 4h in the reaction buffer [50mM Tris-HCL,

10mM $(NH_4)_2SO_4$, 10mM $MaCl_2$, 4mM dithiothreitol, 200μg/ml bovin serum albumin, 50mM dNTP]. After the first rolling circle polymerization with primer1, 10pM of primer2 and primer3 were added to the resultant solution and then the solution was incubated overnight at 30°C.

4.3.5 Monitoring of the gelling process

The mixture for DNA polymerization was incubated in a 96-well microliter plate without Ø29 DNA polymerase. GelGreen, a DNA specific dye, which can stain both single and double stranded DNA, was then added to the mixture which was then incubated for 30min. After Ø29 DNA polymerase was added, the fluorescence intensity of the mixture was evaluated by a fluorescence microplate reader (BioTek Synergy4 Plate Reader, BioTek Instruments, Inc., Winooski, Vermont) at 30°C. After 10 hours, primer2 and primer3 were added. The fluorescence intensity of the mixture was then monitored for 20 hours at 30°C.

4.3.6 Assay of enzymatic degradation of liquid-like DNA hydrogel

A 25μl scale of liquid-like DNA hydrogels was digested with 5.5 U of Exonuclease I in 400 μL of buffered solution (67 mM Glycine-KOH, 6.7 mM $MgCl_2$, 10 mM 2-mercaptoethanol, pH 9.5) for 1 day at 37ºC. 55 U of Exonuclease III was then added to the solution followed by a 1- to 2- day incubation, which was enough to digest the hydrogels completely. After each reaction, the UV absorbance of the supernatant at 260 nm was measured to evaluate the degree of enzymatic degradation.

4.3.7 Scanning Electron Microscope (SEM) imaging

Zeiss Ultra SEM (Zeiss, Germany) was used to obtain high resolution digital images of the DNA gel. A piece of the freeze dried DNA gel was placed onto the top of the SEM holder. The sample was metal-coated with Au/Pd.

4.3.8 Cell characterization

Live cell assays were performed using a live cell dye, CellTracker^{TM} Red CMTPX Probes (Molecular Probes, Eugene, Oregon). Pre-stained HL-60 cells were encapsulated into the pre-made DNA gel by injection. The DNA gel was incubated into a 96-well microliter plate at 37°C. The cell growth in the DNA gel was then evaluated every two days with a fluorescence microscope.

4.3.9 Gel electrophoresis

Linear ssDNA before circularization and circular template DNA were run in 10% denature PAGE gel at 600 volts at 25 °C for 1h with Tris-borate-EDTA (TBE, pH 8.3). The gel was stained using the gel stain SYBR II (Molecular Probes, Oregon) following the manufacturer's protocol.

4.4 Results and Discussions

4.4.1 The efficiency of the circularization reaction

The efficiency of the circularization of linear ssDNA was assessed by gel electrophoresis (Figure 4.1). The circularized DNA templates migrate slower (lane 2) than the linear ssDNA (lane1). Lane 2 shows a single band due to a high yield ligation reaction.

4.4.2 Design of liquid-like DNA hydrogel

First, primer1 was hybridized with a circular DNA template (Figure 4.2). The circular DNA was then polymerized via RCA. The extremely elongated ssDNA **1** was produced with a periodic sequence. Because of the flexibility of the elongated ssDNA, product **1** was sufficiently entangled to create a gel-like substance. Primer2 and primer3 were then added to the solution to reinforce the gel structure without adding more polymerase. Since primer2 was complementary to the portion of rolling circle amplified ssDNA **1**, primer2 was hybridized to the product ssDNA **1** and then polymerized. The resulting product **2** was then hybridized with primer3 to create product **3**. The final polymerized products were highly entangled to form a DNA hydrogel with robust and flexible properties. This DNA hydrogel **4** via RCCR was constructed up to the macro scale.

4.4.3 Gelling profile of liquid-like DNA hydrogel

A DNA hydrogel with entangled RCCA products is shown in Figure 4.3a. To show that the gel was made from DNA, the hydrogel was stained with a DNA specific dye (GelGreen, Ex/Em: 488nm/530nm). The stained DNA hydrogel emitted green fluorescence, suggesting that the hydrogel was composed of DNA molecules (Figure 4.3b and c).

To study the gelation process of DNA hydrogel, the changes in fluorescence intensity were monitored by a fluorescence microplate reader (Figure 4.4). Because the ssDNA elongated by RCA was simultaneously stained with GelGreen, there was increase in fluorescence intensity during gel aging. The fluorescence intensity steeply increased until 4 hours, and then slowly reached the maximum after 9 hours (Figure 4.4a). With five times less circular DNA template (2nM), the fluorescence intensity increased reached half the intensity of the products from 10nM circular DNA

templates. Reducing the concentration of Ø29 DNA polymerase by 5 times, the maximum fluorescence intensity was exactly 5 times less.

For monitoring the process of reinforcement by by chain reaction at the original condition (10nM, 1unit/μl), Primer2 and primer3 were added into the reaction solution. The fluorescence intensity steadily increased until 18 hours (Figure 4.4b). During this reinforcing process, elongated ssDNA was converted to dsDNA and separated into ssDNA repeatedly by chain reaction, resulting in an increase of fluorescence intensity without adding fresh Ø29 DNA polymerase.

4.4.4 Morphological study of liquid-like DNA hydrogel

To investigate the internal structure of the hydrogel based on DNA entanglement, differential interference contrast (DIC) and fluorescence microscopy were used (Figure 4.5). Interestingly, the hydrated DNA gel was composed of several micrometer sized round-shaped features (between 1 to 5μm) suggesting that the resulting DNA products by RCCR were heavily entangled with each other (Figure 4.5a). These balls of DNA threads have a structure similar to relaxed flagelliform protein of spider capture silk[30] allowing for considerable elongation which generates elasticity. Upon the application of stretching force, these DNA balls of thread may digentangled, giving the gel an elastic-like property. In the inset of Figure 4.5a, the overlay image of DIC and fluorescence microscopy showed that the balls of thread emitted green fluorescent light after staining with a DNA-specific fluorescent dye (GelGreen). The result confirms that the balls of thread were DNA products. Although the extended linear DNA does not show in DIC images because of the resolution limits of the microscope, the entire green fluorescence background in the inset of Figure 4.5a suggests that the balls of DNA thread were connected by a variety

of entangled linear DNA. Fluorescence microscope images of the internal structure of DNA hydrogel show a densely connected structure of entangled DNA like a spider web (Figure 4.5b).

To elucidate the physical structure of DNA hydrogel, the surface morphology was studied in a dried state using scanning electron microscopy (SEM). In the dry state, the morphology revealed a pattern similar to a spider web (Figure 4.6a, b, and c). The web-like structures were composed of small fibrils that were interconnected with the larger fibers. High magnification SEM images in Figure 4.6d showed that the fibers were approximately 1-3 μm in diameter. The several micron diameter DNA fibers suggest that DNA strands are heavily entangled together. In addition, a highly porous structure, which is necessary for cell culture matrix, was observed.

4.4.5 Enzymatic degradation profile of liquid-like DNA hydrogel

To investigate the ratio between DNA single and double helices composing the liquid-like DNA hydrogel, enzymatic degradation assays were carried out by ExoI and ExoIII exonucleases, which digested only single and double stranded DNA, respectively. The degradation process was observed by measuring the concentration of degraded DNA strands. Figure 4.7 shows that ExoI digested about 40% of DNA strands of the gel and the remaining 60% of gel were digested by ExoIII. These results indicate that the liquid-like DNA hydrogel consists of 40% ssDNA and 60% ds DNA.

Table 4.1. Oligonucleotide sequences of linear ssDNA and primers for the DNA hydrogel.

Strand	Sequence
Linear ssDNA	5'-Phosphate-TCGTTT**GATGTTCCTAACGTACCA**ACGCAC**ACGCAG TATTATGGACTG**GTAAAAGCTTTCCGAGGTAGCCTGGAGCATAGA GGCATTGGCTG-3'
Primer1	5'-**CAGTCCATAATACTGCGT**-3' (complementary to circular template)
Primer2	5'-**ACGCAGTATTATGGACTG**-3'
Primer3	5'-**TGGTACGTTAGGAACATC**-3' (complementary to circular template)

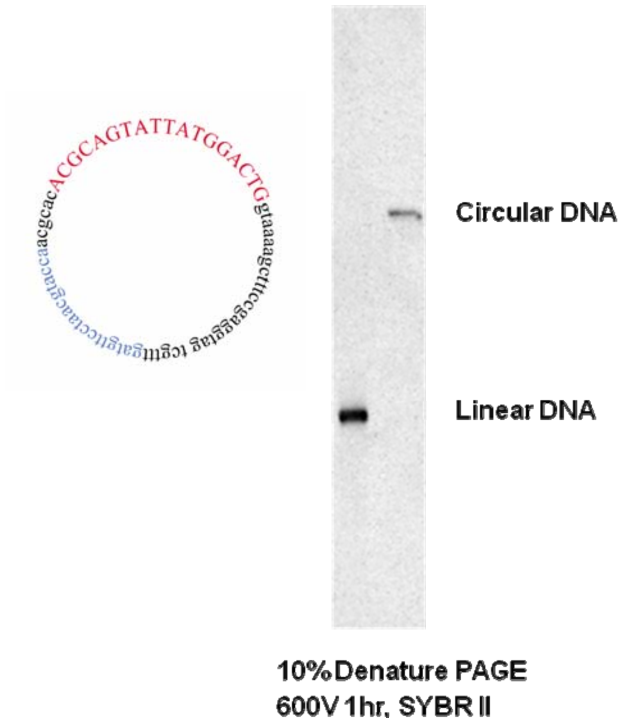

Figure 4.1. Gel electrophoresis image of circular DNA template. Lane2 indicates circular template DNA which shows slower mobility than linear DNA (Lane 1) after circularization.

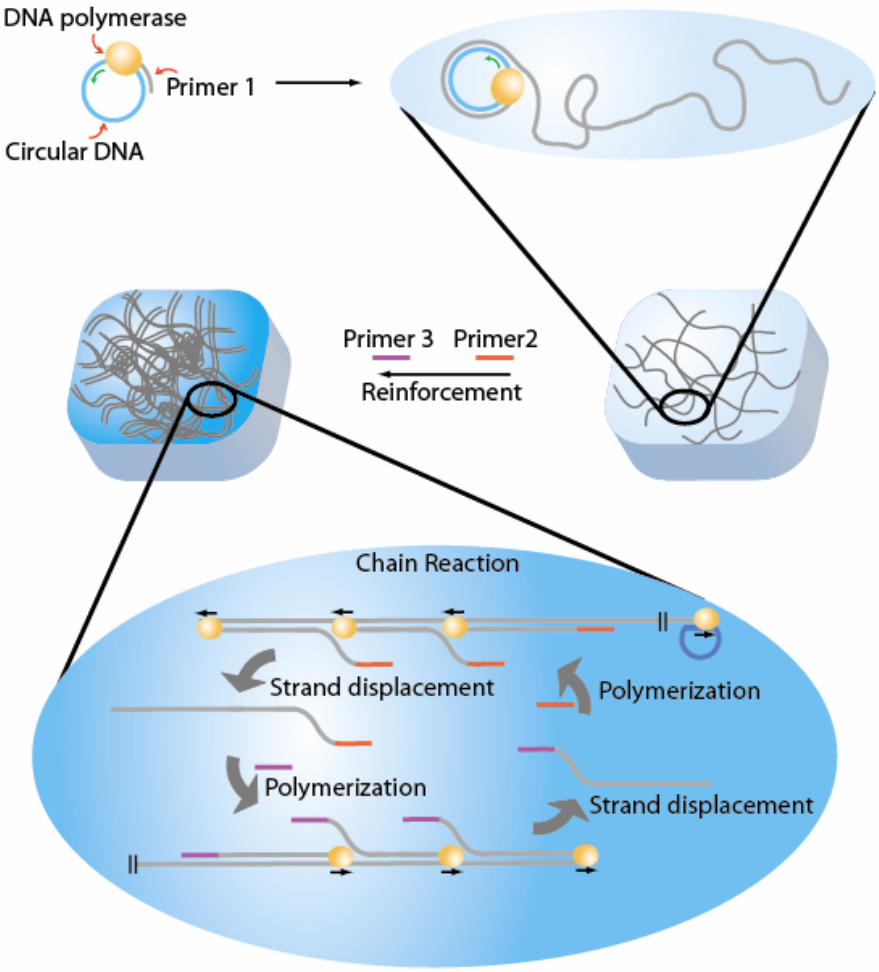

Figure 4.2. Schematic drawing of synthesis of liquid-like DNA hydrogel.

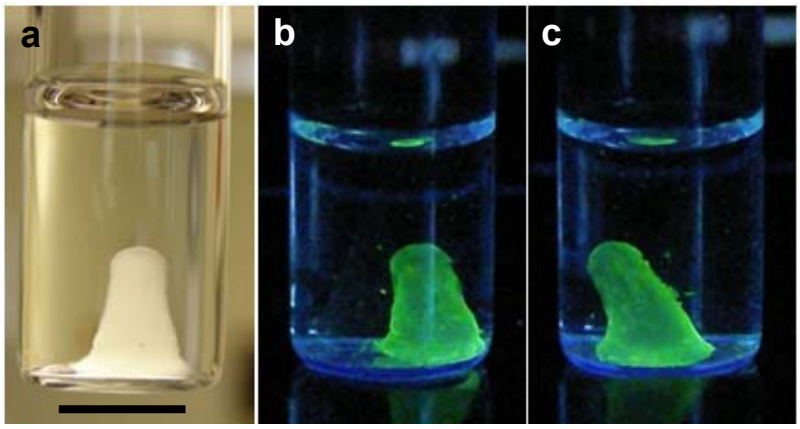

Figure 4.3. DNA hydrogels made entirely from the product of rolling circle chain reaction. **a,** A swollen DNA hydrogel in water. **b, c,** Stained DNA hydrogel with GelGreen, DNA-specific fluorescent dyes. The scale bars is 10 mm.

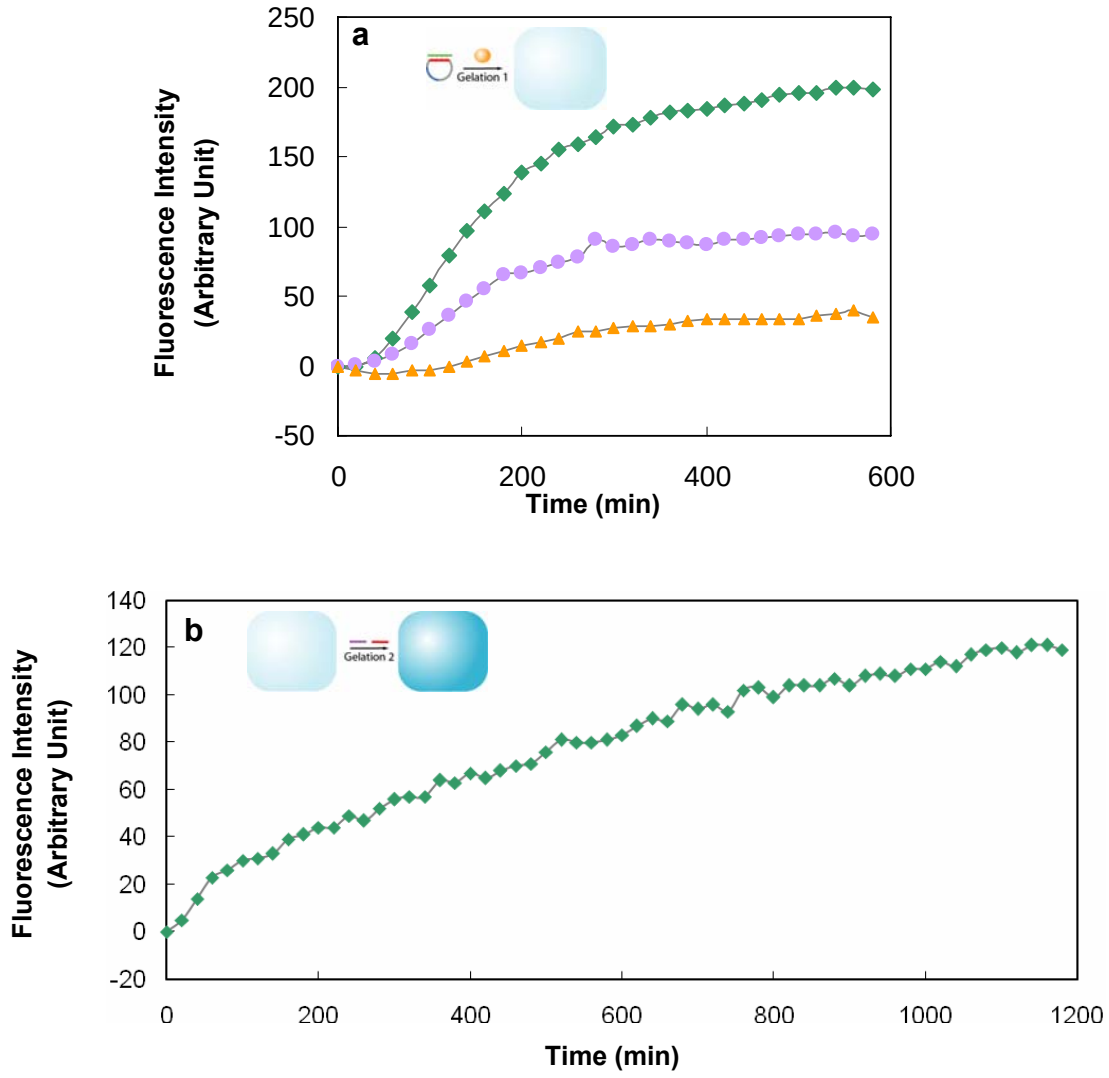

Figure 4.4. Gelation profiles based on the fluorescence intensity. **a,** Profile of initial gelation with three different conditions using 10nM circular DNA templates and 1 unit/μL of Ø29 DNA polymerase (◆), 2nM circular DNA templates and 1 unit/μL of Ø29 DNA polymerase (●), and 10nM circular DNA templates and 0.2 unit/μL of Ø29 DNA polymerase (▲). **b,** Profile of reinforcement from adding 10pM of primer2 and primer3 after gelation1 of the conditions with 10nM circular DNA templates and 1 unit/μL of Ø29 DNA polymerase (◆).

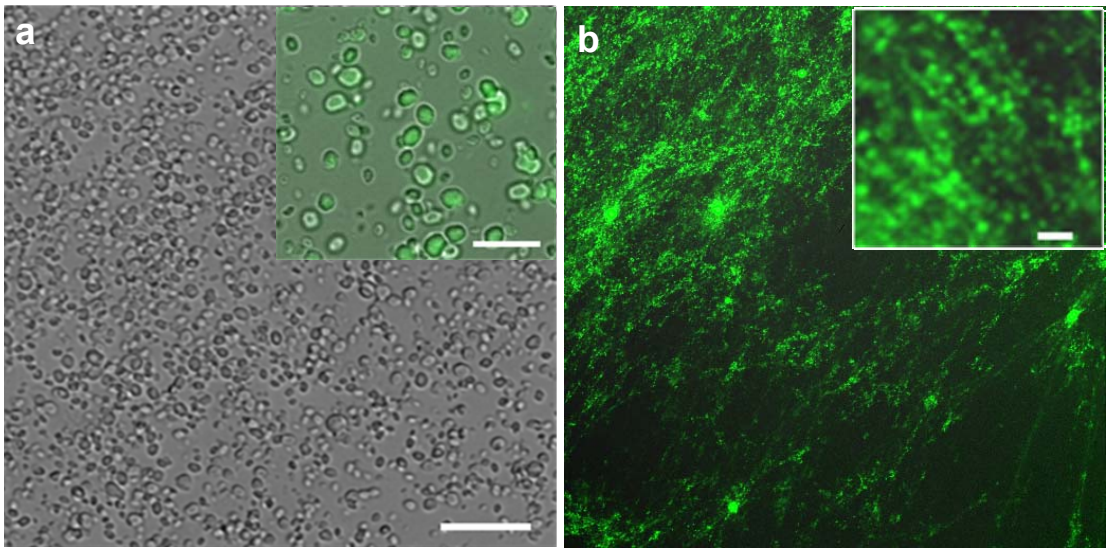

Figure 4.5. Microscopic images of DNA Hydrogel. **a,** DIC images of DNA hydrogel and overlay of DIC and fluorescence image (inset). **b**, Fluorescence microscopic image of the DNA hydrogel. The scale bars are 20 μm for **a** (inset 10 μm) and 50 μm for **b** (Inset 10 μm).

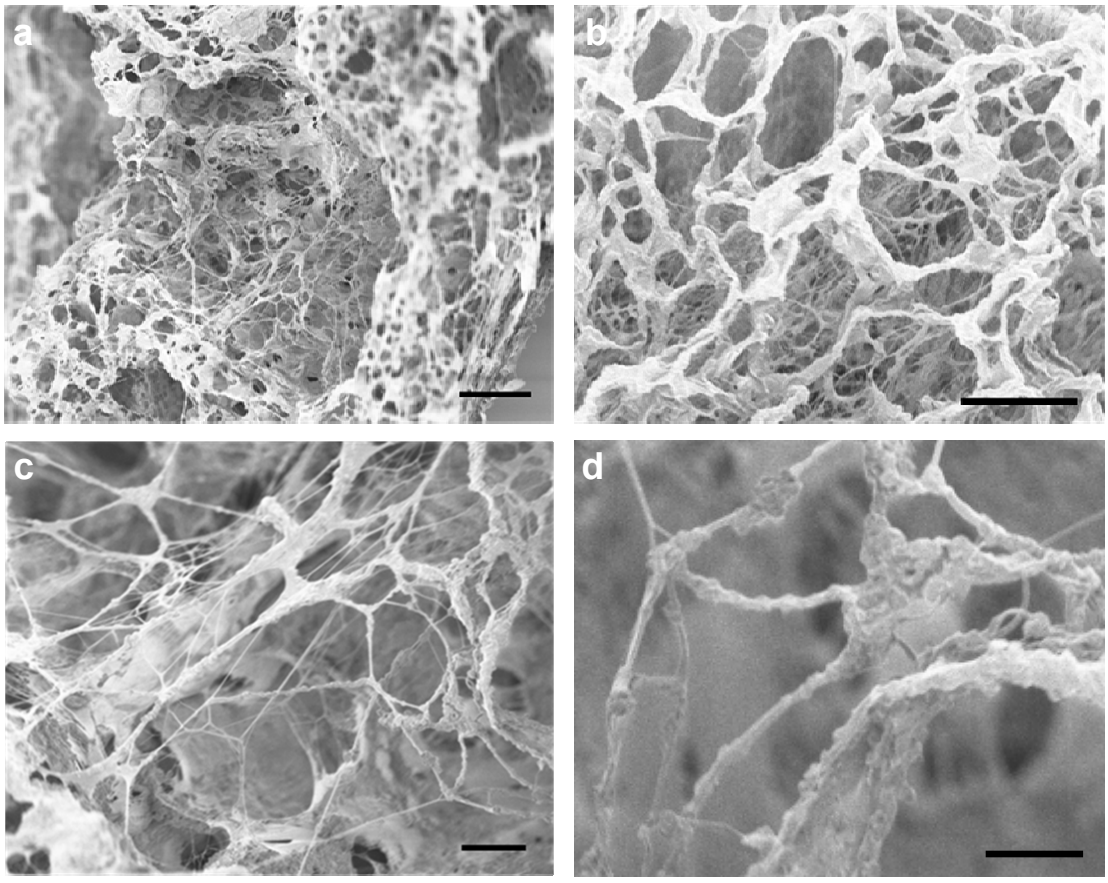

Figure 4.6. Scanning electron microscopy of dried DNA hydrogels. Various magnification images of DNA hydrogel are indicated. The scale bars are 100 μm for **a**, 50 μm for **b**, 20 μm for **c**, and 10 μm for **d**.

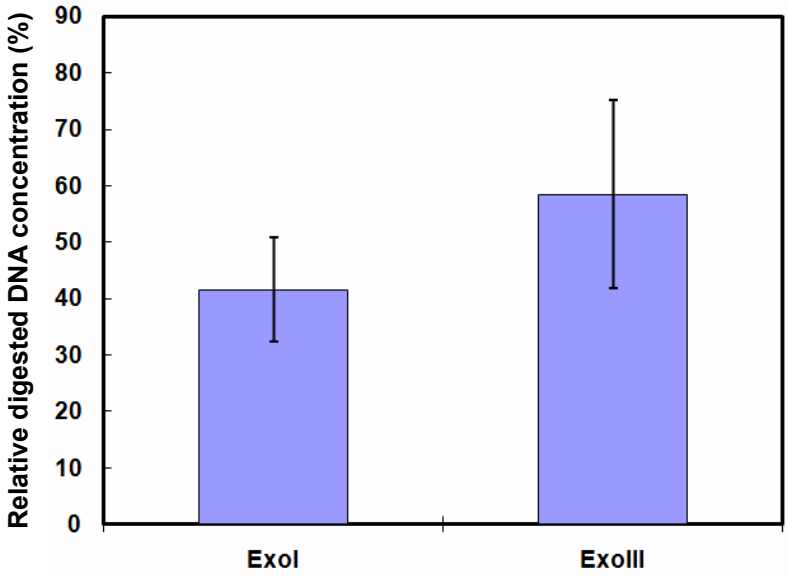

Figure 4.7. Degradation profile of liquid-like DNA hydrogel.

4.4.6 Mechanical property of DNA hydrogel

The mechanical property of DNA hydrogel was measured with a Dynamic Mechanical Analyzer (DMA 2980, TA Instruments, New Castle, DE). To understand the mechanical characteristics of the DNA hydrogel, compression modulus (0.0088Mpa) of the hydrogel was determined by analyzing a linear region of the stress-strain curve (Figure. 4.8). The value of compression modulus of the gel indicates that DNA hydrogels resist deformation by the entanglements of the elongated DNA strands.

4.4.7 Swelling degree of DNA hydrogel

The swelling ratio of DNA hydrogel was investigated with the gel in MilliQ water from the dry state for 336h (14 days). The swelling ratio was determined as

$$[(W_s - W_d) / W_d] \times 100 \qquad (1)$$

where W_s is the weight of the swollen DNA gel, and W_d is the weight of the dry DNA gel. As can be seen in Figure 4.9, the DNA gel swelled up to 700% within one day. However, after 24h, the swelling ratio increased very slowly to reach the equilibrium swelling ratio of 1350 % after 11 more days. This slow swelling process could be due to the highly entangled nature of the long DNA. As a drug carrier, this DNA hydrogel could exhibit good swelling properties for suitable for controlled release over long periods of time.

4.4.8 Moldability and injectability of liquid-like DNA hydrogel

The swelled DNA hydrogels kept their shape in water without dissolving (Figure 4.10a), while they behaved like a liquid outside a water environment (Figure 4.10b). Due to this liquid-like behavior, the DNA hydrogel can be transformed into any shape depending on the shape of the mold (Figure 4.10c). The round shaped DNA

hydrogel was easily transformed to rectangular, triangle, cross, and star shapes. The gel remained intact during the transformation because of its highly entangled nature, which prevented denaturation by physical force.

Unlike classic hydrogels, our liquid-like DNA hydrogel is not only moldable but also injectable after it forms. These properties are significant for fitting into complicated or irregularly-shaped defect sites and cannot be achieved with any other hydrogel. The injectability of liquid-like DNA hydrogel was investigated with very narrow tubes or needles (Figure 4.10d). Although the shape of the gels was elongated after injection, the gel remained intact for needles as narrow as 23G. Because of its robustness, the gel could be used as a biocompatible drug carrier for highly localized drug delivery by injection. In addition, this DNA hydrogel seemed to have relatively good elastic properties since the elongated gel tended to return its original shape.

4.4.8. Thermoplastic property of liquid-like DNA hydrogel

Traditional thermosetting hydrogels, which are prepared by chemical crosslinking, cannot be further processed once formed. Our previous DNA hydrogel, which was enzymatically crosslinked by DNA ligation, also showed thermosetting properties[34]. However, RCCR based DNA gel was not based on base pairing unlike classic DNA hydrogel, it was heatable without changing gel formations. To investigate the thermoplastic properties of DNA hydrogel, triangle-shaped DNA hydrogel was placed into a cross-shaped mold (Figures 4.11a and b). Without heating, when it was stored back in a water solution, the gel easily returned its original shape (triangular) (Figure 4.11c). However, when a triangular gel in a cross-shape mold was heated at 90°C for 15min, the extracted DNA hydrogel maintained a cross-shape in aqueous solution (Figure 4.11d). These results indicate that the liquid-like DNA hydrogel has a

thermoplastic property which allows it to be easily reformed by simple molding and heating.

4.4.9 Cell culture in liquid-like DNA hydrogel

Unlike 3D cell culture systems which require organic solvents or the use of chemical initiators, the physiological gelation conditions of liquid-like DNA hydrogel could provide a favorable cell culture environment. To study cell behavior in the 3D environment of liquid-like DNA hydrogel, HL-60 suspension cells were encapsulated into the gel for one day to eight day incubation periods. After encapsulation of cells, cell growth was analyzed by fluorescence microscope. Fluorescence images of the HL-60 cells are shown in Figure 4.12a-d. Cells were clearly observed to continue proliferating in the 3D gel environment. Cell spreading was quantified by observing cells in selected areas (Figure 4.12e). This DNA hydrogel based 3D cell culture resulted in a significant increase in HL-60 proliferation on days 3, 5, and 8 in comparison to day 1. Thus our novel DNA hydrogel provided a favorable 3D gel matrix for cell culture. These results also suggest that the gel easily permeated cell culture media, nutrients and gases due to its highly porous structure. In addition, the robust nature of hydrogel by physically entangled DNA provides ease of handling to study cell behavior in biologically relevant 3D cell culturing.

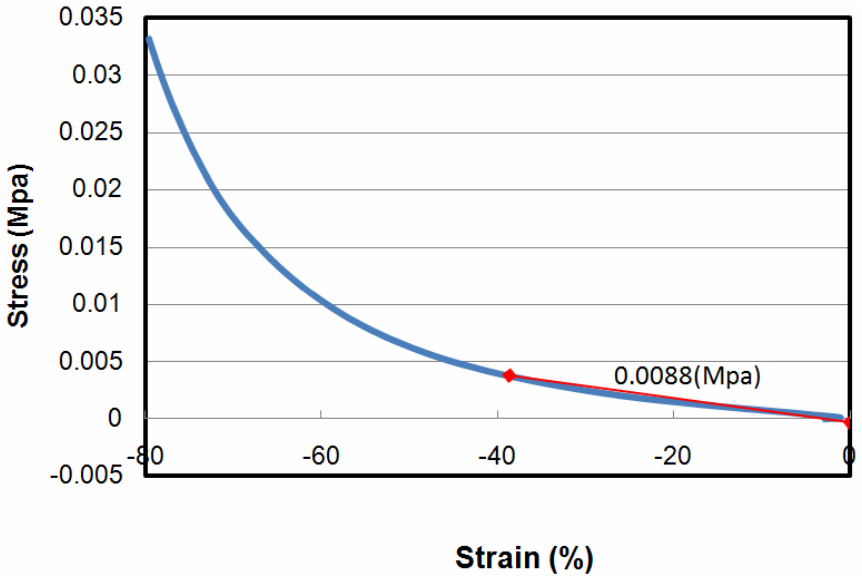

Figure 4.8. Stress-strain curves of hydrogel (Dynamic Mechanical Analysis).

.

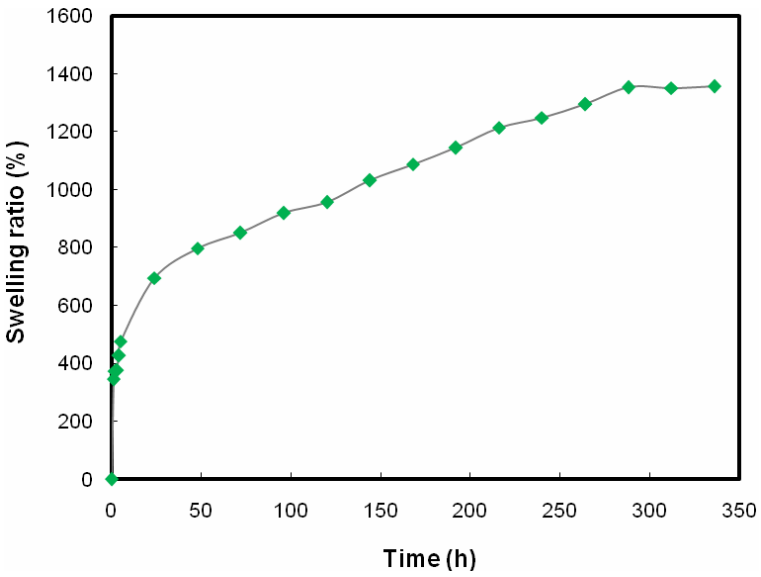

Figure 4.9. Swelling ratio of DNA Hydrogel. The swelling was confirmed in MilliQ water from the dry state for 300h.

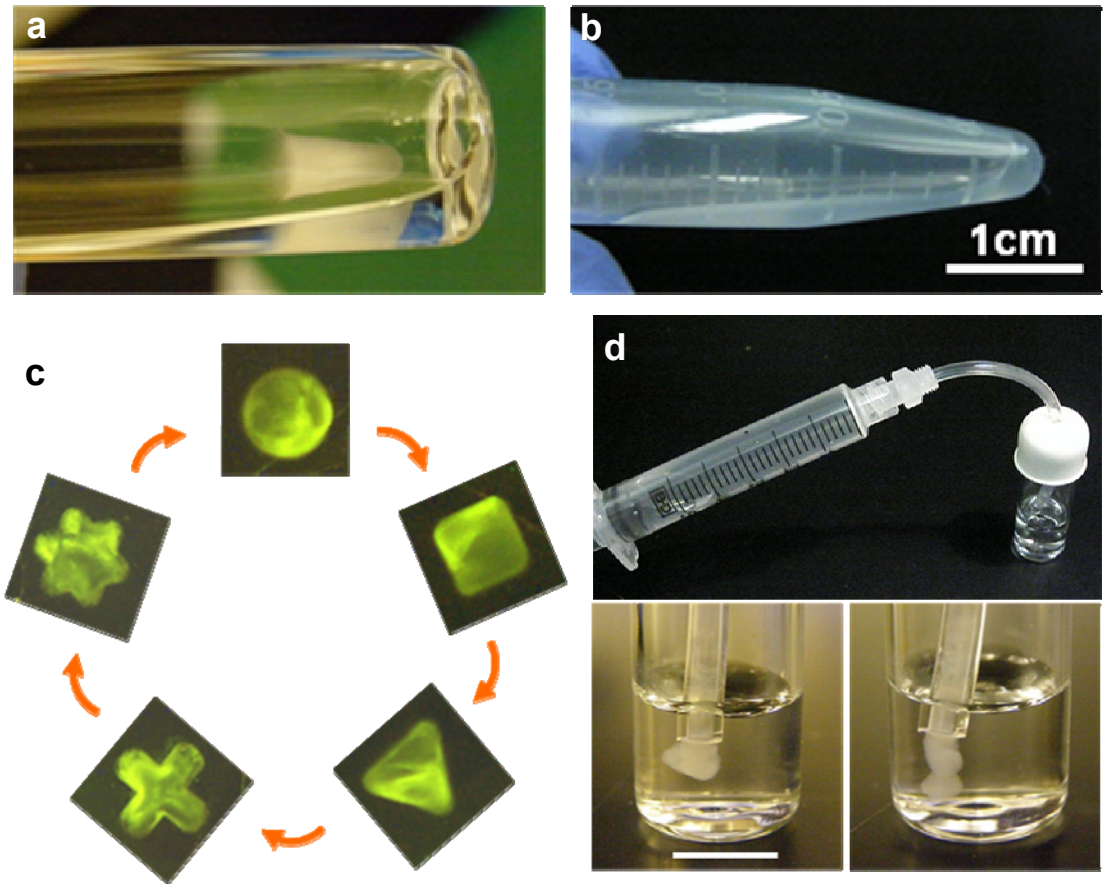

Figure 4.10. a, A swelled liquid-like DNA hydrogel in water, **b**, Liquid-like behavior of DNA gel without water. **c**, Transformation of DNA hydrogel back and forth to any shape depending on the mold. **d**, Images of injecting DNA hydrogel and DNA hydrogel after passing through the narrow tubes. The scale bar is 1cm.

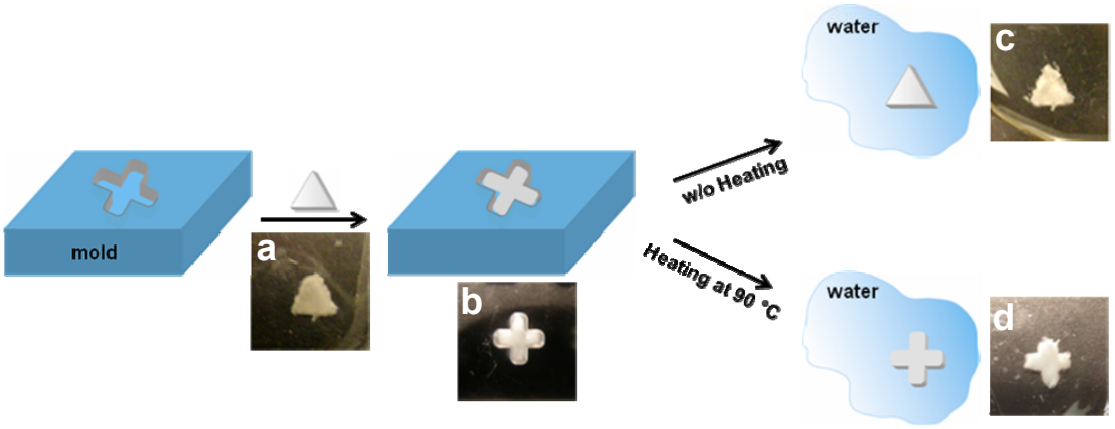

Figure 4.11. Investigation of thermoplastic properties of liquid-like DNA hydrogel **a**, triangle-shaped DNA hydrogel before molding. **b**, Molded DNA hydrogel in cross-shaped mold. **c,** A return to a triangle-shape in water solution after extracting without heating. **d**, Extracted cross-shape after heating at 90°C.

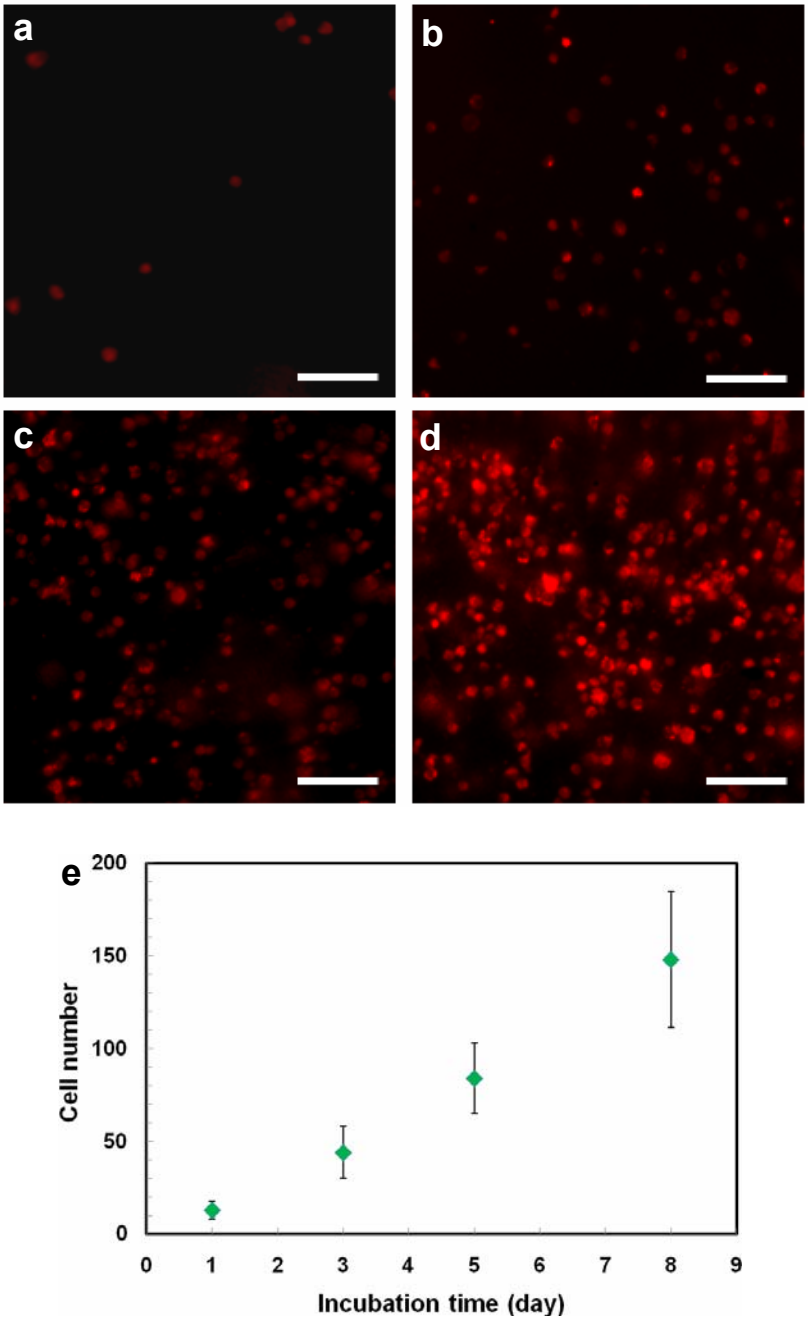

Figure 4.12. Fluorescence images of cells cultured in DNA hydrogel (with red live cell specific dye): **a,** day 1, **b,** day 3, **c,** day 5, and **d,** day 8. All scale bars indicate 100μm. **e**, Proliferation of HL-60 cells in the hydrogel for 8 days. Cell numbers are counted in 500 μm x 500 μm area.

Conclusion

In conclusion, we have demonstrated the generation of a novel hydrogel by the simple approach of combining rolling circle amplification and polymerase chain reaction. The hydrogel consisted of elongated DNA products that became highly entangled to produce physically crosslinked networks. Unlike classic hydrogels, our liquid-like DNA hydrogel was injectable and moldable after it formed. These properties are significant for fitting into complicated or irregularly-shaped defect sites and could not be easily achieved with any other hydrogel. In addition, our novel DNA hydrogel has the ability to be reformed and reshaped by its thermoplastic property. The hydrogel can also efficiently encapsulate and maintain viable cells by mimicking natural cellular environments due to its physically entangled DNA-based 3D geometry and biocompatible nature. The simple and robust manner of generating DNA hydogel could be exploited in biomedical fields such as tissue engineering and drug delivery.

REFERENCE

1. Ladet, S., David, L. & Domard, A. Multi-membrane hydrogels. Nature 452, 76-79 (2008).
2. Khan, F., Tare, R.S., Oreffo, R.O. & Bradley, M. Versatile biocompatible polymer hydrogels: scaffolds for cell growth. Angewandte Chemie (International ed 48, 978-982 (2009).
3. Ho, E., Lowman, A. & Marcolongo, M. Synthesis and characterization of an injectable hydrogel with tunable mechanical properties for soft tissue repair. Biomacromolecules 7, 3223-3228 (2006).
4. Mandracchia, D., Pitarresi, G., Palumbo, F.S., Carlisi, B. & Giammona, G. pH-sensitive hydrogel based on a novel photocross-linkable copolymer. Biomacromolecules 5, 1973-1982 (2004).
5. Wang, C., Stewart, R.J. & Kopecek, J. Hybrid hydrogels assembled from synthetic polymers and coiled-coil protein domains. Nature 397, 417-420 (1999).
6. Ueki, T. & Watanabe, M. Lower critical solution temperature behavior of linear polymers in ionic liquids and the corresponding volume phase transition of polymer gels. Langmuir 23, 988-990 (2007).
7. Lendlein, A., Jiang, H., Junger, O. & Langer, R. Light-induced shape-memory polymers. Nature 434, 879-882 (2005).
8. Shinohara, S., Seki, T., Sakai, T., Yoshida, R. & Takeoka, Y. Photoregulated wormlike motion of a gel. Angewandte Chemie (International ed 47, 9039-9043 (2008).
9. Ehrbar, M., Schoenmakers, R., Christen, E.H., Fussenegger, M. & Weber, W. Drug-sensing hydrogels for the inducible release of biopharmaceuticals. Nature materials 7, 800-804 (2008).

10. Miyata, T., Asami, N. & Uragami, T. A reversibly antigen-responsive hydrogel. Nature 399, 766-769 (1999).
11. Murakami, Y. & Maeda, M. DNA-responsive hydrogels that can shrink or swell. Biomacromolecules 6, 2927-2929 (2005).
12. Pek, Y.S., Wan, A.C., Shekaran, A., Zhuo, L. & Ying, J.Y. A thixotropic nanocomposite gel for three-dimensional cell culture. Nature nanotechnology 3, 671-675 (2008).
13. McGuigan, A.P., Bruzewicz, D.A., Glavan, A., Butte, M. & Whitesides, G.M. Cell encapsulation in sub-mm sized gel modules using replica molding. PLoS ONE 3, e2258 (2008).
14. Gillette, B.M. et al. In situ collagen assembly for integrating microfabricated three-dimensional cell-seeded matrices. Nature materials 7, 636-640 (2008).
15. Lee, J., Cuddihy, M.J. & Kotov, N.A. Three-dimensional cell culture matrices: state of the art. Tissue engineering 14, 61-86 (2008).
16. Liedl, T., Dietz, H., Yurke, B. & Simmel, F. Controlled trapping and release of quantum dots in a DNA-switchable hydrogel. Small (Weinheim an der Bergstrasse, Germany) 3, 1688-1693 (2007).
17. Wei, B., Cheng, I., Luo, K.Q. & Mi, Y. Capture and release of protein by a reversible DNA-induced sol-gel transition system. Angewandte Chemie (International ed 47, 331-333 (2008).
18. Lin, D.C., Yurke, B. & Langrana, N.A. Mechanical properties of a reversible, DNA-crosslinked polyacrylamide hydrogel. Journal of biomechanical engineering 126, 104-110 (2004).
19. Lober, A. et al. Monolithic polymers for cell cultivation, differentiation, and tissue engineering. Angewandte Chemie (International ed 47, 9138-9141 (2008).

20. Dutta, S., Chowdhury, G. & Gates, K.S. Interstrand cross-links generated by abasic sites in duplex DNA. Journal of the American Chemical Society 129, 1852-1853 (2007).

21. Lee, C.K. et al. DNA hydrogel fiber with self-entanglement prepared by using an ionic liquid. Angewandte Chemie (International ed 47, 2470-2474 (2008).

22. Li, Y. et al. Controlled assembly of dendrimer-like DNA. Nature materials 3, 38-42 (2004).

23. Li, Y., Cu, Y.T. & Luo, D. Multiplexed detection of pathogen DNA with DNA-based fluorescence nanobarcodes. Nature Biotechnology 23, 885-889 (2005).

24. Um, S.H. et al. Enzyme-catalysed assembly of DNA hydrogel. Nature materials 5, 797-801 (2006).

25. Fire, A. & Xu, S.Q. Rolling replication of short DNA circles. Proceedings of the National Academy of Sciences of the United States of America 92, 4641-4645 (1995).

26. Beyer, S., Nickels, P. & Simmel, F.C. Periodic DNA nanotemplates synthesized by rolling circle amplification. Nano letters 5, 719-722 (2005).

27. Zhao, W., Gao, Y., Kandadai, S.A., Brook, M.A. & Li, Y. DNA polymerization on gold nanoparticles through rolling circle amplification: towards novel scaffolds for three-dimensional periodic nanoassemblies. Angewandte Chemie (International ed 45, 2409-2413 (2006).

28. Demidov, V.V. Rolling-circle amplification in DNA diagnostics: the power of simplicity. Expert review of molecular diagnostics 2, 542-548 (2002).

29. Fujii, R., Kitaoka, M. & Hayashi, K. Error-prone rolling circle amplification: the simplest random mutagenesis protocol. Nature protocols 1, 2493-2497 (2006).

30. Becker, N. et al. Molecular nanosprings in spider capture-silk threads. Nature materials 2, 278-283 (2003).

CHAPTER 5

Future work

5.1 Multi-drug systems using ABC monomers

Future work on anisotropic branched crosslinkable (ABC) monomers would benefit from synthetic refinements that expand the range of functional moieties that can be attached to the DNA stands. As described in chapter 3, quantum dots, gold nanoparticles, and photo-crosslinkable moieties were successfully labeled with precise control. In addition, successful application of ABC monomers for detection and delivery was achieved by labeling pathogen DNA and ODN.

Although some diseases are the result of monogenic disorders, most diseases are caused by multigenic disorders[1]. To treat diseases arising from multigenic disorders, multivalent drug carriers are necessary. Based on previous achievements, the application of ABC monomers can be extended for delivering not only DNA but also mRNA and siRNA which could easily hybridize with DNA-templated ABC monomers. In addition, it would be easy to functionalize ABC monomers with DNA aptamers which can be used as drugs instead of antibodies[2-5]. Therefore, ABC polymers may be well-suited as a carrier for multi-drug carriers (Figure. 5.1).

5.2. Shape-memory DNA hydrogel

Shape-memory materials, which are stimuli-responsive, have been widely used in a variety of fields[6]. For example, shape-memory metal alloys have been applied in biomedical applications. In addition, several shape-memory polymers have been reported[7].

Creation of DNA hydrogel made from RCA products could lead to new functions which are not easily obtained from traditional polymer based hydrogel. In particular, a shape-memory property can be achieved from highly entangled DNA hydrogel without any complicated chemical reactions. Shape memory DNA hydrogel can be exhibited through the following process. First, the gel receives its permanent

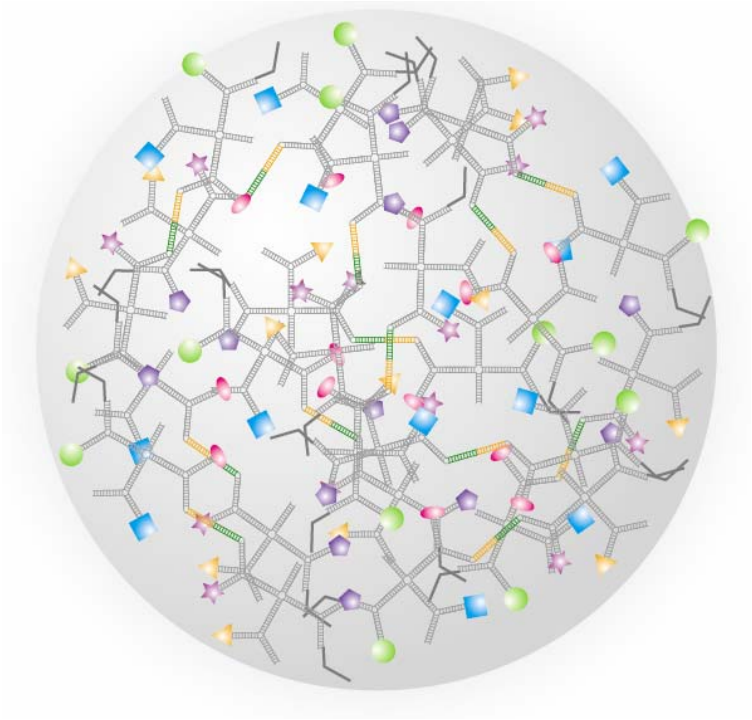

Figure 5.1. Schematic drawing of multi-drug carrier from ABC monomer.

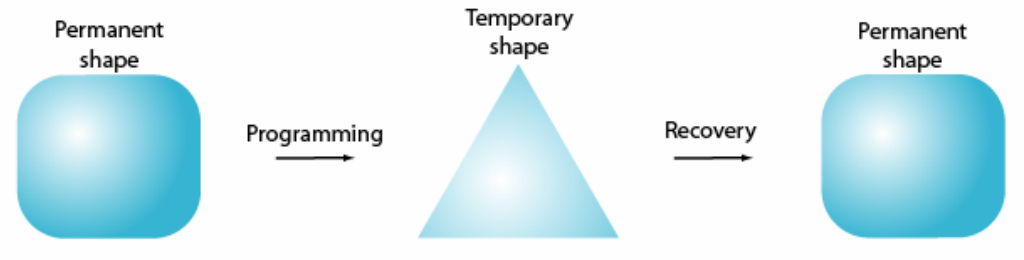

Figure 5.2. Schematic drawing of shape-memory characteristic. The permanent shape of DNA hydrogel can be transferred to the temporary shape by molding. Removing stress from the mold results in the recovery of the permanent shape.

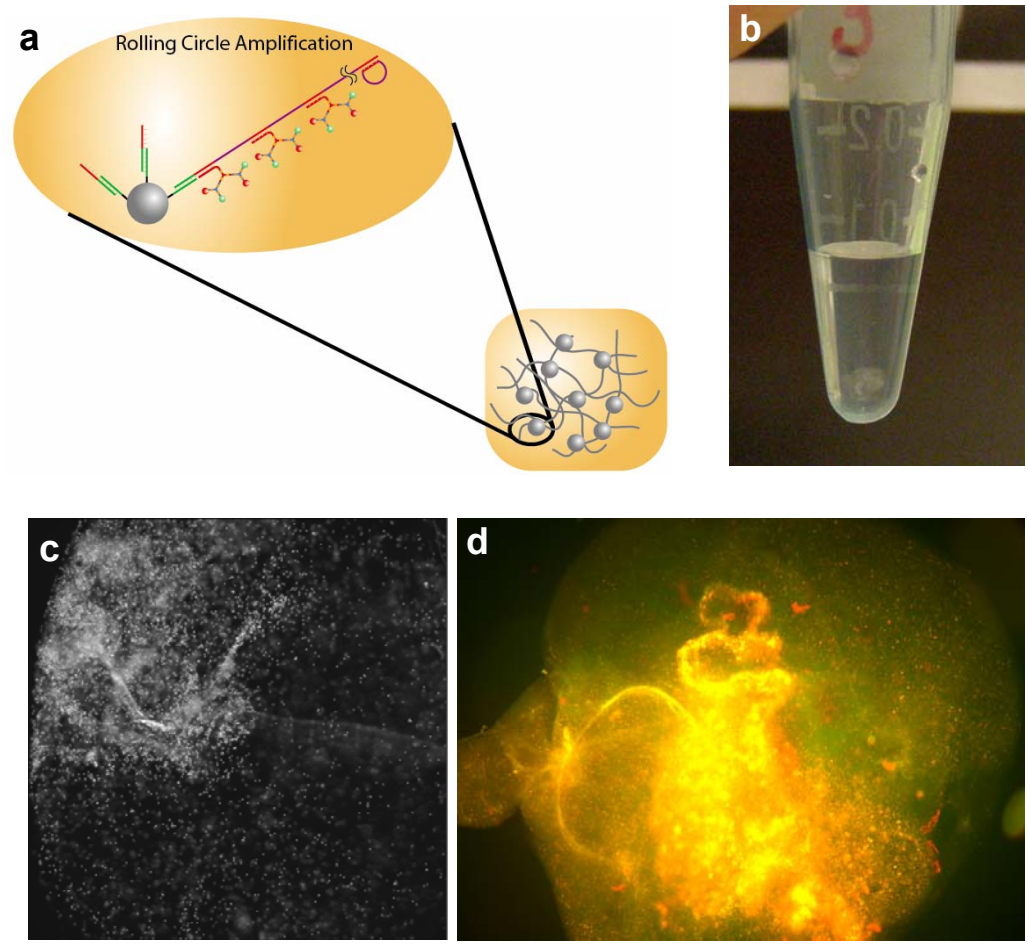

Figure 5.3. a, Schematic drawing of Synthesizing DNA hydrogel by RCA products on microspheres, **b,** DNA hydrogel with embedded microsphere beads, **c,** Microscopic image, and **d,** fluorescence microscopic image.

shape (Figure 5.2). Second, DNA hydrogel deform to take a temporary shape by placing in a mold. Then, the gel can recover its permanent shape after release from the mold. Unlike conventional shape-memory gel, DNA hydrogel can recover its original shape without any additional process such as heating or cooling. Additionally, shape-memory DNA hydrogel can erase its permanent shape by heating and memorize a new permanent shape.

5.3. DNA hydrogel with new functions

Similar to ABC monomer project, DNA hydrogel can be easily interfaced with a variety of nanoparticles and microspheres. It would be interesting to find out how the gel behaves if it has magnetic property by producing elongated DNA stranded on magnetic microspheres (Figure 5.3a). Preliminary data showed the promise to synthesize of DNA hydrogel using microspheres (Figure 5.3b-d). In addition, it should not be difficult to attach most drugs to the DNA strands inside the gel for drug delivery.

REFERENCE

1. Stribley, J., Rehman, K., Niu, H. & Christman, G. Gene therapy and reproductive medicine. *Fertil. Steril.* **77**, 645-657 (2002).
2. Ellington, A. D. & Szostak, J. W., In vitro selection of RNA molecules that bind specific ligands. *Nature* **346,** 818–822 (1990).
3. Bock, L. C., Griffin, L. C., Latham, J.A., Vermaas, E. H. & Toole, J. J., Selection of single-stranded DNA molecules that bind and inhibit human thrombin. *Nature* **355,** 564–6 (1992).
4. Hoppe-Seyler, F. & Butz, K., Peptide aptamers: powerful new tools for molecular medicine. *J. Mol. Med.* **78**, 426–30 (2000).
5. Carothers, J. M., Oestreich, S. C., Davis, J. H. & Szostak, J. W., Informational complexity and functional activity of RNA structures. *J Am Chem Soc.* **126**, 5130–7 (2004).
6. Andreas, L. & Steffen, K., Shape-Memory Polymers. Angew. Chem. Int. Ed. 41, 2034-2057 (2002).
7. Andreas, L., Annette, M. S., & Robert, L., AB-polymer networks based on oligo(ε-caprolactone) segments showing shape-memory properties. PNAS. 98, 842-847 (2001).